2008

Towards an extended microscopic theory for upper-fp-shell nuclei

Kalin Drumev
Louisiana State University and Agricultural and Mechanical College, kdrume1@lsu.edu

TOWARDS AN EXTENDED MICROSCOPIC THEORY FOR UPPER-FP-SHELL NUCLEI

A Dissertation

Submitted to the Graduate Faculty of the
Louisiana State University and
Agricultural and Mechanical College
in partial fulfillment of the
requirements for the degree of
Doctor of Philosophy

in

The Department of Physics and Astronomy

by
Kalin Drumev
M.S., University of Shumen "Konstantin Preslavski", Bulgaria, 1997
May, 2008

Dedication

To those who *truly* believed...

Acknowledgments

First, I would like to express my gratitude to my adviser Professor Jerry P. Draayer for his infinite patience, continuous support and constant encouragement during the long years of research.

I am also indebted to Professors A. Ravi P. Rau, J. Blackmon and J. Wefel from the Department of Physics and Astronomy as well as Professor K. Murray from the Department of Chemistry for serving on my dissertation committee.

Next, my thanks go to the postdocs Dr. Chairul Bahri and Dr. Vesselin Gueorguiev who I had the opportunity to work with for couple of years.

I also acknowledge the help I received from Dr. Gergana Stoitcheva and Dr. Petia Stoytcheva during my first couple of weeks in US and the time spent afterwards.

It is my pleasure to acknowledge my former roommate and colleague Dr. Ionel Stetcu and my colleague Indrajith Senevirathne for their friendship and many fruitfull discussions not only about physics but also about life in general.

I also express my gratitude to Dr. Ana Georgieva for her constant scientific and moral support.

In addition, I extend my appreciation to Dr. Gabriela Popa who has been my long-time colaborator.

Also, I would like to acknowledge the help from Tomas Dytrych in the preparation of the final form of this Dissertation.

Of course, the path to US would be impossible without the support of people from my home country. I would like to thank those who endorsed my coming here, namely, Professors Anton Antonov, Tchavdar Palev and Mario Stoitsov. I also acknowledge my high school physics teacher Christina Baeva who was a constant inspiration during my early years in science.

I extend my appreciation to anyone who took part in the research conducted over the last couple of months and who was around during the countless number of nights with no sleep when many important conclusions for the presented work were made.

Although at times being far from the challenges I was facing, my family was always giving me their infinite support.

Finally, I appreciate the support from the Department of Physics and Astronomy at Louisana State University.

Table of Contents

List of Tables

List of Figures

Abstract

An extended SU(3) shell model that for the first time explicitly includes particles from the unique-parity levels in nuclei is introduced. Its relevance is established through calculations performed with realistic interactions for a group of upper fp-shell isotopes where valence nucleons beyond the N=28=Z core occupy levels of the normal-parity upper fp-shell ($f_{5/2}, p_{3/2}, p_{1/2}$) and the unique-parity $g_{9/2}$ intruder configuration. Specifically, the outcome suggests that the pseudo-SU(3) symmetry is quite good throughout the region and that only part of the configurations are relevant for the structure of the low-lying states. The levels of the upper fp-shell are handled within the framework of an m-scheme basis as well as its pseudo-SU(3) counterpart, and respectively, the $g_{9/2}$ as a single level and as a member for the complete gds shell.

More detailed analyses of the extended SU(3) model are done for two nuclei of special interest in astrophysics, namely the waiting-point nuclei ^{64}Ge and ^{68}Se. The strengths and limitations of the theory are demonstrated by its ability to describe various nuclear characteristics. Specifically, energy spectra, B(E2) transition strengths and wave-function content are compared with the realistic results. In addition, the dominance of configurations with different distribution of particles and the role that several newly-introduced terms play in the Hamiltonian are investigated. The extended SU(3) approach allows one to better probe the effects of deformation and account for these key properties of the system within a highly-truncated model space.

The model also promises to be useful for nuclei from the rare-earth and actinide regions. Specifically, by ensuring a robust number of collective degrees of freedom and Hamiltonians with a larger number of degrees of freedom, it should allow one to give a satisfactory explanation of the experimentally-observed existence of an abundance of low-lying 0^+ states and very strongly enhanced B(E2) strengths found in these nuclei. This version of the theory will extend previous results from the pseudo-SU(3) model where the role of nucleons in the intruder levels was relegated to a very simple renormalization of the dynamics defined by nucleons in the normal-parity spaces only.

Chapter 1

Introduction

The nuclear shell model [1] has been applied successfully for the description of various aspects of nuclear structure, in large part because it is based on a minimum number of assumptions. Although direct diagonalization of the Hamiltonian matrix in the full Hilbert space would be desirable, the dimensionality of such a space is often too large to allow calculations of this type to be done. Recently, in order to relax this restriction dramatically, various stochastic approaches, for instance, the Shell-Model Monte Carlo Method [2], have been suggested. Alternatively, algebraic models using the symmetry properties of the systems under investigation have been developed (e.g.[3, 4]).

Intruder levels are present in heavy deformed nuclei where the strong spin-orbit interaction destroys the underlying harmonic oscillator symmetry of the nuclear mean-field potential. The role they play for the overall dynamics of the system has been the topic of many questions and debates [5, 6, 7, 8]. Until now, the problem has been either approached within the framework of a truncation-free toy model [5] or by just considering the role of the single intruder level detached from its like-parity partners [6, 8]. It was argued in [5] that particles in these levels contribute in a complementary way to building the collectivity in nuclei. However, some mean-field theories suggest that these particles play the dominant role in inducing deformation [7]. In order to build a complete shell-model theory, these levels need to be included in the model space especially if experimentally observed high-spin or opposite-parity states are to be described.

Until recently, SU(3) shell-model calculations - real SU(3) [3] for light nuclei and pseudo-SU(3) [4] for heavy nuclei - have been performed in either only one space (protons and neutrons filling the same shell, e.g. the *ds* shell) or two spaces (protons and neutrons filling different shells, e.g. for rare-earth and actinide nuclei). Various results for low-energy features, like energy spectra and electromagnetic transition strengths, have been published over the years [9, 10, 11]. These applications confirm that the SU(3) model works well for light nuclei and the pseudo-SU(3) scheme, under an appropriate set of assumptions, for rare-earth and actinide species. Up to now, SU(3)-based methodologies have not been applied to nuclei with mass numbers $A = 56$ to $A = 100$, which is an intermediate region where conventional wisdom suggests the break down of the assumptions that underpin their use in the other domains.

In particular, the $g_{9/2}$ intruder level that penetrates down from the shell above due to the strong spin-orbit splitting appears to be as spectroscopically relevant to the overall dynamics as the normal-parity $f_{5/2}, p_{3/2}, p_{1/2}$ levels. Specifically, in this region the effect of the intruder level cannot be ignored or mimicked through a "renormalization" of the normal-parity dynamics which is how it has been handled to date.

The upper-$fp + g_{9/2}$ shell is the lightest region of nuclei where the intruder level must be taken into account. Its presence poses a significant challenge and opens a sequence of questions, many of them still unanswered. For example, if the pseudo-SU(3) symmetry proves to be a good scheme for characterizing upper-fp shell configurations, should one integrate the $g_{9/2}$ intruder into this picture by treating it as a single j-shell that is independent of couplings to the other members $(g_{7/2}, d_{5/2}, d_{3/2}, s_{1/2})$ of the gds shell, or should one take the complete gds shell into account? While the treatment of the $g_{9/2}$ intruder as a single additional orbit is possible for only a few exceptional nuclei within the m-scheme shell-model calculations, an SU(3) approach to the problem could allow the inclusion of the $g_{9/2}$ intruder as a member of the full gds shell and can be applied to all upper-fp nuclei. It is the purpose of this work to introduce and establish the benefits of a new and extended SU(3) shell model which, for the first time, explicitly includes particles from the complete unique-parity sector and therefore can be used to explore the role that intruder levels play in the dynamics of the system.

In the next two chapters, the two well-known microscopic algebraic models based on the $SU(3)$ symmetry, namely, the Elliott's SU(3) model for the description of ds-shell nuclei [3] and its pseudo realization in heavy nuclear systems [12], are reviewed. The main features and advantages of both models are pointed out, with the need for an extension of the latter seeming obvious and natural. Next, in Chapter 4 the appropriate choice of model space for this extension is established in the upper fp-shell region of nuclei by calculating, using a realistic Hamiltonian, the occupancies of the single-particle orbitals and the symmetry properties of some typical representative isotopes. Then, a brief introduction of the basics of the extended SU(3) model follows in Chapter 5 along with a description of the algorithms using existing and newly developed computer codes. The following chapter of the dissertation, Chapter 6, presents results from the first calculations within the framework of the introduced extended SU(3) shell model performed for two nuclei of major importance in astrophysics, namely, the waiting-point $N = Z$ nuclei ^{64}Ge and ^{68}Se [13]. Both the strengths and the limitations of the model are demonstrated and discussed. Energy spectra, B(E2) transition strengths and the wave function content are calculated and compared with the realistic predictions. Also, the meaning and the importance of the model space truncation scheme is underscored. We conclude with a discussion about various future applications of the model and the possible challenges along the way of its introduction in other nuclear domains. Finally, a summary of the primary goals, used methods and accomplished results as well as the prospects for future investigations can be found in the Conclusion, Chapter 7.

Chapter 2

Elliott's SU(3) Model

As one of the most successful theories of the last century, quantum mechanics can be used to explain a wide range of physical phenomena. However, there are only a very limited number of problems that can be solved exactly. That set includes certain one-dimensional potentials, the three-dimensional harmonic oscillator, and hydrogen-like systems. The solvability question for such systems is inextricably linked to the symmetries they possess.

Symmetry is a unifying concept that was introduced in physics during the second part of the nineteenth century. At that time it was primarily used to describe geometric arrangements of constituent parts of an extended object as it is with atoms in molecules and crystals. If the system remains unchanged under the full set of transformations that generate the symmetry then it is called an **exact symmetry**. In this case the transformations give rise to a degenerate multiplet of states that span a representation of a group. It is well-known that energy conservation is due to time translational symmetry, linear momentum conservation is due to space translational symmetry, and angular momentum conservation is related to rotational symmetry of the system under consideration. Other examples of exact symmetry are the spherical oscillator and the Coulomb potentials which possess SU(3) and SO(4) symmetry, respectively.

Even in cases when the strong requirement for existence of an exact symmetry can not be met, the symmetry concept can still be useful. A second symmetry type is a **dynamical symmetry**. In this case the system is not necessarily left invariant under the symmetry operations, but the eigenstates can still be associated with a single irreducible representation of a group. The lifting of the degeneracy is then generated by the occurrence of generators (or function of generators) of a group which does not alter the irreducible representation of the eigenstates in the Hamiltonian (or Lagrangian) characterizing the system. In the early sixties dynamical symmetries were introduced in particle physics (flavor) and later in molecular physics.

Since the atomic nucleus is a complex many-particle system which does not yield to a statistical description, many group theoretical approaches have been developed over the years. For instance, the Interacting Boson Model [14] (with underlying symmetry $U(6)$) which considers the nucleus as consisting of bosonic proton

and neutron pairs coupled to spin zero and angular momentum zero or two. Another example is the fermion algebraic models originating from the Elliott model [3, 15] (with $SU(3)$ as an underlying symmetry). Group theoretical methods allow for a mathematically elegant treatment of complex physical systems that have specific symmetry properties.

2.1 $SU(3)$ Symmetry

In the nuclear shell model, where the three-dimensional isotropic harmonic oscillator is used as an approximation for the nuclear mean field, $SU(3)$, which is the symmetry group of the harmonic oscillator, emerges as an important symmetry. $SU(3)$ becomes a dynamical symmetry if a quadrupole-quadrupole interaction is added to the mean field. It remains useful as an approximate symmetry even if small $SU(3)$ symmetry breaking single-particle or pairing terms are added to the nuclear Hamiltonian. This is due to the dominance of the quadrupole-quadrupole interaction in the mid-shell region.

The Hamiltonian for a particle with mass m in a three dimensional isotropic harmonic oscillator is

$$H_0 = \frac{\mathbf{p^2}}{2m} + \frac{1}{2}m\omega^2\mathbf{r^2} \tag{2.1}$$

In order to reveal its symmetry character we rewrite it in terms of boson creation and annihilation operators $b_i^\dagger = \sqrt{\frac{m\omega}{2\hbar}}(x_i + i\frac{p_i}{m\omega})$ and $b_i = \sqrt{\frac{m\omega}{2\hbar}}(x_i - i\frac{p_i}{m\omega})$ where $b_i^\dagger$ and its hermitian conjugated operator b_i, respectively, increases or reduces the number of oscillator quanta in the i-th direction. With these two operators that satisfy the commutation relations

$$\begin{aligned} \left[b_i, b_j^\dagger\right] &= \delta_{ij} \\ \left[b_i, b_j\right] &= \left[b_i^\dagger, b_j^\dagger\right] = 0, \end{aligned} \tag{2.2}$$

the Hamiltonian for an harmonic oscillator can be written as

$$H_0 = \hbar\omega(\mathbf{b}^\dagger.\mathbf{b} + \frac{3}{2}). \tag{2.3}$$

where

$$A_{ij} = b_i^\dagger b_j \tag{2.4}$$

are the generators of the group $U(3)$ that shift an oscillator quantum from the i-th to the j-th direction. The harmonic oscillator Hamiltonian thus clearly conserves the $SU(3)$ symmetry and basically counts the total number of quanta in the x, y and z direction.

The commutation relations for the $U(3)$ generators introduced in Eq. (2.4) can easily be derived from the ones between the space and momentum coordinates ($\left[x_i, p_j\right] = i\hbar\delta_{ij}$) and are:

$$\left[A_{ij}, A_{kl}\right] = \delta_{jk}A_{li} - \delta_{il}A_{kj} \tag{2.5}$$

The three Casimir operators that exist for $U(3)$ can be expressed by the shift operators as:

$$\begin{aligned} N &= \sum_i A_{ii} \\ C_2 &= \frac{3}{2}\sum_{i,j} A_{ij}A_{ji} \\ C_3 &= \sum_{i,j,k} A_{ij}A_{jk}A_{ki} \end{aligned} \tag{2.6}$$

where the factor 3/2 reflects a common convention. It is easy to show (using the commutation relation given in Eq. (2.2)) that N, C_2 and C_3 commute with all generators as necessary.

Furthermore, the generators of the $U(3)$ Lie algebra given in Eq. (2.4) can be modified to $SU(3)$ generators by removing the trace. This amounts to subtracting the boson number operator

$$A'_{ij} = A_{ij} - \frac{1}{3}\delta_{ij} \tag{2.7}$$

which leaves the physics described in either the $SU(3)$ or $U(3)$ picture unchanged.

Since the total number of quanta is conserved, the $SU(3)$ irreducible representations [16] (or simply irreps) only depend on the relative difference in the number of quanta along the three axes and only two quantum numbers are necessary to classify these. Usually, they are given by the so-called highest weight state characterized by a maximum number of quanta along the z-axis and the maximum of the remainder along the x-axis as:

$$\begin{aligned} \lambda &= n_z - n_x \\ \mu &= n_x - n_y \end{aligned} \tag{2.8}$$

In the special case of a single particle in the η-th shell the $SU(3)$ irrep is thus given by $(\lambda, \mu) = (\eta, 0)$.

Different options exist for a further classification of the $SU(3)$ irreps (λ, μ) with the sublabels depending on the choice of subgroups. For applications in the shell model which use the $SU(3)$ symmetry it is convenient to make use of the rotational invariance of the system by selecting $SO(3)$ as a subgroup. To do so, a set of $SU(3)$ generators that transform as rotational tensors should be chosen. They can be expressed by the $U(3)$ generators A_{ij} introduced in Eq. (2.4) that correspond to a cartesian scheme and shift oscillator quanta in the x, y or z direction, as:

$$\begin{aligned} L_{10} &= i(A_{32} - A_{23}), \\ L_{1\pm1} &= -\frac{1}{\sqrt{2}}(A_{12} - A_{21} \pm i(A_{31} - A_{13})), \\ Q^a_{20} &= 2A_{11} - A_{22} - A_{33}, \\ Q_{2\pm1} &= \sqrt{\frac{3}{2}}(A_{12} - A_{21} \pm i(A_{13} + A_{31})), \\ Q_{2\pm2} &= \sqrt{\frac{3}{2}}(A_{22} - A_{33} \pm i(A_{23} + A_{32})) \end{aligned} \tag{2.9}$$

This set of $SU(3)$ generators consists of the three components of the angular momentum operator L_i and the five components of the algebraic quadrupole operator $Q^a_{2\mu}$. The algebraic quadrupole operator has angular momentum 2 and can be expressed in cartesian coordinates as:

$$Q^a_{2\mu} = \sqrt{\frac{4\pi}{5r_0^4}}(r^2 Y_{2\mu}((\mathbf{r})) + r_0^4 p^2 Y_{2\mu}(\mathbf{p})), \quad \mu = -2, -1, 0, 1, 2. \tag{2.10}$$

The $SU(3)$ generators from Eq. (2.9) satisfy the following commutation relations:

$$\begin{aligned} \left[L_{1\mu}, L_{1\nu}\right] &= -\sqrt{2}\,\langle 1\mu, 1\nu|1\mu+\nu\rangle\, L_{1\mu+\nu}, \\ \left[L_{1\mu}, Q^a_{2\nu}\right] &= -\sqrt{6}\,\langle 1\mu, 2\nu|2\mu+\nu\rangle\, Q^a_{2\mu+\nu}, \\ \left[Q^a_{2\mu}, Q^a_{2\nu}\right] &= 3\sqrt{10}\,\langle 2\mu, 2\nu|1\mu+\nu\rangle\, L_{1\mu+\nu}, \end{aligned} \tag{2.11}$$

where $\langle l_1 m_1, l_2, m_2|l_3, m_3\rangle$ is the usual notation for a Clebsch-Gordan coefficient.

This choice of $SU(3)$ generators, using the three components of the angular momentum, makes clear that $SO(3)$ is a subgroup of $SU(3)$. A classification scheme for the spatial part of harmonic oscillator states is thus given by the group chain $SU(3) \supset SO(3) \supset SO(2)$ where $SO(2)$ is the group of rotations around one axis that gives the m projection quantum number.

From the solutions of the harmonic oscillator it is known that in the single-particle case the allowed angular momenta within the η-th shell are given by:

$$L = \eta, \eta - 2, ...1 \quad \text{or} \quad 0 \tag{2.12}$$

reflecting the fact that all states within a fixed shell have the same parity $P = (-1)^\eta$.

In the many-particle case, where the $SU(3)$ irrep (λ, μ) is not restricted to $(\eta, 0)$, the total angular momentum is given by a generalization of the rule above [3]:

$$L = \lambda + \mu, \lambda + \mu - 2, ..., 1 \quad \text{or} \quad 0 \tag{2.13}$$

for $K = 0$ and

$$L = k, k+1, k+2, ..., \lambda + \mu - k \tag{2.14}$$

for $K \neq 0$ where K is given by

$$K = \min(\lambda, \mu), \min(\lambda, \mu) - 2, ..., 1 \quad or \quad 0 \tag{2.15}$$

The quantum number K (sometimes called Elliott "K" quantum number) reflects the fact that in this classification scheme multiple occurrences of L are possible within a certain $SU(3)$ irrep (λ, μ). This label also has a physical interpretation that will be discussed in a later section.

Alternatively, a multiplicity label κ can be introduced to distinguish between multiple occurrences of an angular momentum L. It runs from 0 to k_{max} with the value of k_{max} given by

$$k_{max} = \left[\frac{\lambda + \mu + 2 - L}{2}\right] - \left[\frac{\lambda + 1 - L}{2}\right] - \left[\frac{\mu + 1 - L}{2}\right] \tag{2.16}$$

Here, $\left[...\right]$ is the notation for the greatest integer (or Gauss) function.

A harmonic oscillator eigenstate can thus be labeled by the two $SU(3)$ quantum numbers λ, μ plus the three additional sublabels L, m_L and κ.

2.2 Basics and Advantages of the $SU(3)$ Model

In the late fifties, Elliott developed an algebraic theory that is able to describe collective phenomena and treats the nucleus as a many-particle fermionic system. It invokes special group symmetries associated with collective behavior in an attempt to achieve a tractable microscopic description of nuclear phenomena. The Elliott or $SU(3)$ shell model [3] uses the three-dimensional isotropic oscillator as an approximation for the nuclear mean field and makes use of the associated symmetry group $SU(3)$ for the classification of the many-particle states and the construction of the Hamiltonian. An important feature of the model which allows for a geometric interpretation of the $SU(3)$ eigenstates is its relation to the rotor picture. Thus it succeeds in bridging the gap between collective and single-particle theories .

It is expected that any microscopic description of nuclei in terms of fermion degrees of freedom will result in large dimensionalities of the many-particle configuration space. A basic assumption usually used that greatly reduces the size of the model space is that only particles in an open (so called valence) shell have to be considered for the many-particle wave function. So, the filled shells are treated as an inert spherical core. They have no direct effect on the nuclear properties, thus allowing one to truncate significantly the configuration space.

It may turn out that this truncation is not enough and even the configuration space restricted to one oscillator shell η for which $n = (\eta + 1)(\eta + 2)/2$ levels are available, remains large with a binomial growth of the dimension that for m fermions in n levels is approximately given by n^m. For many realistic applications this growth prohibits or severely slows down calculations even on today's computers. Group theoretical methods provide an elegant solution for this dillema by making use of symmetry properties of the Hamiltonian. A crucial ingredient is the construction of a realistic nuclear Hamiltonian using the generators of a specific group. For a symmetry-adapted basis, no mixing between the basis vectors belonging to a fixed group irrep occurs if the Hamiltonian describes a system with exact or dynamical symmmetry. An appropriate choice of a subspace can then be made which will lead to a drastic reduction of the configuration space.

For the Elliott model, this is achieved by introducing a nuclear Hamiltonian with $SU(3)$ symmetry, the symmetry group of the unitary transformations in an oscillator shell. As is already known from the single-particle shell model, the harmonic oscillator can be used as an approximation for the nuclear mean field of a realistic Hamiltonian. However, additional terms are necessary that have to conserve the $SU(3)$ symmetry but at the same time be able to produce an energy spectrum specific to the systems we would like to be able to describe like a typical rotational spectrum.

The key piece of the $SU(3)$ Hamiltonian which can do this and that was introduced by Elliott is the algebraic quadrupole operator

$$Q^a_{2\mu} = \sqrt{\frac{4\pi}{5b^2}}\big((\frac{r_s^2}{b^2}Y_{2\mu}(\mathbf{r_s}) + b^2 p_s^2 Y_{2\mu}(\mathbf{p_s})\big) \quad (b = \sqrt{\frac{\hbar}{m\omega}}). \tag{2.17}$$

Elliott first realized the advantage of using the algebraic quadrupole operator instead

of the usual collective quadrupole operator

$$Q^c_{2\mu} = \sqrt{\frac{16\pi}{5}} \frac{r_s^2}{b^2} Y_{2\mu}(\mathbf{r_s}) \tag{2.18}$$

which lies in the fact that the five components of the former one together with the three components of the angular momentum are generators of $SU(3)$, as was discussed in the previous section.

Within a major oscillator shell the matrix elements of Q^c and Q^a are identical, but since Q^c couples states belonging to the η-th shell with those of the η'-th shell that differs by two quanta, $\eta = \eta \pm 2$, it introduces a mixing between these shells. For small and medium deformations however, the effect of both operators is comparable.

It can be shown [17] that the long-range part of the nucleon-nucleon interaction is given by the quadrupole-quadrupole interaction and it is an important part of any realistic nuclear Hamiltonian. For the description of the well-deformed nuclei away from the magic numbers the quadrupole-quadrupole term is essential and will to a great extent determine the dynamics of the system.

The rotationally invariant quadrupole-quadrupole operator $Q^a.Q^a$ is thus diagonal in a $SU(3)$ basis with its eigenvalues $E_{Q^a.Q^a}$ given by

$$E_{Q^a.Q^a} = 4C_2 - 3L(L+1), \tag{2.19}$$

where L is the angular momentum and C_2 is the second degree Casimir operator of $SU(3)$ which has an expectation value given by

$$\langle (\lambda,\mu)|C_2|(\lambda,\mu)\rangle = (\lambda+\mu)(\lambda+\mu+3) - \lambda\mu. \tag{2.20}$$

The L^2 dependence of the $Q^a.Q^a$ eigenvalue allows one to reproduce a rotational spectrum with a $SU(3)$ conserving Hamiltonian that is constructed using the harmonic oscillator potential plus the quadrupole-quadrupole interaction:

$$H_{SU(3)} = H_{osc} - \frac{\chi}{2} Q^a.Q^a. \tag{2.21}$$

Thus, the simplest version of the $SU(3)$ model Hamiltonian is able to describe a collective feature that is not included in the single-particle model. It can also account for another important collective feature, namely, the enhanced E2 transitions between members of identical bands.

As was mentioned earlier, the large dimensionality of the configuration space for many-particle wave functions makes an effective truncation scheme essential for practical applications. The structure of the $Q^a.Q^a$ eigenvalue provides a natural choice for this truncation scheme. Because of its C_2 dependence, the rotational band with lowest energy can be associated with the $SU(3)$ band that has the largest C_2 value possible for a given particle configuration. This so-called leading irrep with a few additional $SU(3)$ irreps that come next in an ordering scheme according to the value of C_2 are sufficient to describe the low-energy spectrum of a well-deformed nucleus. This simple truncation scheme yields a dramatic reduction of

the configuration space. In later sections we will introduce some more elaborate choices of truncation schemes in the cases when two types of particles are involved in constructing the basis states and when various spatial configurations or relatively strong mixing terms are involved.

Proton-neutron wave functions may be built using two approaches depending on whether we deal with light or heavy nuclei. Since for light nuclei the protons and neutrons share the same single-particle levels, the isospin degree of freedom is introduced with the protons and neutrons treated as different states of an isospin 1/2 doublet. Thus, the total number of states within an oscillator shell is $N = 4\Omega$ (where $\Omega = \frac{(\eta+1)(\eta+2)}{2}$ is the spatial dimension of the η-th oscillator shell and the factor 4 comes from the spin-isospin part). In case of heavy nuclei, for each type of particles we have $N = 2\Omega$ states. According to the Pauli principle, an m-particle wavefunction must transform like the totally antisymmetric representation $[f^m] = [1^m]$ of $U(k\Omega)$ (where k=2 or k=4).

A classification of the m-particle wave function into irreps of the unitary group in N dimensions $U(N)$ simultaneously specifies the irrep of the permutation group on m objects (S_m) to which each of the m-particle wavefunctions belongs [18]. This $U(N)$ and S_m correspondence means that it is sufficient to give further consideration to only one of the two, a result that applies to bosonic as well as fermionic schemes. In most cases, the focus moves on the group $U(N)$ because it is simpler to deal with. The irreps of $U(N)$ are labeled by the symbol $\big[f\big] = \big[f_1, f_2, ..., f_N\big]$ which has a simple pictorial representation called a Young diagram consisting of placing f_1 boxes directly adjacent to each other in a horizontal row, with $f_2 < f_1$ boxes left justified in a second row below and adjacent to the first set, etc. As each box corresponds to one particle, $\sum_i f_i = m$ for an m-particle configuration.

Since $N = k\Omega$, an m-particle fermionic wavefunction belongs to the antisymmetric irrep of the unitary group in $k\Omega$ dimensions, $U(k\Omega)$, which also means that it belongs to the antisymmetric irrep of the permutation group. For m particles, this antisymmetric irrep is the one with all the f_i's equal to 1, $\big[f\big] = \big[1, 1, ..., 1\big] \equiv \big[1^m\big]$. However, the full shell model space can be further partitioned into space and spin, or space and spin-isospin parts, with spatial dimensionality Ω. When this is done, each part can have any allowed m-particle symmetry, so long as its complement has the conjugate symmetry to insure that the product remains totally antisymmetric under particle permutation. The unitary symmetries associated with a factorization of the valence space into a direct product of two are denoted as $U(k\Omega) \supset U(\Omega) \times U(k)$ where $k = 2$ for the spin and $k = 4$ for the spin-isospin cases. Overall antisymmetry in $U(k\Omega)$ requires that the $U(k)$ irrep be conjugate to the irrep of $U(\Omega)$. So, the $\big[f\big]$ irrep of $U(\Omega)$ and the conjugate irrep $\big[f^c\big]$ of $U(k)$ are related to one-another by row-column interchange.

The spatial part of the wavefunction may be further classified according to the group chain $U(\Omega) \supset SU(3)$, thus making use of the $SU(3)$ symmetry of the Hamiltonian. Here, a multiplicity label α has to be introduced in order to distinguish between multiple occurrences of a $SU(3)$ irrep (λ, μ) in a $U(\Omega)$ irrep $[f]$. Next, the spatial part can be further classified by the $SU(3) \supset SO(3)$ subchain, a reduction

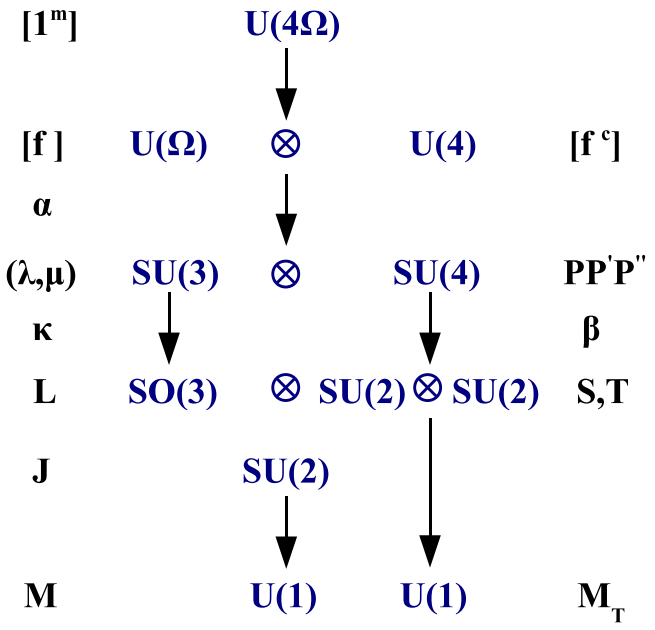

Figure 2.1: Decomposition of the $U(4\Omega)$ space in light ($A \leq 28$) nuclei. The associated irrep labels for the spatial symmetries are given on the left, and those for the intrinsic spin-isospin ones on the right.

we discussed earlier (see section 2.1) where we also introduced the multiplicity label κ.

The unitary group $U(k)$ - corresponding to the intrinsic part of the wave function - can be reduced similarly: $U(2) \supset SU(3) \supset SU_S(2)$ for identical particles, where the spin S, which labels the $SU(2)$ irrep, is fixed once $[f^c]$ is specified, since $S = (f_1^c - f_2^c)/2$. In the spin-isospin formalism, one has the reduction $U(4) \supset SU_S(2) \otimes SU_T(2)$, which yields quantum numbers βST, where S and T denote spin and isospin and β gives the multiplicity of (ST) in the $U(4)$ irrep $[f^c]$.

This way we can construct m-particle states

$$\big|m\big[f\big]\alpha(\lambda,\mu)\kappa L, S; JM\big\rangle \tag{2.22}$$

for an identical-particle system, and

$$\big|m\big[f\big]\alpha(\lambda,\mu)\kappa L, \beta(ST)JM, M_T\big\rangle \tag{2.23}$$

in the spin-isospin formalism. The quantum numbers that identify the irrep of $U(k)$ are suppressed in the last two equations since they are fixed by the labels $[f]$ of $U(\Omega)$ and the requirement of overall antisymmetry. Basis states for light nuclei ($A \leq 28$) are of the form (2.23). The full group decomposition in this case is shown in Fig. 2.1.

For heavy nuclei, where protons and neutrons occupy different shells, the totally antisymmetric wave functions for protons and neutrons, each having the form

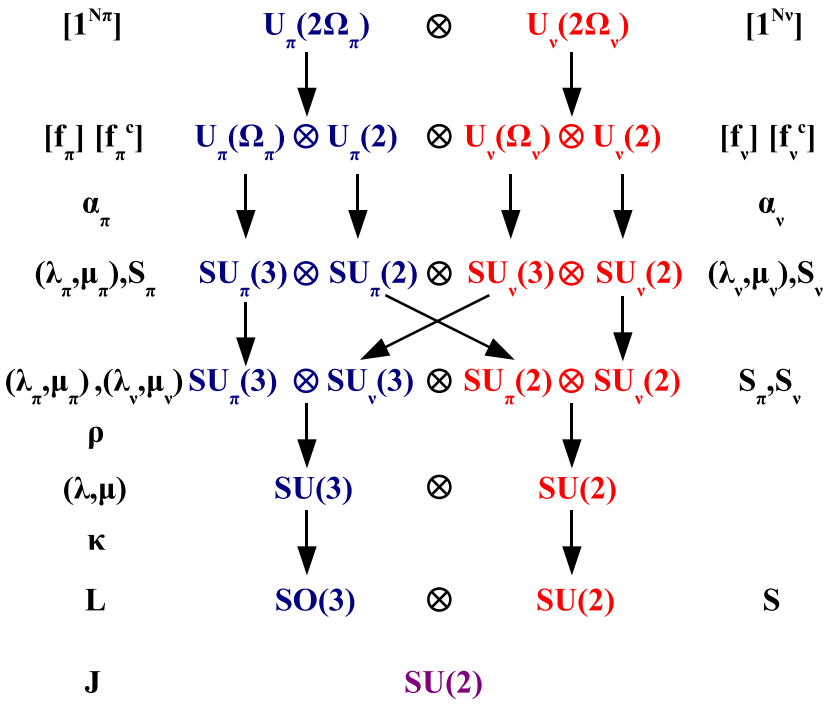

Figure 2.2: Proton-neutron decomposition in heavy nuclei. The associated irrep labels on the left are for the protons, and those for the neutrons - on the right.

given in Eq. (2.22) must be coupled to a total wavefunction, where the coupling may be done on different levels. We may have states in $J_\pi - J_\nu$ coupled ($SU(3)$ uncoupled) scheme

$$|\{N_\pi[f_\pi]\alpha_\pi(\lambda_\pi,\mu_\pi)\kappa_\pi L_\pi,[f_\pi^c]S_\pi;J_\pi\}\{N_\nu[f_\nu]\alpha_\nu(\lambda_\nu,\mu_\nu)\kappa_\nu L_\nu[f_\nu^c]S_\nu;J_\nu\}JM\rangle\,, \quad (2.24)$$

or in a $SU(3)$ coupled scheme

$$|\{N_\pi[f_\pi]\alpha_\pi(\lambda_\pi,\mu_\pi),N_\nu[f_\nu]\alpha_\nu(\lambda_\nu,\mu_\nu\}\rho(\lambda,\mu)\kappa L,\{[f_\pi^c]S_\pi,[f_\nu^c]S_\nu\}S;JM\rangle\,. \quad (2.25)$$

The group decomposition corresponding to the $SU(3)$-coupled scheme is given in Fig. 2.2.

The choice of scheme to use depends on the dynamics generated by the Hamiltonian. If the residual proton-neutron interaction reenforces the deformation generated in the separate proton and neutron spaces, then the $SU(3)$-coupled scheme is appropriate to use. The JJ-coupled scheme would be appropriate when the residual interaction favors strong pairing correlations.

2.2.1 Coupling of Two $SU(3)$ Irreps

As will be explained in more detail later, in order to obtain the state (2.25) we have to perform a unitary transformation between the uncoupled proton and neutron basis

states (2.22) and this coupled state. The elements of this transformation are the Wigner coefficients (see Appendix A). The outer multiplicity label $\rho = 1, 2, ..., \rho_{\max}$ in (2.25) (where $\rho_{\max}$ denotes the number of possible couplings) can be thought of as labeling different relative orientations of the proton (λ_π, μ_π) and neutron (λ_ν, μ_ν) shapes that give rise to the same final proton-neutron shape (λ, μ) [19]. The possible (λ, μ) irreps in the final product can be obtained by coupling the appropriate Young diagrams which we briefly mentioned earlier.

The standard procedure for decomposing a product of two $SU(3)$ representations into its irreducible parts [1] is to apply the Littlewood rules for the coupling of two two-rowed Young diagrams [20]. In order to probe quantitatively the allowed $SU(3)$ product configurations, we can express this "prescription" in mathematical terms by introducing new quantum numbers mimicking the construction process of a $SU(3)$ product irrep through the Littlewood rules. These rules can be summarized in the following way:

- Step 1 - Compose the Young diagrams for each of the two representations;
- Step 2 - Mark in the second diagram all the boxes in the first row an "a", the ones in the second row with a "b", etc.
- Step 3 - Add all the boxes marked with an "a" to the right-hand ends of the first diagram having in mind the following restrictions:

  (a) there must be never more than two or more boxes marked with an "a" in the same column;

  (b) the diagram must remain regular which means that no row contains less elements than the row beneath.
- Step 4 - Repeat the same procedure for those boxes marked with a "b" keeping in mind the following additional restrictions:

  (a) reading from right to left, the number of boxes marked with a "b" does not become larger than the ones marked with an "a";

  (b) diagrams with more than N rows are prohibited for the case of an $U(N)$ symmetry;
- Step 5 - Repeat step 4 for all additional rows of the second factor.

For instance, using these rules for the representations $(\lambda_1, \mu_1) = (1, 1)$ and $(\lambda_2, \mu_2) = (1, 1)$ results in 6 coupled irreps - (2,2), (3,0), (0,3), (1,1) (appearing twice) and (0,0).

Alternatively, we may follow a slightly different approach. For reasons of simplicity it is useful to start with the leading $SU(3)$ representation given by

$$(\lambda_\pi, \mu_\pi) \otimes (\lambda_\nu, \mu_\nu) \rightarrow (\lambda, \mu) = (\lambda_\pi + \lambda_\nu, \mu_\pi + \mu_\nu). \tag{2.26}$$

[1] The unimodular group $SU(3)$ is obtained from $U(3)$ by removing those transformations which simply introduce an overall change of phase. As a consequence, those representations of $SU(3)$ which correspond to diagrams differing only in the number of complete columns become equivalent.

The corresponding Young diagram consists of $\lambda_\pi + \mu_\pi + \lambda_\nu + \mu_\nu$ boxes in the first and $\mu_\pi + \mu_\nu$ boxes in the second row. Any other representation can only be obtained by removing a certain number of boxes, m, from the first row and distributing them to the second and third row, respectively. If n denotes the number of boxes added to the second row, the Young diagram assumes the following structure:

$$\begin{array}{lll} \text{first row:} & \lambda_\pi + \lambda_\nu + \mu_\pi + \mu_\nu - m & \text{boxes,} \\ \text{second row:} & \mu_\pi + \mu_\nu & \text{boxes,} \\ \text{third row:} & m - n & \text{boxes,} \end{array} \tag{2.27}$$

which is equivalent to a

$$(\lambda, \mu) = (\lambda_\pi + \lambda_\nu - m - n, \lambda_\pi + \lambda_\nu + 2n - m) \tag{2.28}$$

representation. Repeating the upper procedure for the second row, with k denoting the number of boxes shifted from the second to the third row, the Young diagram transforms into

$$\begin{array}{lll} \text{first row:} & \lambda_\pi + \lambda_\nu + \mu_\pi + \mu_\nu - m & \text{boxes,} \\ \text{second row:} & \mu_\pi + \mu_\nu + n - k & \text{boxes,} \\ \text{third row:} & m - (n - k) & \text{boxes.} \end{array} \tag{2.29}$$

Hence, any possible (λ, μ) configuration is of the form

$$(\lambda, \mu) = (\lambda_\pi + \lambda_\nu - m - (n - k), \mu_\pi + \mu_\nu + 2(n - k) - m). \tag{2.30}$$

Notice that n and k appear only as a difference, i.e. a $SU(3)$ product representation does not distinguish between different combinations of n and k as long as their difference remains constant; possible multiple occurrences of the same value of (n-k) generates cases with multiplicity $\rho > 1$. So, the result for the tensor product is given by

$$\begin{aligned} (\lambda, \mu) &= (\lambda_\pi, \mu_\pi) \otimes (\lambda_\nu, \mu_\nu) \\ &= \bigoplus_{m,n,k} (\lambda_\pi + \lambda_\nu - m - (n - k), \mu_\pi + \mu_\nu + 2(n - k) - m), \end{aligned} \tag{2.31}$$

where, according to the Littlewood rules, the limits for summation over m,n and k are given by

$$\begin{array}{lll} n \geq 0 & m - n \leq \mu_\pi & m + k - 2n \leq \mu_\pi, \\ k \geq 0 & m - n \leq \lambda_\nu & n \leq \lambda_\pi, \\ m \geq n & m - k \leq \lambda_\nu & k \leq \mu_\nu. \end{array} \tag{2.32}$$

2.3 The $SU(3)$ Hamiltonian

An important property of the $SU(3)$ model is its relation to the rotor model. Since the simple $SU(3)$ Hamiltonian (2.21) with quadrupole-quadrupole interaction is

able to reproduce a rotational spectrum where the ground state band is given by a unique $SU(3)$ irrep, such a relation can already be anticipated. It allows for an interpretation of $SU(3)$ irreps in terms of the shape variables β and γ that are commonly used as a measure for the axial and triaxial deformation thus bridging the gap between a microscopic and a macroscopic description of nuclei [21].

It turns out that the Hamiltonian (2.21) is too schematic to reproduce the details of realistic rotational spectra. Specifically, states of a given $SU(3)$ irrep (λ, μ) which have the same angular momentum are degenerate, whereas in experimental spectra one finds individual rotational bands - corresponding to different multiplicity labels κ - which are shifted relatively to each other [22, 23, 24] (a phenomenon referred to as "K-band splitting"). The problem can be resolved if we generalize our Hamiltonian by adding terms that are rotationally invariant and conserve the $U(3)$ symmetry of the system.

2.3.1 The Rotor and $SU(3)$

The rotor has always enjoyed a prominent role in physics. It was also one of the first problems addressed with the quantum methods developed independently by Heisenberg, Born, Jordan [25] and Schrödinger [26]. Casimir [27] established a relationship between the eigenfunctions of the rotor and the irreducible representations of the rotation group in three dimensions clearly demonstrating the advantages of using algebraic techniques over analytic methods when the Hamiltonian possesses a known symmetry.

The dynamics of a quantum rotor found its earliest application in the fields of atomic and molecular physics. With the advent of nuclear structure data showing rotational features, it quickly became a model of choice in nuclear physics as well and it is now commonly applied in the study of nuclei with spectra that show rotational characteristics.

The Hamiltonian of a triaxial rotor H_{ROT} is given by

$$H_{\mathrm{ROT}} = A_x I_x^2 + A_y I_y^2 + A_z I_z^2, \tag{2.33}$$

where the operators I_α^2 ($\alpha = x, y$ and z) are the squares of the projections of the total angular momentum operator I on the α-th axis in the body-fixed frame of reference and $A_\alpha = 1/2\mathcal{J}_\alpha$ is the corresponding inertia parameter. The inertia parameters A_α are usually chosen using the convention $A_y \leq A_x \leq A_z$. An asymmetry parameter κ, related to the inertia ellipsoid and defined by

$$\kappa = \frac{2A_x - A_y - A_z}{A_z - A_y}, \tag{2.34}$$

is commonly used to describe the shape of the rotor: $\kappa = -1$ when $A_x = A_y < A_z$, a prolate shape; $\kappa = +1$ when $A_y < A_x = A_z$, an oblate geometry; and $\kappa = 0$ when $A_x = \frac{A_y + A_z}{2}$, the most asymmetric configuration. For the cases of axial symmmetry, the Hamiltonian is diagonal with eigenvalues

Table 2.1: Classification of the eigenstates of the triaxial rotor according to symmetry classes of the Vierergruppe D_2.

Symmetry	Transformation				Index		Dimension	
type	E	T_1	T_2	T_3	λ	μ	I(even)	I(odd)
A	1	1	1	1	e	e	(I+2)/2	(I-1)/2
B_1	1	1	-1	-1	e	o	I/2	(I+1)/2
B_2	1	-1	1	-1	o	o	I/2	(I+1)/2
B_3	1	-1	-1	1	o	e	I/2	(I+1)/2

$$\begin{aligned} E_{\mathrm{k=-1}} &= A_y I(I+1) + (A_z - A_y)K^2 \qquad \text{for} \quad \mathrm{k=-1} \\ E_{\mathrm{k=+1}} &= A_z I(I+1) + (A_z - A_x)K^2 \qquad \text{for} \quad \mathrm{k=+1}, \end{aligned} \tag{2.35}$$

with K being the eigenvalue of the projection of the angular momentum on the intrinsic z axis. So, in these limiting cases, the spectrum shows a rotational characteristic with $I(I+1)$ spacing for each value of K.

The rotor Hamiltonian is invariant under rotations by an angle of π about the principal axis. This set of transformations, $\{E, T_\alpha\}$ where E is the identity and $T_\alpha = exp(i\pi_\alpha)$, generates the Vierergruppe (D_2). As a consequence the hamiltonian matrix, which has dimension $2I+1$ for angular momentum I, can be brought into block diagonal form with the submatrices labelled by the symmetry classes of D_2, see Table (2.1). A convenient representation for the eigenstates of the general Hamiltonian (2.33) is given by

$$\Psi^{(\lambda\mu)\nu I}_{\mathrm{ROT}\ M} = \sum_{K\geq 0}{}' C^{(\lambda\mu)\nu IK} \Psi^{(\lambda\mu)KI}_{\mathrm{sym}\ \ M}, \tag{2.36}$$

where

$$\Psi^{(\lambda\mu)KI}_{\mathrm{sym}\ \ M} = \Big(\frac{2I+1}{16\pi^2(1+\delta_{K0})}\Big)^{1/2} \big[D^I_{MK} + (-1)^{\lambda+\mu+I} D^I_{M-K}\big]. \tag{2.37}$$

Here, the D^I_{MK} are the standard $SO(3)$ rotation matrices. For the axially symmetric case ($\kappa = -1$) the magnitude of K, which is the eigenvalue of I_3, is a good quantum number but, as indicated, eigenstates of the asymmetric rotor ($\kappa \neq -1$) involve a linear combination of states with different K values. The prime on the summation indicates either all even or all odd values for K. In Eq. (2.37), λ can be even or odd, and μ is even for K even and odd for K odd. The traditional choice replaces the $\lambda + \mu + I$ expression by a single quantity γ and a rather cumbersome rule for assigning it a value. Note how simply λ and μ specify the symmetry class of D_2 to which the eigenstates belong, see Table 2.1.

So, in the cases of both the symmetric and asymmetric rotor, the eigenstates can be labeled by the angular momentum, its third projection along the body-fixed axis K, and M-its third projection on the laboratory-fixed axis. They can be grouped

in bands of a certain K-value, so we have the ground-state band corresponding to $K = 0$, and the other K-bands of odd or even values according to the γ-value ($\gamma = \lambda + \mu + I$).

The collective aspects of the nuclear interaction can be described naturally within the framework of the $SU(3)$ model. The close relation between the rotor and the $SU(3)$ group translates into the ability of a $SU(3)$ symmetry preserving Hamiltonian to describe the rotational spectrum of well-deformed nuclei and also allows one to map $SU(3)$ eigenstates $|(\lambda, \mu)\rangle$ onto shapes parametrized by the deformation parameters β and γ of the quantum rotor [28, 29].

The rotor group $T_5 \wedge SO(3)$ is generated by the five moments of the collective quadrupole operator (see Eq. (2.18)) which coincide with the moments of the corresponding inertia tensor and three components of the angular momentum. The commutation relation between these generators of the semi-direct product of T_5 and $SO(3)$ are:

$$\begin{aligned} \left[L_\mu, L_\nu\right] &= -\sqrt{2}\,\langle 1\mu, 1\nu|1\mu+\nu\rangle\, L_{\mu+\nu}, \\ \left[L_\mu, Q^c_\nu\right] &= -\sqrt{6}\,\langle 1\mu, 2\nu|2\mu+\nu\rangle\, Q^c_{\mu+\nu}, \\ \left[Q^c_\mu, Q^c_\nu\right] &= 0, \end{aligned} \tag{2.38}$$

reflecting the typical structure of a semi-direct product group with two sets of generators, each separately closed under commutation ($\left[T_5, T_5\right] \to T_5$, $\left[SO(3), SO(3)\right] \to SO(3)$) but with the commutator of an element of one group with an element of the other yielding an element of only one of the sets ($\left[T_5, SO(3)\right] \to T_5$). These commutation relations are similar to the ones between the algebraic quadrupole operator, Q^a_μ and the angular momentum, L, that are generators of $SU(3)$, namely,

$$\begin{aligned} \left[L_\mu, L_\nu\right] &= -\sqrt{2}\,\langle 1\mu, 1\nu|1\mu+\nu\rangle\, L_{\mu+\nu}, \\ \left[L_\mu, Q^a_\nu\right] &= -\sqrt{6}\,\langle 1\mu, 2\nu|2\mu+\nu\rangle\, Q^a_{\mu+\nu}, \\ \left[Q^a_\mu, Q^a_\nu\right] &= 3\sqrt{10}\,\langle 2\mu, 2\nu|1\mu+\nu\rangle\, L_{\mu+\nu}, \end{aligned} \tag{2.39}$$

where only the last commutation relation for the quadrupole operators are different, giving zero in the rotor case and non-zero in the $SU(3)$ case.

$SU(3)$ is a compact group with a maximum value for the angular momentum, L, whereas the one for the rotor is noncompact with unbound L. However, the $SU(3)$ algebra contracts to that of the rotor when the angular momentum L is small compared to $(\lambda + \mu)$, which can be seen by rescaling Q^a as $\frac{Q^a}{\sqrt{C_2}}$ [30]. The procedure leaves the first two commutation relations unchanged but implies $[Q^a_\mu, Q^a_\nu] \approx 0$ for $C_2 >> L$ in the $SU(3)$ case. This is equivalent to the statement that the $SU(3)$ model describes rotational states very well as long as

$$L << (\lambda + \mu). \tag{2.40}$$

Since both the rotor and $SU(3)$ theory are describing the same physical phenomena - that is, a rotational spectrum - and their algebras are closely related, it is natural to require a correspondence between the invariants of both groups. The eigenvalues

of the two invariants C_2 and C_3 of the rank two group $SU(3)$ can be expressed by the $SU(3)$ labels (λ, μ) as:

$$\begin{aligned} < C_2 > &= (\lambda+\mu)(\lambda+\mu+3) - \lambda\mu, \\ < C_3 > &= \frac{1}{9}(\lambda-\mu)(\lambda+2\mu+3)(2\lambda+\mu+3). \end{aligned} \tag{2.41}$$

The symmetry group of the rotor $T_5 \wedge SO(3)$, also has two invariants, the traces of the square ($Tr[(Q^c)^2] = \frac{1}{6}Q^c.Q^c$) and cube ($Tr[(Q^c)^3] = -\frac{1}{36}\sqrt{\frac{35}{2}}(Q^c \otimes Q^c \otimes Q^c)^0$) of the collective quadrupole matrix which have the following eigenvalues:

$$\begin{aligned} < Tr[(Q^c)^2] > &= \lambda_1^2 + \lambda_2^2 + \lambda_3^2, \\ < Tr[(Q^c)^3] > &= \lambda_1\lambda_2\lambda_3. \end{aligned} \tag{2.42}$$

Here, the λ_α are the expectation values of the quadrupole matrix in its body-fixed principal axis frame ($Q^c_{\alpha\beta} = \lambda_\alpha \delta_{\alpha\beta}$) that can be parametrized by the shape variables (β, γ) as:

$$\lambda_\alpha = \sqrt{\frac{5}{\pi}}\frac{Ar_0^2}{3}\beta cos(\gamma - \frac{2\pi\alpha}{3}) \qquad\qquad \alpha = 1, 2, 3, \tag{2.43}$$

where A denotes the number of like particles and r_0 is a dimensionless root-mean-square radius.

Requiring a correspondence between the invariants of the two groups, i.e. $C_2 \sim Tr[(Q^c)^2]$ and $C_3 \sim Tr[(Q^c)^3]$, leads to the following relation between the $SU(3)$ labels (λ, μ) and the λ_i's:

$$\begin{aligned} \lambda_1 &= -\frac{1}{3}(\lambda-\mu), \\ \lambda_2 &= -\frac{1}{3}(\lambda+\mu+3), \\ \lambda_3 &= \frac{1}{3}(2\lambda+\mu+3). \end{aligned} \tag{2.44}$$

This set of equations translates into the following relation between the shape variables (β, γ) and the $SU(3)$ irreps (λ, μ):

$$\begin{aligned} \beta^2 &= \frac{4\pi}{5}\frac{1}{(Ar_0^2)^2}(\lambda^2 + \lambda\mu + \mu^2 + 3(\lambda+\mu+1)), \\ \tan\gamma &= \frac{\sqrt{3}(\mu+1)}{2\lambda+\mu+3}. \end{aligned} \tag{2.45}$$

This relation can be interpreted also as a mapping between the labels (λ, μ) and spherical coordinates $(k\beta, \gamma) \leftrightarrow (r, \gamma)$ where the abbreviation $k = \sqrt{5/9\pi}Ar_0$ has been used:

$$\begin{aligned} k\beta\cos\gamma &= k\beta_x = (2\lambda+\mu+3)/3, \\ k\beta\sin\gamma &= k\beta_y = \frac{\mu+1}{\sqrt{3}}. \end{aligned} \tag{2.46}$$

Following these equations, each irrep (λ, μ) corresponds to a unique parametrization in terms of shape by (β, γ). For example, Eq. (2.58) implies that for $\mu = 0$ the deformation parameter γ is close to zero. A $SU(3)$ irrep with $\mu = 0$ thus corresponds to a prolate (cigar-like) shape. For the case $\lambda = \mu$ the $SU(3)$ irrep describes a particle distribution with maximum triaxiality, $\gamma = 30°$. A $SU(3)$ irrep with $\lambda = 0$ corresponds to an oblate (pancake-like) shape with $\gamma = 60°$.

The fermionic nature of the nucleons, a feature that is not included in the collective models, is reflected in the $SU(3)$ model through the values the quantum numbers λ and μ can assume. Each (λ, μ) corresponds to an unique shape parametrized by (β, λ), but the opposite is not always true. While β and γ can vary continuously, the group structure $U(\Omega) \supset SU(3)$ dictates a limited set of allowed (λ, μ) values depending upon the number of nucleons in a shell.

2.3.2 Shell-Model Operator for K-band Splitting

The realization of a shell-model expression for an operator $\mathcal{K}^2$ that produces K-band splitting was an important step in the development of the $SU(3)$ shell model. Since K^2 is the eigenvalue of the special rotor Hamiltonian, namely I_3^2, where I_3^2 is the projection of the total angular momentum on the body-fixed symmetry axis, this result led to a $\mathcal{K}$-operator, and provided analytic expressions for its matrix elements in the Elliott $SU(3) \supset SO(3)$ basis [23, 24]. The eigenvalue of the $\mathcal{K}^2$ operator is exactly K^2 in the limit $L << \min(\lambda, \mu)$, where K is the Elliott K quantum number defined through projection on an intrinsic state of maximum deformation.

To derive the $SU(3)$ model equivalent of the K^2 operator which is necessary for a realistic description of the rotational structure, the relation between the $SU(3)$ algebra and the rotor algebra is used. Ideally, in addition to being a rotational invariant, such a $SU(3)$ model equivalent of K^2 should conserve the $SU(3)$ symmetry of the system. In the case of S=0, by employing a special minimal set of $SO(3)$ scalars, the so-called $SU(3) \rightarrow SO(3)$ integrity basis, which has been shown [31] to contain five operators that give rise to real symmetric matrix forms, the Hamiltonian can be rewritten in a frame-independent expression. The operators can be chosen to be the Casimir invariants L^2, C_2 and C_3, and two non-$SU(3)$ invariant rotational scalars, labeled X_3^a and X_4^a, which are of degree three and four, respectively, in the $SU(3)$ generators:

$$\begin{aligned} X_3^a &= \sum_{i,j} L_i Q_{ij}^a L_j, \\ X_4^a &= \sum_{i,j,k} L_i Q_{ij}^a Q_{jk}^a L_k. \end{aligned} \tag{2.47}$$

Since only the operators X_3^a and X_4^a are able to couple and mix multiple occurrences of a given $SO(3)$ irrep in $SU(3)$, they have to be part of a $SU(3)$ Hamiltonian that is able to reproduce a more complex rotational spectrum. In the most general case, this Hamiltonian has the form

$$H_{SU(3)} = a_1 C_2 + a_2 C_3 + a_3 L^2 + a_4 X_3^a + a_5 X_4^a. \tag{2.48}$$

In order to extract the shell-model equivalent of the K^2 operator from this Hamiltonian, the collective version of the three terms in $H_{SU(3)}$ with an angular momentum dependence has been rewritten, replacing the algebraic quadrupole operator with its collective counterpart that is diagonal in the body-fixed principle axis frame ($Q^c_{\alpha\beta} = \lambda_\alpha \delta_{\alpha\beta}$):

$$\begin{aligned} L^2 &= \sum_i L_i L_i = \sum_i I_i^2, \\ X_3^c &= \sum_{i,j} L_i Q^c_{i,j} L_j = \sum_i \lambda_i I_i^2, \\ X_4^c &= \sum_{i,j,k} L_i Q^c_{i,j} Q^c_{j,k} L_k = \sum_i \lambda_i^2 I_i^2. \end{aligned} \tag{2.49}$$

Here, the notation I and L is used for the angular momentum in the body-fixed and lab-frame, respectively. This set of equations (2.49) can be inverted [23] to yield the following expression for the I_i^2 in terms of L^2 and X^c's:

$$I_i^2 = [(\lambda_1\lambda_2\lambda_3)L^2 + (\lambda_i^2)X_3^c + (\lambda_i)X_4^c)]/D_i, \qquad D_i = 2\lambda_i^3 + \lambda_1\lambda_2\lambda_3. \tag{2.50}$$

Substituting these expressions into the Hamiltonian for an asymmetric rotor

$$H_{\rm ROT} = A_x I_x^2 + A_y I_y^2 + A_z I_z^2, \tag{2.51}$$

gives a frame-independent expression for H_{ROT}, namely,

$$H_{\rm ROT} = aL^2 + bX_3^c + cX_4^c, \tag{2.52}$$

where the parameters a, b and c are given as

$$\begin{aligned} a &= \sum_i \lambda_1\lambda_2\lambda_3 A_i/D_i, \\ b &= \sum_i \lambda_i^2 A_i/D_i, \\ c &= \sum_i \lambda_i A_i/D_i. \end{aligned} \tag{2.53}$$

To derive a $SU(3)$ shell model image of $K^2 = I_3^2$ from this Hamiltonian, the operators X_3^c and X_4^c that couple shells differing by two quanta have to be changed back to their algebraic counterparts that were introduced in Eq. (2.47). As it was shown [21], this substitution does indeed yield a shell-model Hamiltonian that is able to reproduce the rotor results and observed rotational phenomena in nuclei. The algebraic equivalent of H_{ROT} in Eq. (2.52) for the special case $A_x = A_y = 0$ and $A_z = 1$ is thus a natural definition for a shell-model operator K^2

$$K^2 = (\lambda_1\lambda_2 L^2 + \lambda_3 X_3^a + X_4^a)/(2\lambda_3^2 + \lambda_1\lambda_2). \tag{2.54}$$

From the correspondence between the invariants of the rotor group $T_5 \wedge SO(3)$ and $SU(3)$, the parameters λ_i are given as a function of the $SU(3)$ labels λ and μ by

$$\begin{aligned} \lambda_1 &= -\frac{1}{3}(\lambda - \mu), \\ \lambda_2 &= -\frac{1}{3}(\lambda + 2\mu + 3), \\ \lambda_3 &= \frac{1}{3}(2\lambda + \mu + 3). \end{aligned} \tag{2.55}$$

Since the $SU(3)$ irreps are related to the shape of nuclear distribution, this can be seen as a generalization of the rotor Hamiltonian given in Eq. (2.51) where the coefficients are determined by the moments of inertia.

As in the case of rotational spectra generated by the quadrupole-quadrupole operator, the correspondence between the $\mathcal{K}$ operator in the $SU(3)$ and rotor pictures is best for small values of L. This reflects the fact that $SU(3)$ is a compact group with finite-dimensional irreps, while the symmetry group of the rotor is non-compact with infinite-dimensional representations. The K-band splitting was reproduced in the ^{24}Mg and ^{168}Er by applying this theory to only the leading representations of these nuclei [23].

So far, the $\mathcal{K}^2$ operator we talk about, is actually $\mathcal{K}_L^2$, since the total spin considered was $S = 0$, and therefore $J = L$. Following the development of a shell-model operator to describe the K-band splitting in even-even nuclei, a shell-model operator that generates K_J-band splitting in odd-A nuclei was introduced [24]. $K_J = K_L + K_S$ is the projection of the total angular momentum, $J = L + S$, on the principal symmetry axis of the system. The appropriate form for $\mathbf{S} = \mathbf{0}$ states, has to reduce to the algebraic equivalent of $\mathcal{K}_L^2$ for $\mathbf{S} = \mathbf{0}$ in even-A nuclei.

In this case the Hamiltonian of a generalized triaxial rotor is given by Eq. (2.51) where I, ($I^2 = I_x^2 + I_y^2 + I_z^2$) is now the total angular momentum that can be either half-integral or integral.

$$\begin{aligned} J^2 &= \sum_i J_i J_i = \sum_i I_i^2, \\ X_3^c &= \sum_{i,j} J_i Q_{ij}^c J_j = \sum_i \lambda_i I_i^2, \\ X_4^c &= \sum_{i,j,k} J_i Q_{ij}^c Q_{jk}^c J_k = \sum_i \lambda^2 I_i^2. \end{aligned} \tag{2.56}$$

Equations (2.56) can be solved for the I_i's to obtain a frame independent rotor Hamiltonian that in turn gives a frame-independent expression for K_J^2 with the inertia parameters $A_x = A_y = 0$ and $A_z = 1$:

$$K_J^2 = [(\lambda_1\lambda_2 J^2 + \lambda_3 X_3^c + X_4^c)]/(2\lambda_3^2 + \lambda_1\lambda_2). \tag{2.57}$$

Replacing X_3^c and X_4^c with their algebraic counterparts-for which the algebraic quadrupole operator $Q_{\alpha\beta}^a$ is used instead of its collective version - is then a natural definition for a $SU(3)$ shell-model image of K_J^2.

For the evaluation of the matrix elements of the X_3^a and X_4^a operators and therefore of K_J^2 in the angular-momentum projected spin-coupled basis of the $SU(3)$ scheme [24],

$$|\gamma(\lambda,\mu)\kappa LSJM_J\rangle \qquad \text{with} \quad \gamma = N[f]\alpha[f^c]\beta TM_T, \tag{2.58}$$

it is useful to express these operators in a tensor notation:

$$X_3^a = \sum_{\alpha\beta} J_\alpha Q_{\alpha\beta} J_\beta = \frac{1}{6}\sqrt{30}[[J\otimes Q]^1\otimes J]^0, \tag{2.59}$$

and

$$X_4^a = \sum_{\alpha\beta\gamma} J_\alpha Q_{\alpha\beta} Q_{\beta\gamma} J_\gamma = -\frac{5}{18}\sqrt{3}[[J\otimes Q]^1\otimes [J\otimes Q]^1]^0. \tag{2.60}$$

Since the reduced matrix elements of Q^a are known, the reduced matrix elements for $[[J\otimes Q]^1\otimes J]^0$ and $[[J\otimes Q]^1\otimes [J\otimes Q]^1]^0$ (with $k=1$ for X_4^a) and therefore of X_3^a and X_4^a, which are diagonal in all but κ and L, can be evaluated using

$$\begin{aligned}&\langle\gamma(\lambda,\mu)\kappa LSJ\|X_3^a\|\gamma(\lambda,\mu)\kappa' L'SJ\rangle = \\ &\sqrt{\frac{5}{6}}J(J+1)\sqrt{2J+1}W(J1J1;J2)\langle(\lambda,\mu)\kappa LSJ\|Q^a\|(\lambda,\mu)\kappa' L'SJ\rangle,\end{aligned} \tag{2.61}$$

and

$$\begin{aligned}&\langle\gamma(\lambda,\mu)\kappa LSJ\|X_4^a\|\gamma(\lambda,\mu)\kappa' L'SJ\rangle = \\ &\frac{5}{6}J(J+1)\sqrt{2J+1}\sum_{\kappa'' L'' J''}(-1)^{J-J''}W(J1J1;J2)^2 \\ &\langle(\lambda,\mu)\kappa LSJ\|Q^a\|(\lambda,\mu)\kappa'' L''SJ\rangle\langle(\lambda,\mu)\kappa'' L''SJ\|Q^a\|(\lambda,\mu)\kappa' L'SJ\rangle,\end{aligned} \tag{2.62}$$

where the reduced matrix elements for Q^a, which has $SU(3)$ tensor character $(\lambda_0,\mu_0)\kappa_0 L_0 = (1,1)12$ is given by

$$\begin{aligned}&\langle(\lambda,\mu)\kappa LSJ\|Q^a\|(\lambda,\mu)\kappa' L'SJ'\rangle = \\ &(-1)^\phi 2\sqrt{C_2(\lambda,\mu)(2J'+1)(2J+1)}W(SJ'L2;L'J) \\ &\langle(\lambda,\mu)\kappa' L';(1,1)12\|(\lambda,\mu)\kappa L\rangle_{\rho=1}.\end{aligned} \tag{2.63}$$

Here, the W(...) is an SU(2) Racah coefficient and $\langle(\lambda,\mu)\kappa' L';(1,1)12\|(\lambda,\mu)\kappa L\rangle_{\rho=1}$ denotes a reduced $SU(3)\supset SO(3)$ coupling coefficient. The phase factor, $(-1)^\phi = -1$ if $\mu\neq 0$ and $+1$ if $\mu = 0$, is required for consistency with the definition of $SU(3)$ coupling coefficients [32, 33]. The matrix elements for K_J^2 reduce to those of the simpler K_L^2 operator in the $S=0$ configurations.

Eigenvalues of the $\mathcal{K}_J^2$ operator determined in the leading normal (or pseudo) $SU(3)$ irrep were calculated for ^{25}Mg $[(\lambda,\mu)=(9,3), S=\frac{1}{2}]$ and two heavy nuclei - ^{159}Dy $[(\lambda,\mu)=(28,6), S=\frac{1}{2}]$ and ^{165}Er $[(\lambda,\mu)=(29,8), S=\frac{1}{2}]$ [24]. The results show (see Fig. 2.3) that for low-J values in each band the calculated eigenvalues are almost equal to the collective-model values: $(\frac{1}{2})^2$, $(\frac{3}{2})^2$, $(\frac{5}{2})^2$, etc. It is also seen that the values for higher K_J's fall off from the expected rotor values with the fall off being more pronounced the higher the K_J and J. Due to the bigger dimensionality of the irrep though (determined by $d(\lambda,\mu)=\frac{(\lambda+\mu+2)(\lambda+1)(\mu+1)}{2}$), the fall off is not as sharp as in the case of light nuclei like ^{25}Mg.

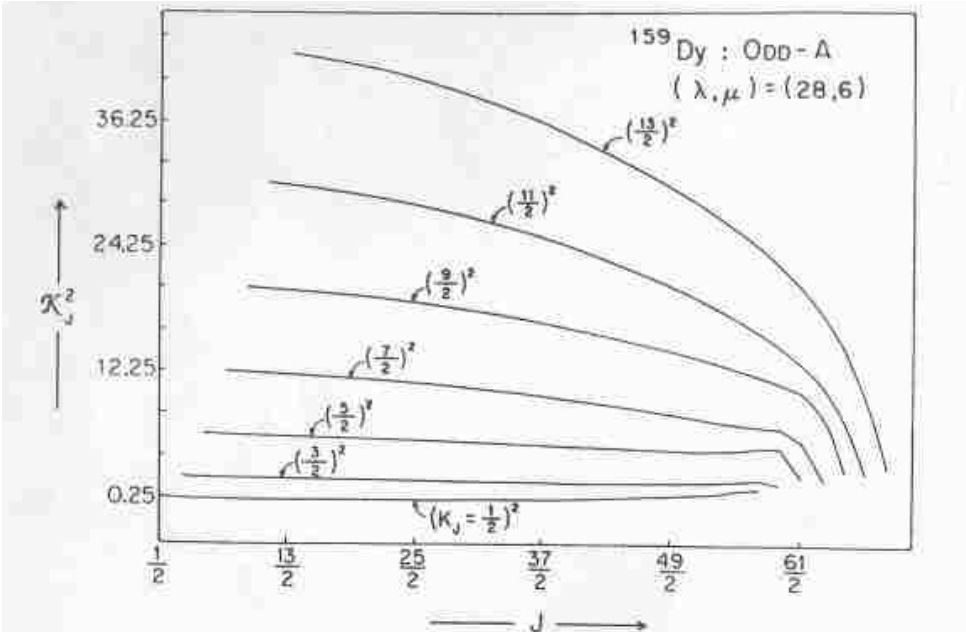

Figure 2.3: Eigenvalues of the $\mathcal{K}_J{}^2$ operator for the leading pseudo-$SU(3)$ representation of the rare-earth nucleus ^{159}Dy, namely, $(\lambda, \mu) = (28, 6)$ (Taken from [24]).

2.4 More Realistic Hamiltonians - Addition of Symmetry-Breaking Terms

Since for real nuclei $SU(3)$ is only an approximate symmetry, we need a more realistic Hamiltonian than the one we discussed so far. Symmetry-breaking parts, like single-particle energies and pairing interaction terms, that are one- and two-body interactions, respectively, should be added. The modification of the Hamiltonian is possible since the $SU(3)$ model is a many-particle theory able to account for single-particle degrees of freedom even though these terms do not appear naturally in the $SU(3)$ formalism. In this section, the matrix elements for single-particle energies and the pairing interactions will be given in the framework of the $SU(3)$ model.

The importance of the spin-orbit and orbit-orbit terms has been demonstrated through the success of the single-particle shell model. Moreover, the observation that the last unpaired nucleon determines the spin of the nucleus reflects on the importance of the pairing interaction which lowers the energy of nucleon pairs coupled to total angular momentum zero. The pairing-plus-quadrupole model [34] has been used to simulate both few-particle non-collective and many-particle collective features in nuclei [35]. The addition of this two-body interaction is thus an important step towards a more realistic Hamiltonian. Pairing correlations are normally attributed to the short-range part of the nucleon-nucleon interaction. Since the spatial overlap of two-nucleon densities is at its maximum if the nucleons have the same l and $|m|$ value, this configuration is energetically favored by a short-range attractive interaction.

Experimentally, an energy gap of about 1 MeV can be seen in the spectrum of even-even nuclei that are just a few nucleons away from a closed shell. This observation is important and gives an estimate for the strength of the pairing interaction. The "pairing gap" occurs between the $J^\pi = 0$ ground state and a set of nearly degenerate states ($J^+ = 2^+, 4^+, 6^+...$) and corresponds to the energy necessary to break apart a nucleon pair.

A realistic Hamiltonian that accounts for single-particle effects as well as collective properties is given by the expression

$$H = -\frac{\chi}{2} Q.Q + G_\pi H_P^\pi + G_\nu H_P^\nu + \sum_{i,\sigma=\pi,\nu} (D_\sigma l_{i\sigma}^2 + C_\sigma l_{i\sigma}.s_{i\sigma}) + aK_J^2 + bJ^2, \quad (2.64)$$

where i runs over all particles in the shell. The spin-orbit force breaks both the $SU(3)$ symmetry and (by mixing different spins) the $U(3)$ symmetry of the system. It tends to keep a nucleus from realizing its maximum deformation, that is, it drives the system towards smaller $k\beta$ values while not affecting the γ-deformation significantly. A strong spin-orbit succeeds in softening the $k\beta$ and γ deformations to the point where a shape can no longer be defined [36].

A general one-body operator that acts symmetrically on a system of identical particles is given by the expression

$$\mathcal{F} = \sum_s f(\mathbf{r_s}, \sigma_\mathbf{s}), \quad (2.65)$$

where $\mathbf{r_s}$ and $\sigma_\mathbf{s}$ represent the position and the spin coordinates of the s-th particle. The one-body operator takes the following form in the second quantization formalism:

$$\mathcal{F} = \sum_{\rho,\rho'} \langle \rho' | f(\mathbf{r_s}, \sigma_\mathbf{s}) | \rho \rangle a_{\rho'}^\dagger a_\rho. \quad (2.66)$$

In this formalism, a fermion creation operator $a_\rho^\dagger$ is defined by its action on a vacuum state $|0\rangle$ which results in the single-particle state $|\rho\rangle$

$$a_\rho^\dagger |0\rangle = |\rho\rangle , \quad (2.67)$$

and the conjugate operator a_ρ annihilates a particle. Its action on the single-particle state gives the vacuum state

$$a_\rho |\rho\rangle = |0\rangle . \quad (2.68)$$

The set of anti-commutation relations for the fermion creation and annihilation operators ($a_\rho^\dagger$ and a_ρ) requires that a many-particle fermionic wavefunction must be totally antisymmetric,

$$\begin{aligned} \{a_\rho^\dagger, a_{\rho'}\} &= a_\rho^\dagger a_{\rho'} + a_{\rho'} a_\rho^\dagger = \delta_{\rho,\rho'}, \\ \{a_\rho^\dagger, a_{\rho'}^\dagger\} &= \{a_\rho, a_{\rho'}\} = 0. \end{aligned} \quad (2.69)$$

For a proton in the η-th shell, for example, the abbreviation $|\rho\rangle$ corresponds to the state $\left|(\eta, 0), l, m_l, \frac{1}{2}, m_s, \pi\right\rangle$ if the $SU(3) \supset SO(3)$ group chain is used and angular

momentum and spin are not coupled. Here, the single-particle $SU(3)$ irrep label $(\lambda,\mu) = (\eta,0)$ is used in place of the principal quantum number. This is done to stress the fact that the single-particle creation operator is an $(\eta,0)$ irreducible tensor of $SU(3)$. The corresponding annihilation operator transforms according to the conjugate representation $(0,\eta)$. The annihilation operator introduced above is not a proper $SU(3)$ tensor, but an operator $\tilde{a}_\gamma$ that has good $SU(3)$ transformation behavior under $SU(3)$ only differs from a_γ by a phase factor [37]:

$$\tilde{a}_\rho = \tilde{a}_{(0,\eta)l,m_l,\frac{1}{2},m_s} = (-1)^{\eta+l+m+\frac{1}{2}+m_s} a_{(\eta,0)l,-m_l,\frac{1}{2},-m_s}. \tag{2.70}$$

Let us introduce a one-body unit tensor, which according with the general formula for coupling $SU(3)$ tensor operators (see (C.5) from Appendix C) is simply a tensor product of $SU(3)$ creation and annihilation operators,

$${}^{(1,1)}\mathcal{F}^{(\lambda,\mu)\kappa LM_L SM_S}_{(\eta',0)(0,\eta)\frac{1}{2}\frac{1}{2}} = \big[a^\dagger_{(\eta',0)\frac{1}{2}} \otimes \tilde{a}_{(0,\eta)\frac{1}{2}}\big]^{(\lambda,\mu)\kappa LM_L SM_S}. \tag{2.71}$$

We may also write it in an ls coupled form

$$\begin{aligned} \mathcal{U}^{(\lambda\lambda)LSJ}_{\eta\eta'} &\equiv {}^{(1,1)}\mathcal{U}^{(\lambda,\mu)\kappa LSJM_J}_{(\eta',0)(0,\eta)\frac{1}{2}\frac{1}{2}} = [a^\dagger_{(\eta',0);\frac{1}{2}} \otimes \tilde{a}_{(0,\eta);\frac{1}{2}}]^{(\lambda,\mu)\kappa LSJM_J} \\ &= \sum_{M_L M_S} \langle LM_L, SM_S|JM\rangle\, [a^\dagger_{(\eta,0);\frac{1}{2}} \otimes \tilde{a}_{(0,\eta);\frac{1}{2}}]^{(\lambda,\mu)\kappa LM_L SM_S} \end{aligned} \tag{2.72}$$

which (when $\mathbf{J}=0$) is useful for the expansion of one-body operators that have to be rotationally invariant. The tensor expansions for the single-particle spin-orbit and orbit-orbit interactions are [12]:

$$\begin{aligned} \sum_i l_i.s_i = \sum_{(\lambda,\lambda)l} \big[a^\dagger_{(\eta,0)l\frac{1}{2}} \otimes \tilde{a}_{(0,\eta)l\frac{1}{2}}\big]^{(\lambda,\lambda)0,0,0}_0 \langle(\eta,0)l;(0,\eta)l\|(\lambda,\lambda)0\rangle \\ (-)^\eta \big[\frac{1}{2}l(l+1)(2l+1)\big]^{\frac{1}{2}}, \end{aligned} \tag{2.73}$$

and

$$\begin{aligned} \sum_i l_i^2 = \sum_{(\lambda,\lambda)l} \big[a^\dagger_{(\eta,0)l\frac{1}{2}} \otimes \tilde{a}_{(0,\eta)l\frac{1}{2}}\big]^{(\lambda,\lambda)1,1,0}_0 \langle(\eta,0)l;(0,\eta)l\|(\lambda,\lambda)1\rangle \\ (-)^\eta \big[l(l+1)\big]\big[2(2l+1)\big]^{\frac{1}{2}}. \end{aligned} \tag{2.74}$$

Similarly, we can introduce a two-body $SU(3)$ unit tensor ${}^{(2,2)}\mathcal{F}$, as a product of a unit tensor ${}^{(2,0)}\mathcal{F}$ that creates a pair of particles and one ${}^{(0,2)}\mathcal{F}$ that annihilates a particle pair,

$${}^{(2,2)}\mathcal{F}^{\rho(\lambda,\mu)\kappa LM_L SM_S}_{(\lambda_1,\mu_1)(\lambda_2,\mu_2),S_1,S_2} \equiv \big[{}^{(2,0)}\mathcal{F}^{(\lambda_1,\mu_1),S_1}_{(\eta_1',0)(\eta_1,0)\frac{1}{2}\frac{1}{2}} \otimes^{(0,2)} \mathcal{F}^{(\lambda_2,\mu_2),S_2}_{(0,\eta_2')(0,\eta_2)\frac{1}{2}\frac{1}{2}}\big]^{\rho(\lambda,\mu)\kappa LM_L SM_S}, \tag{2.75}$$

where the pair creation and annihilation unit tensors are defined as:

$$\begin{aligned} {}^{(2,0)}\mathcal{F}^{(\lambda,\mu)\kappa LM_L SM_S}_{(\eta',0)(\eta,0)\frac{1}{2}\frac{1}{2}} &\equiv \big[a^\dagger_{(\eta',0)\frac{1}{2}} \otimes a^\dagger_{(\eta,0)\frac{1}{2}}\big]^{(\lambda,\mu)\kappa LM_L SM_S} \\ {}^{(0,2)}\mathcal{F}^{(\mu,\lambda)\kappa LM_L SM_S}_{(0,\eta')(0,\eta)\frac{1}{2}\frac{1}{2}} &\equiv \big[\tilde{a}_{(0,\eta')\frac{1}{2}} \otimes \tilde{a}_{(0,\eta)\frac{1}{2}}\big]^{(\mu,\lambda)\kappa LM_L SM_S}. \end{aligned} \tag{2.76}$$

A general two-body operator,

$$G = \sum_{i<j=1}^{N} g(x_i\sigma_i, x_j\sigma_j), \tag{2.77}$$

can be expressed in second quantization as

$$G = \sum_{\beta,\gamma,\delta,\epsilon} \langle\beta\gamma|f|\delta\epsilon\rangle a^\dagger_\beta a^\dagger_\gamma a_\delta a_\epsilon, \tag{2.78}$$

where $\langle\beta\gamma|f|\delta\epsilon\rangle$ are normalized antisymmetric two-particle states. As an example, consider the pairing interaction which can be written in second quantization as

$$V_P = -\frac{1}{4}G\sum_{\gamma,\gamma'} a^\dagger_\gamma a^\dagger_{\tilde{\gamma}} a_{\gamma'} a_{\tilde{\gamma'}}, \tag{2.79}$$

where $\tilde{\gamma}$ and $\tilde{\gamma'}$ denote the time-reversed partners of single-particle states γ and γ', respectively, and G is the strength of the pairing interaction. The expansion has the following form [36]:

$$\begin{aligned} V_P = \frac{G}{2} \sum_{(\lambda_1,\mu_1)(\lambda_2,\mu_2)} \sum_{\eta\eta'} P_{\eta\eta'}((\lambda_1,\mu_1)(\lambda_2,\mu_2)\rho_0(\lambda_0,\mu_0)) \\ \left[\left[a^\dagger_\eta \otimes a^\dagger_\eta\right]^{(\lambda_1\mu_1)} \otimes \left[\tilde{a}^\dagger_{\eta'} \otimes \tilde{a}^\dagger_{\eta'}\right]^{(\mu_2\lambda_2)}\right]^{\rho_0(\lambda_0,\mu_0)\kappa_0=1 l_0=s_0=0}, \end{aligned} \tag{2.80}$$

where the coefficients $P_{\eta\eta'}(...)$ involve a sum over the product of three $SU(3)$ reduced coupling coefficients

$$\begin{aligned} &P_{\eta\eta'}((\lambda_1,\mu_1)(\lambda_2,\mu_2)\rho_0(\lambda_0,\mu_0)) = (-1)^{l-l'}\sqrt{(2l+1)(2l'+1)} \\ &\langle(\eta,0)l;(\eta,0)l\|(\lambda_1,\mu_1)10\rangle \\ &\langle(\eta',0)l;(\eta',0)l\|(\lambda_2,\mu_2)10\rangle\langle(\lambda_1,\mu_1)l;(\lambda_2,\mu_2)l\|(\lambda_0,\mu_0)10\rangle_{\rho_0}. \end{aligned} \tag{2.81}$$

It was shown [36] that when the pairing-plus-quadrupole model is realized in the framework of the $SU(3)$ scheme, the pairing force breaks the $SU(3)$ symmetry and removes almost all degeneracies which occur in the pure symmetry limits of the theory.

Adding the one-body spin-orbit and orbit-orbit interactions, and the two-body pairing interaction to a $SU(3)$ Hamiltonian breaks the $SU(3)$ symmetry. If a dominating quadrupole-quadrupole interaction is assumed, however, $SU(3)$ still remains extremely useful as an approximate symmetry. Specifically, this allows one to restrict the configuration space to $SU(3)$ irreps with a large C_2 value and to use group theoretical tools for the evaluation of all required matrix elements.

For a proton-neutron system, the reduced matrix elements of the Hamiltonian (2.64) can be calculated using the following expression [38]:

$$
\begin{aligned}
&\langle\{N'_\pi[f'_\pi]\alpha'_\pi(\lambda'_\pi,\mu'_\pi),N'_\nu[f'_\nu]\alpha'_\nu(\lambda'_\nu,\mu'_\nu)\}\rho'(\lambda',\mu')\kappa'L'\{S'_\pi,S'_\nu\}S';J'\\
&||^{\pi\nu}\,T^{J_0}_{\{\pi\}\{\nu\}}\,||\\
&\{N_\pi[f_\pi]\alpha_\pi(\lambda_\pi,\mu_\pi),N_\nu[f_\nu]\alpha_\nu(\lambda_\nu,\mu_\nu)\}\rho(\lambda,\mu)\kappa L\{S_\pi,S_\nu\}S;J\rangle\\
&=\sum_{(\lambda_0,\mu_0)\kappa_0L_0S_0}\chi\begin{Bmatrix}L&L_0&L'\\S&S_0&S'\\J&J_0&J'\end{Bmatrix}\\
&\sum_{\tilde\rho}\langle(\lambda,\mu)\kappa L,(\lambda_0,\mu_0)\kappa_0L_0\,||\,(\lambda',\mu')\kappa'L'\rangle_{\tilde\rho}\\
&\langle\{N'_\pi[f'_\pi]\alpha'_\pi(\lambda'_\pi,\mu'_\pi),N'_\nu[f'_\nu]\alpha'_\nu(\lambda'_\nu,\mu'_\nu)\}\rho'(\lambda',\mu'),\{S'_\pi,S'_\nu\}S'\\
&|||^{\pi\nu}\,T_{\{\pi\}\{\nu\}}\,|||\\
&\{N_\pi[f_\pi]\alpha_\pi(\lambda_\pi,\mu_\pi),N_\nu[f_\nu]\alpha_\nu(\lambda_\nu,\mu_\nu)\}\rho(\lambda,\mu),\{S_\pi,S_\nu\}S\rangle,
\end{aligned}
\tag{2.82}
$$

with

$$
\begin{aligned}
&\langle\{N'_\pi[f'_\pi]\alpha'_\pi(\lambda'_\pi,\mu'_\pi),N'_\nu[f'_\nu]\alpha'_\nu(\lambda'_\nu,\mu'_\nu)\}\rho'(\lambda',\mu'),\{S'_\pi,S'_\nu\}S'\\
&|||^{\pi\nu}\,T_{\{\pi\}\{\nu\}}\,|||\\
&\{N_\pi[f_\pi]\alpha_\pi(\lambda_\pi,\mu_\pi),N_\nu[f_\nu]\alpha_\nu(\lambda_\nu,\mu_\nu)\}\rho(\lambda,\mu),\{S_\pi,S_\nu\}S\rangle\\
&=\chi\begin{Bmatrix}S_\pi&S_{\pi_0}&S'_\pi\\S_\nu&S_{\nu_0}&S'_\nu\\S&S_0&S'\end{Bmatrix}\\
&\sum_{\rho_\pi\rho_\nu}\chi\begin{Bmatrix}(\lambda_\pi,\mu_\pi)&(\lambda_{\pi_0},\mu_{\pi_0})&(\lambda_\pi,\mu'_\pi)&\rho_\pi\\(\lambda_\nu,\mu_\nu)&(\lambda_{\nu_0},\mu_{\nu_0})&(\lambda'_\nu,\mu'_\nu)&\rho_\nu\\(\lambda,\mu)&(\lambda_0,\mu_0)&(\lambda',\mu')&\tilde\rho\\\rho&\rho_0&\rho'&\end{Bmatrix}\\
&\langle N'_\pi[f'_\pi]\alpha'_\pi(\lambda'_\pi,\mu'_\pi)S'_\pi\,|||^\pi\,T^{(\lambda_{\pi_0},\mu_{\pi_0}),S_{\pi_0}}\,|||\,N_\pi[f_\pi]\alpha_\pi(\lambda_\pi,\mu_\pi)S_\pi\rangle_{\rho_\pi}\\
&\langle N'_\nu[f'_\nu]\alpha'_\nu(\lambda'_\nu,\mu'_\nu)S'_\nu\,|||^\nu\,T^{(\lambda_{\nu_0},\mu_{\nu_0}),S_{\nu_0}}\,|||\,N_\nu[f_\nu]\alpha_\nu(\lambda_\nu,\mu_\nu)S_\nu\rangle_{\rho_\nu},
\end{aligned}
\tag{2.83}
$$

where $\chi\{...\}$ denotes a unitary $9j$ or Jahn-Hope symbol [39, 40] and $\chi\{....\}$ its $SU(3)$ extension called a $9-(\lambda,\mu)$ coefficient [41]. The triple-barred matrix elements that enter the equation, are reduced with respect to both $SU(3)$ and $SO(3)$, and can be evaluated for operators of physical interest with the code now under development [42].

2.5 Electromagnetic Transition Operators in the SU(3) Model

We conclude this chapter by giving the expressions that are used in the $SU(3)$ model to calculate electromagnetic transition strengths which are quantities of great

importance in nuclear physics. In general, the electric and magnetic transition operators for a system of A nucleons in the long-wavelength approximation are given by [43]:

$$\begin{aligned} T^L_M(E) &= b_0^L \sum_\sigma \sum_i e_\sigma r^L_\sigma(i) Y_{LM}(\hat{\mathbf{r}}_\sigma(i)), \\ T^L_M(M) &= b_0^{L-1}\mu_N \sum_\sigma \sum_i \{ \big[g^s_\sigma \mathbf{s}^\sigma(i) + \frac{2g^o_\sigma}{L+1}\mathbf{l}^\sigma(i)\big] . \big[\nabla_\sigma(i) r^L_\sigma(i) Y_{LM}(\hat{\mathbf{r}}_\sigma(i))\big]\}, \end{aligned} \tag{2.84}$$

where $\sigma = \pi$ or ν, $b_0 = A^{1/6}$ is the harmonic oscillator size parameter, g^s and g^o are spin and orbital g factors, e is the charge and μ_N denotes the nuclear magneton. Using the following operators:

$$\begin{aligned} L^\sigma_\mu &= \sum_i l^\sigma_\mu(i) = \frac{1}{\sqrt{2}} \sum_i \big[\mathbf{r}_\sigma(i) \times \mathbf{p}_\sigma(i)\big]_{1\mu}, \\ S^\sigma_\mu &= \sum_i s^\sigma_\mu(i), \\ Q^\sigma_M &= \sum_i q^\sigma_M(i) = \sum_i \sqrt{\frac{16\pi}{5}} r^2_\sigma(i) Y_{2M}(\hat{\mathbf{r}}_\sigma(i)), \end{aligned} \tag{2.85}$$

the M1 and E2 transition operators can be rewritten as:

$$\begin{aligned} T^1_\mu(M) &= \sqrt{\frac{3}{4\pi}}\mu_N \sum_\sigma \{ g^o_\sigma L^\sigma_\mu + g^s_\sigma S^\sigma_\mu \}, \\ T^2_M(E) &= \sqrt{\frac{5}{16\pi}} b_0^2 \sum_\sigma e_\sigma Q^\sigma_M. \end{aligned} \tag{2.86}$$

We can write down these operators in another form using the derivation in Appendix C. The $SU(3)$ and $SU(2)$ tensor forms for the corresponding single-particle operators are given by [37]

$$\begin{aligned} l_\mu &= f^{(1,1);0}_{11\mu 0}, \\ s_\mu &= f^{(0,0);1}_{100\mu}, \\ q_m &= \sqrt{\frac{1}{3}} f^{(1,1);0}_{12m0}. \end{aligned} \tag{2.87}$$

The triple-barred matrix elements for the orbital angular momentum, spin, and quadrupole operators are listed below [44]:

$$\begin{aligned} \langle (\eta,0); \frac{1}{2} ||| \mathbf{l} ||| (\eta,0); \mathbf{\frac{1}{2}} \rangle &= [\frac{4}{3} C_2(\eta,0)]^{1/2}, \\ \langle (\eta,0); \frac{1}{2} ||| \mathbf{s} ||| (\eta,0); \mathbf{\frac{1}{2}} \rangle &= [\frac{3}{4}]^{1/2}, \\ \langle (\eta,0); \frac{1}{2} ||| \mathbf{q} ||| (\eta,0); \mathbf{\frac{1}{2}} \rangle &= [4 C_2(\eta,0)]^{1/2}, \end{aligned} \tag{2.88}$$

where $C_2(\lambda,\mu)$ indicates the eigenvalue of the second order Casimir invariant of $SU(3)$ in the (λ,μ) irrep. Substituting the last three formulas into Eq. (C.6) derived in Appendix C we find

$$\begin{aligned} L_\mu &= [\frac{1}{3}\dim(\eta,0)C_2(\eta,0)]^{1/2}\{a^\dagger_{(\eta,0);1/2}\otimes\tilde{a}_{(0,\eta);1/2}\}_1^{(1,1);110}{}_{\mu}, \\ S_\mu &= [\frac{1}{2}\dim(\eta,0)]^{1/2}\{a^\dagger_{(\eta,0);1/2}\otimes\tilde{a}_{(0,\eta);1/2}\}_1^{(1,1);101}{}_{\mu}, \\ Q_M &= [\dim(\eta,0)C_2(\eta,0)]^{1/2}\{a^\dagger_{(\eta,0);1/2}\otimes\tilde{a}_{(0,\eta);1/2}\}_2^{(1,1);120}{}_{M}. \end{aligned} \tag{2.89}$$

Chapter 3

Pseudo-Spin Symmetry and the Pseudo-$SU(3)$ Model

The success of the $SU(3)$ shell model for light deformed nuclei [3, 15] has led physicists to explore similar concepts in heavy deformed systems. Specifically, attention has been directed to the well-deformed rotational nuclei of the rare-earth and actinide regions. It is the purpose of this chapter to describe the conditions under which we arrive at a model capable to describe heavy deformed systems, namely, the pseudo-$SU(3)$ model.

The three-dimensional isotropic harmonic oscillator, H_0, with eigenvalue $n\hbar\omega$ where n is the shell number, augmented with the one-body $l.s$ and l^2 interactions,

$$H = H_0 + Cl.s + Dl^2, \tag{3.1}$$

is known to be a good approximation for the nuclear single-particle Hamiltonian [1]. The l^2 term ($D < 0$) pushes high angular momentum states down relative to those with lower l values, a feature that occurs automatically when a Woods - Saxon form is used for the central potential, while the phenomenological $l.s$ term ($C < 0$), which couples space and spin degrees of freedom, is required to achieve shell closures at the magic nucleon numbers $2, 8, 20, 50, 82, 126$ and 184. Unfortunately, the required value for C is so large that the spin-orbit term completely destroys the underlying $SU(3)$ symmetry of the oscillator for all but light ($A < 28$) nuclei, thereby making it useless in attempts at unraveling the structure of heavy ($A > 100$) systems. Specifically, for heavy nuclei the $j = \eta + 1/2$ orbital of the η-th oscillator shell ($\eta = 0, 1, ...$) which includes levels with $j = l \pm 1/2$ with $l = \eta, \eta - 2, ..., 1$ or 0, is pushed down among the orbitals of the next lower shell and becomes part of the core (this orbital is called a defector level). This yields new shells with normal parity $j = 1/2, 3/2, ..., \eta - 1/2$ orbitals plus a $j = (\eta + 1) + 1/2 = \eta + 3/2$ unique-parity level (also called intruder level) from the $\eta + 1$-th shell immediately above.

In this chapter, it is shown that this seemingly unfavorable situation gives way to a much more favorable one because for heavy nuclei $C \approx 4D$ or the Nilsson parameter $\mu = 2D/C \approx 0.5$. First of all, this condition insures that at the $0\hbar\omega$ level pseudo-spin is a good symmetry because the level splitting generated by the $l.s$ and l^2 interactions can be duplicated by a pseudo-oscillator Hamiltonian plus a pseudo

l^2 interaction, with at most a very small breaking of the pseudo-spin symmetry by a pseudo $l.s$ term [45, 46]. Since common residual interactions are pseudo-spin scalar operators, a many-particle pseudo-LS coupled shell-model scheme can be employed, and the basis truncated to leading pseudo-spin symmetries, without loss of important physics. Furthermore, the pseudo LS scheme extends to pseudo-$SU(3)$ when deformation dominates [12].

3.1 Pseudo-Spin Symmetry

In the single-particle picture, the pseudo-spin concept means a division of the total particle angular momentum into *pseudo* ($\mathbf{j} = \tilde{\mathbf{l}} + \tilde{\mathbf{s}}$) [1] rather than *normal* ($\mathbf{j} = \mathbf{l} + \mathbf{s}$) orbital and spin parts, so $\tilde{l} \pm \frac{1}{2} = l \mp \frac{1}{2}$. A straightforward way to gain an immediate appreciation for the simplicity and significance of the pseudo-spin concept [45, 46] is shown in Figure 3.1 where eigenvalues of H are plotted as a function of the Nilsson parameter $\mu = 2D/C$. For the special value $\mu = 0.5$, the orbital pairs with $j = l + 1/2$ and $j = (l + 2) - 1/2$ are degenerate for all l values. Furthermore, the splitting of these pairs follows a $\tilde{l}(\tilde{l} + 1)$ rule where $\tilde{l}$ is the average l value of the pair, $\tilde{l} = (l + (l + 2))/2 = l + 1$. This mapping of the $(ls)j$ coupled single-particle states onto $(\tilde{l}\tilde{s})j$ pairs can be expressed as a special "normal $\rightarrow$ pseudo" unitary transformation [48, 49] which takes the quantum numbers η, l, s and j into the pseudo partners, $\tilde{j} = \tilde{l} + \tilde{s}$, where $\tilde{j} = j$, $\tilde{l} = l + 1$, $\tilde{\eta} = \eta - 1$ and $\tilde{s} = \frac{1}{2}$,

$$\left|\tilde{\eta}(\tilde{l}, \tilde{s})\tilde{j}\tilde{m}\right\rangle = U_{\eta jm,\tilde{\eta}\tilde{j}\tilde{m}}(l, \tilde{l}) \left|\eta(l, s)j, m\right\rangle , \tag{3.2}$$

and $U_{\eta jm,\tilde{\eta}\tilde{j}\tilde{m}}(l, \tilde{l})$ is simply a relabeling of the basis states that associates all levels of the η-th shell, except the defector with $j = \eta + \frac{1}{2}$, with levels of the $\tilde{\eta}$-th shell of a "pseudo" oscillator, $\tilde{\eta} = \eta - 1$. This unitary transformation can be written in the following label-independent operator form:

$$U_{\eta jm,\tilde{\eta}\tilde{j}\tilde{m}}(l, \tilde{l}) = 2(\eta.\xi + 2\mathbf{l}.\mathbf{s} + 3)^{-1/2}(\xi.\mathbf{s}), \tag{3.3}$$

where η creates while ξ annihilates oscillator quanta, and l and s are the single-particle orbital angular momentum and spin operators, respectively. The structure of the unitary pseudo-spin transformation has been extensively investigated during the years [50].

The single-particle Hamiltonian transforms under this mapping as follows:

$$H_0 + Cl.s + Dl^2 \quad \begin{array}{c} \leftarrow normal - - \\ - - - - - - - - - \\ - - pseudo \rightarrow \end{array} \quad \tilde{H}_0 + (4D - C)\tilde{l}.\tilde{s} + D\tilde{l}^2 + (\hbar\omega + 2D - C) \tag{3.4}$$

where $H_0 = \tilde{n}\hbar\tilde{\omega} = (n - 1)\hbar\tilde{\omega}$, $\tilde{l}.\tilde{s} = -(l.s + 1)$ and $\tilde{l}^2 = l^2 + 4l.s + 2$. Since the term $(\hbar\omega + 2D - C)$ is a constant, the pseudo form $\tilde{H} = \tilde{H}_0 + (4D - C)\tilde{l}.\tilde{s} + D\tilde{l}^2$

[1] From now on we will write a tilde over a quantity to denote its pseudo realization.

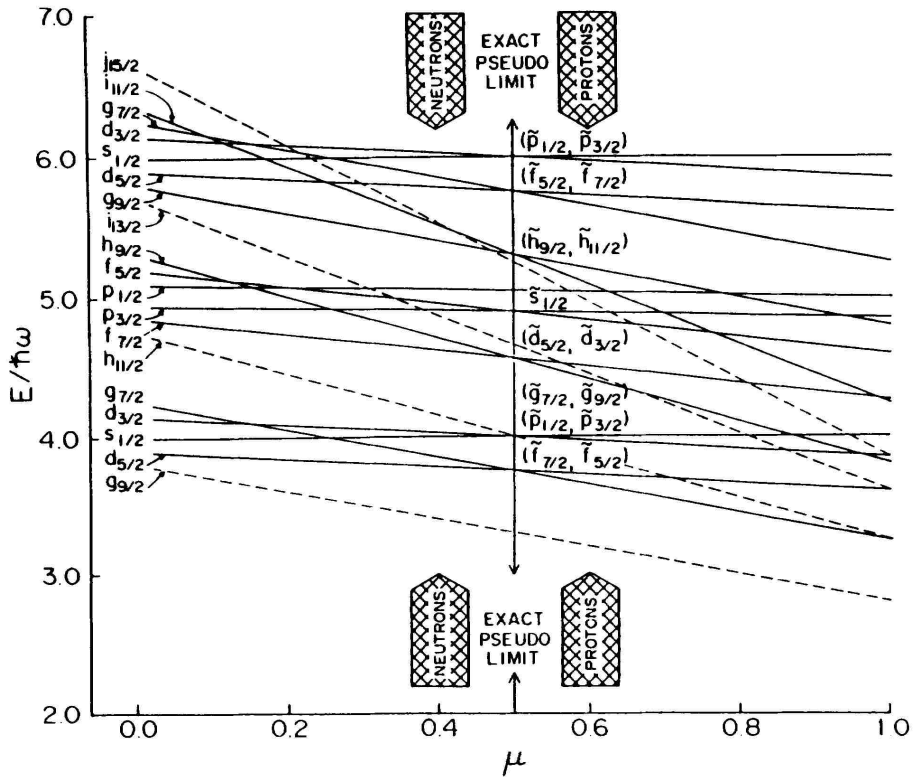

Figure 3.1: Eigenvalues of the single-particle Hamiltonian $\frac{H}{\hbar\omega} = \eta - \kappa(2l.s + \mu l^2)$, where $\mu = \frac{2D}{C}$ and $\kappa = -\frac{C}{2\hbar\omega} \approx \frac{1}{4}A^{-1/3}$, for the specific value $\kappa = 0.05$ and $0.0 \leq \mu \leq 1.0$ Each pseudo shell is accompanied by a unique-parity intruder level (dashed lines) with $j = \eta + \frac{3}{2}$ from the shell above (Taken from [47]).

has the same excitation spectrum as the normal one, $H = H_0 + Cl.s + Dl^2$, when $\hbar\tilde{\omega} = \hbar\omega$, $\tilde{C} = (4D - C)$ and $\tilde{D} = D$. This transformation is meaningful because $C \approx 4D$ so $\tilde{C} = 0$. Specifically, as indicated in the figure, $\mu_\pi \approx 0.6$ and $\mu_\nu \approx 0.4$ (π for protons and ν for neutrons). This places heavy nuclei very close to the exact pseudo-spin limit ($\mu = 0.5$) of the theory [51]. In particular, the average value for μ is exactly 0.5. The familiar single-particle shell-model Hamiltonian for heavy nuclei can therefore be replaced by a less familiar but equivalent pseudo form which is inherently simpler because it has a much smaller spin-orbit term.

3.2 Relativistic Mean-Field Results

The pseudo-spin concept may be better understood by comparing an intuitive result for the parameter D with relativistic nuclear mean-field predictions for the parameter C. Starting with the usual Dirac equation (with only the time component of the scalar and vector potentials taken into account) and using a nonrelativistic re-

duction of the relativistic mean-field theory, the spin-orbit interaction potential can be expressed as

$$V_{ls} = \frac{\hbar^2}{2M}\frac{2}{r}\frac{d}{dr}\Big(\frac{1}{1-B\frac{\rho}{\rho_0}}\Big)\mathbf{l.s}, \tag{3.5}$$

where the parameters ρ and ρ_0 are the nucleon density at radius r and the nuclear matter density. In the simplest version of the theory, the dimensionless quantity $B = \frac{1}{2}(B_s + B_v)$, with its scalar ($i$=$s$) and vector ($i$=$v$) components given by $B_i = \frac{g_i^2\rho_0}{\mu_i^2 Mc^2}$, where μ_i and g_i denote meson masses and coupling constants, respectively. The spin-orbit strength, C, can be obtained by averaging V_{ls} over the region inside the nucleon radius R as

$$C = \frac{-\hbar^2}{2MR}\frac{1-B}{3B}. \tag{3.6}$$

In determining this result, the fact that $\frac{d\rho}{dr}$ vanishes everywhere, except near the surface of the nucleus, has been used.

To find an estimate for the strength of the orbit-orbit interaction, one can use the fact that the origin of the $\mathbf{l^2}$ term lies in the flatness of the mean field in the interior region as compared with the quadratic oscillator form used in the shell model Hamiltonian. In the large mass limit ($A \to \infty$) a more realistic potential is that of a spherical well with finite depth. If this potential is replaced by one with an infinite depth, the single-particle energies are given by

$$E_{nl} = \frac{\hbar^2}{2MR^2}x_{nl}^2, \tag{3.7}$$

where M is the nucleon mass, R is the radius of the well, and the x_{nl} are the zeroes of spherical Bessel functions that are approximately given by $x_{nl}^2 \approx [(\frac{1}{2}n{+}1)\pi]^2{-}l(l{+}1)$. The energy splitting thus follows an $l(l+1)$ rule and the orbit-orbit strength, D, is given by

$$D = -\frac{\hbar^2}{2MR^2}. \tag{3.8}$$

With the estimates for C and D that were obtained, μ can be approximated by the ratio

$$\mu = \frac{2D}{C} = \frac{1-B}{3B}, \tag{3.9}$$

which is independent of the mass number.

Using estimates for B derived in the Nambu Jona-Lasinio model [52] which starts with massless quarks and generates the hadron masses by spontaneous symmetry breaking, gives $\mu = 0.686$. Also, other microscopic models like the Walecka model [53] and a derivative coupling model due to Zimanyi and Moszkowski [54], that give $\mu = 0.447$ and 0.635 respectively, yield reasonable results for μ. The pseudo-spin symmetry thus appears to be a feature of the nuclear interaction that can also be seen on a more fundamental level.

3.3 Pseudo-$SU(3)$ Shell Model

A consequence of good pseudo-spin symmetry is that a $\tilde{L}\tilde{S}$-coupling scheme (with distinct $\tilde{S}$ multiplets that are decoupled and ordered) is expected to be a good starting point for describing many-particle phenomena in heavy nuclei. The $\tilde{N}$-particle valence spaces (where $\tilde{N} = \tilde{N}_\pi$ for protons and $\tilde{N} = \tilde{N}_\nu$ for neutrons, which occupy different major shells) divide into subspaces: $\tilde{S} = 0, 1, 2, 3, ..., \tilde{S}_{\max}$ for $\tilde{N}$ even or $\tilde{S} = \frac{1}{2}, \frac{3}{2}, \frac{5}{2}, ..., \tilde{S}_{\max}$ for $\tilde{N}$ odd with $\tilde{S}_{\max} = \min(\frac{\tilde{N}}{2}, \tilde{\Omega} - \frac{\tilde{N}}{2})$ where $\tilde{\Omega} = \frac{(\tilde{\eta}+1)(\tilde{\eta}+2)}{2}$ is the pseudo-shell degeneracy. The proton - neutron $\tilde{L}\tilde{S}$-coupled states $\left|\Psi^J\right\rangle = \left|\left[(\tilde{\alpha}_\pi \tilde{L}_\pi, \tilde{\alpha}_\nu \tilde{L}_\nu)^{\tilde{L}} \otimes (\tilde{S}_\pi, \tilde{S}_\nu)^{\tilde{S}}\right]^J\right\rangle$ ($\tilde{\alpha}$ labeling $\tilde{L}$ multiplicity) with $\tilde{S}_\pi = \tilde{S}_{\pi_{\min}}$, $\tilde{S}_\nu = \tilde{S}_{\nu_{\min}}$ and $\tilde{S} = \tilde{S}_{\min} = |\tilde{S}_{\pi_{\min}} - \tilde{S}_{\nu_{\min}}|$ are expected to dominate, because realistic interactions favor pseudo-space symmetric (pseudo-spin antisymmetric) configurations.

This truncation to the lowest $\tilde{S}_\pi$, $\tilde{S}_\nu$ and $\tilde{S}$ is usually insufficient to reduce the model space to a reasonable and workable size. Fortunately, another symmetry for strongly deformed nuclei can be invoked to effect a further truncation. Just as for light nuclei, pseudo-$SU(3)$ of the pseudo oscillator which lies between $\tilde{U}(\tilde{\Omega})$ and $\widetilde{SO_L}(3)$ can be used to organize the states within each $\tilde{S}$ multiplet according to their deformation [3, 15]. In this case the deformation is realized in terms of the pseudo (not normal) space symmetry. Nonetheless, this gives rise to strongly enhanced $B(E2)$ transition strengths because the electric quadrupole operators $\tilde{Q}$ and Q are known to differ very little from one another [37]. This way, we finally arrive at a theory (the pseudo-$SU(3)$ model) which has the same advantages as the Elliott's $SU(3)$ model for light nuclei.

3.4 Pseudo-$SU(3)$ Model Framework for Rare-Earth and Actinide Nuclei

In rare-earth and actinide nuclei, the valence protons π and valence neutrons ν fill different major shells. Thus, for a given nucleus, there are two open shells, one for protons and one for neutrons, each of them comprised of a set of normal-parity levels and the associated unique-parity level. The normal-parity space is partitioned into irreps of pseudo $SU(3)$ and the unique-parity space is spanned by configurations of identical particles in a single j shell. Since, in a restricted space like a single j shell, the pairing part of the residual interaction tends to dominate, the seniority coupling scheme is appropriate for a description of the unique-parity configurations. If the $\pi - \nu$ interaction is of the quadrupole-quadrupole ($Q.Q$) type then the yrast states are approximated well by strong-coupled $SU(3)$ wavefunctions. In a previous study it was shown that this is true even if the $\pi - \pi$ and $\nu - \nu$ interactions are very different from the $Q.Q$ type [55].

If these assumptions are valid then the low-energy structure of the normal-parity part of the space will be dominated by a few irreps of pseudo $SU(3)$. In the

unique-parity parts of the proton and neutron shells, we expect the configurations with low seniority to be the most important ones. Arrangements with high seniority are not favored because the pairing gap is large as compared to the spacing of low-lying rotational levels. The strong-coupled normal-parity states, $|NJ_NM_N\rangle$, are coupled to the unique-parity basis states, $|UJ_UM_U\rangle$, to yield states of good total angular momentum,

$$|JM\rangle \equiv \{|NJ_N\rangle \otimes |UJ_U\rangle\}^J_M. \tag{3.10}$$

Here, $\{-\}^J_M$ denotes angular momentum coupling.

Now we will write down explicitly the group theoretical structure of the normal- and unique-parity spaces. This gives a complete labelling scheme for basis states of the model. The many-particle states of N nucleons in a shell of dimension Ω are characterized by the totally antisymmetric irrep of a unitary group of dimension Ω, that is,

$$\begin{array}{ccc} U(\Omega) & \leftarrow & \text{group symbol,} \\ \left[1^N\right] & \leftarrow & \text{irrep label.} \end{array} \tag{3.11}$$

This group can be reduced to a direct sum of two unitary groups associated with the normal- and unique-parity spaces,

$$\begin{array}{ccccc} U(\Omega) & \rightarrow & U(\Omega_N) & + & U(\Omega_U) \\ \left[1^N\right] & & \left[1^{n_N}\right] & & \left[1^{n_U}\right]. \end{array} \tag{3.12}$$

The quantum numbers n_N and n_U denote the number of nucleons in the normal- and unique-parity spaces, respectively. These satisfy the inequalities

$$0 \le n_N \le N, \qquad 0 \le n_U \le N, \qquad N = n_N + n_U. \tag{3.13}$$

Normally, only the normal- and unique-parity spaces associated with the most probable values of n_N and n_U are considered and these are determined from the appropriate Nilsson diagrams; see Fig. 3.2. Each level is filled with a pair of protons (neutrons) in order of increasing energy. For well-deformed nuclei a value of the deformation $\epsilon \sim 0.25$ is considered appropriate. This can be checked by confirming that it yields the greatest binding energy as compared to configurations with $(n_N \pm 2, n_U \mp 2)$ when a realistic Hamiltonian is diagonalized.

In the rare-earth region, the normal-parity spaces are built by single-particle orbits of the pseudo-harmonic oscillator shells $\tilde{N} = 3$ (protons) and $\tilde{N} = 4$ (neutrons). The corresponding intruder levels are the $h_{11/2}$ and $i_{13/2}$, respectively. For the actinide nuclei, the single-particle orbits of the $\tilde{N} = 4$ (protons) and $\tilde{N} = 5$ oscillator shells form the normal-parity proton and neutron subspaces and the intruder levels are $i_{13/2}$ and $j_{15/2}$, respectively. The dimensions of these spaces are given by

$$\Omega_\pi = 32 \qquad \Omega^\pi_N = 20 \qquad \Omega^\pi_U = 12, \tag{3.14}$$

$$\Omega_\pi = 44 \qquad \Omega^\pi_N = 30 \qquad \Omega^\pi_U = 14, \tag{3.15}$$

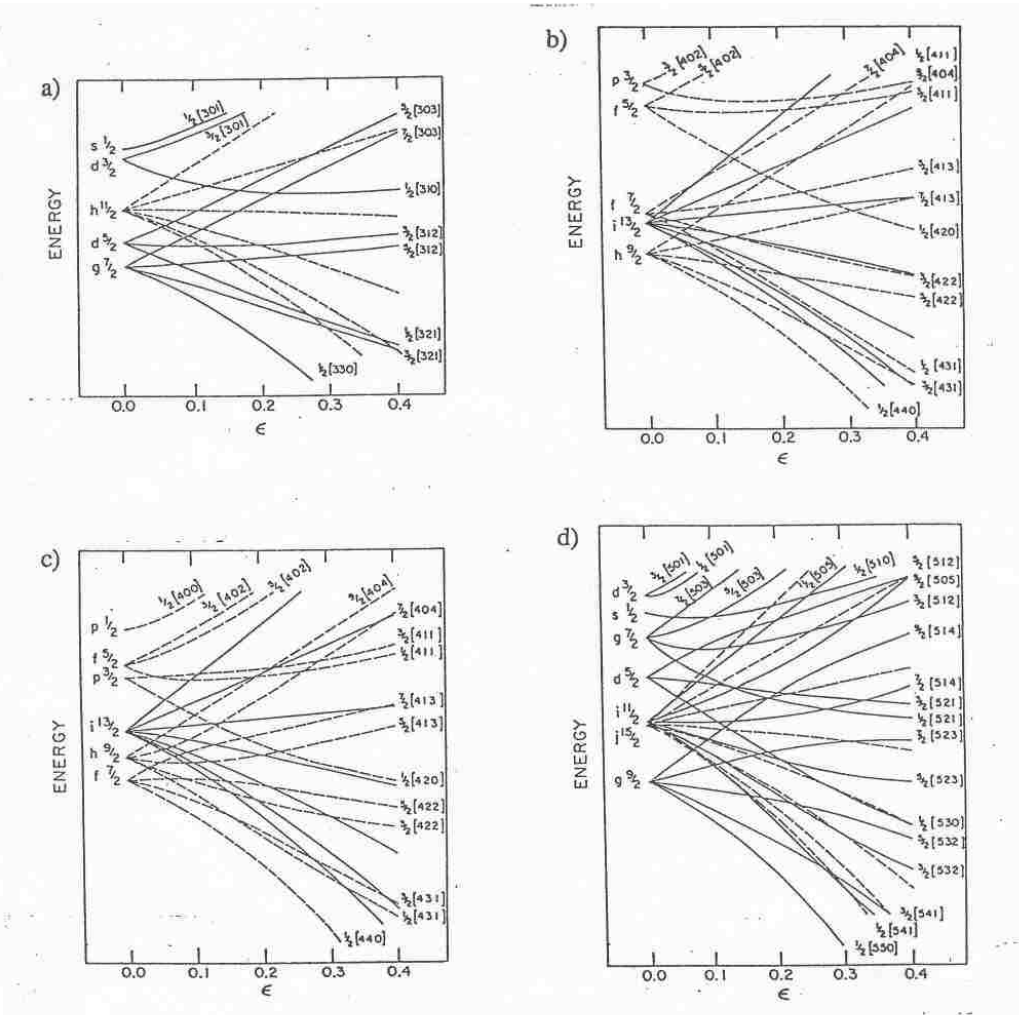

Figure 3.2: Nilsson diagrams for rare-earth and actinide nuclei. a) Level scheme for the $N = 4$ proton shell, b) for the $N = 5$ proton shell, c) for the $N = 5$ neutron shell, d) for the $N = 6$ neutron shell (Taken from [56]).

for the rare-earth and

$$\Omega_\pi = 44 \qquad \Omega_N^\pi = 30 \qquad \Omega_U^\pi = 14, \tag{3.16}$$

$$\Omega_\pi = 58 \qquad \Omega_N^\pi = 42 \qquad \Omega_U^\pi = 16, \tag{3.17}$$

for the actinide nuclei. Here and until the end of the section, the tilde on symbols referring to pseudo-shell labels will be omitted when its presence can be inferred from context.

If the most probable occupancy of the normal- and unique-parity spaces is given,

$$N_\sigma = n_N^\sigma + n_U^\sigma, \tag{3.18}$$

where σ is π or ν for protons and neutrons, respectively, the basis states are specified in terms of the group chains

$$\begin{array}{ccccccccc} U(\Omega_N^\sigma) & \rightarrow & U(\Omega_N^\sigma/2)\otimes U(2) & \rightarrow & SU(3)\otimes SU(2) & \rightarrow & O(3)\otimes SU(2) & \rightarrow & SU(2) \\ \left[1^{n_N^\sigma}\right] & & \{f_\sigma\} \quad \{\tilde{f}_\sigma\} & & \alpha_\sigma(\lambda_\sigma,\mu_\sigma) & & S_\sigma \quad \kappa_\sigma L_\sigma & & J_N^\sigma \end{array} ,$$

$$\begin{array}{ccccc} U(\Omega_U^\sigma) & \rightarrow & Sp(\Omega_U^\sigma) & \rightarrow & O(3) \\ \left[1^{n_U^\sigma}\right] & & \left[1^{\nu_\sigma}\right] & & \beta_\sigma J_U^\sigma \end{array} . \tag{3.19}$$

As in Eqs. (3.11) and (3.12) above, underneath each group the quantum numbers that characterize its irreps are given. The indices α, κ, and β are multiplicity labels of the indicated reductions. Note that the decomposition of $U(\Omega_N)$ into $U(\Omega_N/2)\otimes U(2)$ is a factorization of the normal-parity space into orbital and spin degrees of freedom. This is an LS-coupling scheme. The unique-parity space, on the other hand, is a single j shell so a jj-coupled geometry is appropriate. As shown, the seniority quantum number of that space is an irrep label of the symplectic group, $Sp(\Omega_U)$. Of course, $O(3)$ is the orbital angular momentum group and the final $SU(2)$ refers to the total angular momentum.

As it has been the case for almost all pseudo-$SU(3)$ studies to date [2], the intruder level with opposite parity in each major shell has been removed from active consideration and its role considered implicitly. The nucleons in these levels are taken to renormalize the dynamics that is described using only nucleons in normal-parity states - a choice reflected, for example, through the use of effective charges to describe quadrupole electromagnetic transitions that are larger than those usually employed in shell-model calculations. With this restriction in mind, the pseudo-$SU(3)$ strong coupled basis states are given by

$$\begin{aligned} &|f_\pi(\lambda_\pi,\mu_\pi), f_\nu(\lambda_\nu,\mu_\nu); \rho(\lambda,\mu)\kappa JM\rangle = \\ &\sum_{\kappa_\pi,\kappa_\nu,L_\pi,L_\nu} \langle(\lambda_\pi,\mu_\pi)\kappa_\pi L_\pi; (\lambda_\nu,\mu_\nu)\kappa_\nu L_\nu \| (\lambda,\mu)\kappa J\rangle_\rho \\ &\left[|\{f_\pi\}(\lambda_\pi,\mu_\pi)\kappa_\pi L_\pi\rangle \otimes |\{f_\nu\}(\lambda_\nu,\mu_\nu)\kappa_\nu L_\nu\rangle\right]^J_M . \end{aligned} \tag{3.20}$$

In Eq. (3.20) $\langle -; - \| - \rangle_\rho$ is a reduced $SU(3) \supset SO(3)$ coupling coefficient and as in Eq. (3.10), $\left[-\right]^J_M$ denotes angular momentum coupling.

Initially, the pseudo-$SU(3)$ model calculations have been done with highly schematic interactions [37, 56]. The development of a computer code that is able to calculate reduced matrix elements for any type of physical operator between different $SU(3)$ irreps [57] has made it possible to include realistic $SU(3)$ symmetry breaking terms, like the pairing interaction, in $SU(3)$-model Hamiltonians. Indeed, results using this code show that the pairing interaction is closely tied to the development of triaxiality in strongly deformed systems [36, 38, 58]. Furthermore, complete model space calculations in the fp shell [59, 60] show that a very good description of the low-energy spectra can be obtained when the Hilbert space is truncated, albeit not

[2] One exception, for example, is the study performed within the framework of a toy model [5] on the role of the intruder levels for the dynamics of a nuclear system.

so severely, following the same logic as used in the ds-shell, namely, a dominance of the quadrupole-quadrupole interaction. These same calculations also showed that the pairing interaction is critical for a correct description of the moments of inertia.

During the last decade, two approaches of using realistic Hamiltonians have been followed in the applications of the pseudo-$SU(3)$ model. The first type of studies has focused on a Hamiltonian that is built from $SU(3)$ generators plus residual interactions [61, 62, 63] and has the form

$$\begin{aligned} H &= H_{SU(3)} + H_{int} \\ &= -(a_2 + a_{sym})C_2 + a_3 C_3 + bK_J^2 + cJ^2 \\ &+ D_\pi \sum_{i_\pi} l_{i_\pi}^2 + D_\nu \sum_{i_\nu} l_{i_\nu}^2 - G_\pi H_P^\pi - G_\nu H_P^\nu. \end{aligned} \tag{3.21}$$

This Hamiltonian was very successful in describing low-energy structure of heavy deformed nuclei. Furthermore, the model was successful in explaining the scissors mode and served to introduce a new oscillation mode, called twist mode [64]. In order to describe the fragmentation in the $M1$ strength distribution, a residual interaction was included to generate configuration mixing. In the pure $SU(3)$ limit of the theory the model predicts at most four $M1$ transitions from the ground state 0^+ of even-even nuclei, while the experimental situations show that there may be more such transitions. By introducing proton and neutron single-particle energies and pairing interactions as residual terms in the Hamiltonian, and fitting their interaction strengths to reproduce the low-energy spectra, a good reproduction of the fragmentation in the $M1$ distribution was obtained [61, 62]. Unfortunately, this procedure yielded an apparent lack of consistency in choices for Hamiltonian parameters.

In most recent works [65, 66, 67], this lack of consistency in the choice of parameters was removed by reconsidering the structure of the Hamiltonian and by studying the effect of some interactions in the presence of the others. The Hamiltonian that was used was of the form

$$\begin{aligned} H &= H_{sp}^\pi + H_{sp}^\nu - \frac{\chi}{2} Q.Q - G_\pi H_P^\pi - G_\nu H_P^\nu \\ &+ aJ^2 + bK_J^2 + a_3 C_3 + a_{sym} C_2. \end{aligned} \tag{3.22}$$

The main idea in these studies was to fix the strength of the proton and neutron single-particle energies, quadrupole-quadrupole and pairing interactions and to consider the other parameters only as fine tuning. This idea is supported by the observation that the correct band structure is already formed by considering only the first five terms mentioned above. This can be considered a great result having in mind that only $Q.Q$ is part of the $SU(3)$ model and single-particle energies and pairing interactions are associated with destroying the $SU(3)$ symmetry. It was found that considering single-particle energies with Nilsson parameters [22] in a $Q.Q$ Hamiltonian does not destroy the $SU(3)$ structure. It does introduce a strong mixing but the $SU(3)$ band structure is maintained.

As a result of these developments, a very powerful shell-model theory for the description of normal-parity states in heavy deformed nuclei has emerged. In

case that only normal-parity configurations with the highest spatial symmetry (and $S_{\pi,\nu} = 0$ or $\frac{1}{2}$ for even or odd number of nucleons, respectively), have been taken into consideration, a successful description of up to four low-lying bands [62, 65, 68] has not been a problem. Adding more spatial configurations (those with $S_{\pi,\nu} = 1$ or $\frac{3}{2}$ for even or odd number of nucleons) allowed the description of up to nine bands [67, 69].

The matrix elements of the Hamiltonian in the pseudo-$SU(3)$ model are still calculated using Eq. (2.83), introduced in Chapter 2. It should be noted though that some of the terms in the Hamiltonian may need a rescaling of their parameters in order to reflect the effect of the pseudo-spin transformation on the corresponding operator (as it is the case for the $Q.Q$ operator that we will comment in detail later).

3.5 Electromagnetic Transition Operators in the Pseudo-$SU(3)$ Model

Similar to Chapter 2, we conlude this chapter by giving the form of the electromagnetic transition operators used in the pseudo-$SU(3)$ model. Starting from the definition of these operators given in Eq. (2.86), namely:

$$\begin{aligned} T^1_\mu(M) &= \sqrt{\frac{3}{4\pi}}\mu_N \sum_\sigma \{g^o_\sigma L^\sigma_\mu + g^s_\sigma S^\sigma_\mu\}, \\ T^2_M(E) &= \sqrt{\frac{5}{16\pi}} b^2_0 \sum_\sigma e_\sigma Q^\sigma_M, \end{aligned} \tag{3.23}$$

and employing the pseudo-$SU(3)$ tensorial expressions for the orbital and spin angular momentum operators and that of the quadrupole operator (see Eq. (D.5) from Appendix D), the transition operators can be written as

$$\begin{aligned} \mathcal{T}^{J_0}_{M_0} &= \sum_{\sigma=\pi,\nu} \mathcal{T}^{J_0}_{M_0}(\sigma) \\ &= \sum_\sigma A_{J_0} C^{J_0}_t(\tilde{\eta}; \tilde{\lambda_0}, \tilde{\mu_0}, \tilde{\kappa_0}, \tilde{L_0}, \tilde{S_0}) \\ &\quad \times \{a^\dagger_{(\tilde{\eta_\sigma},0)1/2} \otimes a^\dagger_{(0,\tilde{\eta_\sigma}),1/2}\}^{(\tilde{\lambda_0},\tilde{\mu_0});\tilde{S_0},J_0}_{\tilde{\kappa_0}\tilde{L_0}\quad M_0}, \end{aligned} \tag{3.24}$$

where

$$\begin{aligned} A_1 &= \sqrt{\frac{3}{4\pi}}\mu_N, \\ A_2 &= \sqrt{\frac{5}{16\pi}} b^2_0, \\ A_3 &= \sqrt{\frac{105}{16\pi}}\mu_N b^2_0, \end{aligned} \tag{3.25}$$

and the tensor expansion coefficients can be evaluated using Eq. (D.6) from Appendix D.

From Eq. (3.23) we see immediately that the tensorial coefficients for the magnetic dipole transition operator can be written as

$$\begin{aligned} C^1_t(\tilde{\eta_\sigma};\tilde{\lambda_0},\tilde{\mu_0},\tilde{\kappa_0},\tilde{L_0},\tilde{S_0}) = \quad & g^o_\sigma C^1_l(\tilde{\eta_\sigma};\tilde{\lambda_0},\tilde{\mu_0},\tilde{\kappa_0},\tilde{L_0},\tilde{S_0}) \\ & + g^s_\sigma C^1_s(\tilde{\eta_\sigma};\tilde{\lambda_0},\tilde{\mu_0},\tilde{\kappa_0},\tilde{L_0},\tilde{S_0}), \end{aligned} \tag{3.26}$$

where C^1_l and C^1_s are the coefficients of the orbital and spin angular momenta, respectively. To calculate these two coefficients, we need to calculate first the reduced matrix elements of $\mathbf{l}$ and $\mathbf{s}$ with respect to the single-particle states (see Eq. (2.88)) and then substitute the result in the Eq. (D.5) derived in Appendix D. The result is

$$\begin{aligned} & C^1_l(\tilde{\eta};\tilde{\lambda_0},\tilde{\mu_0},\tilde{\kappa_0},\tilde{L_0},\tilde{S_0}) = \\ & \sum_l \sum_{j,j'} [2(2l+1)l(l+1)/(2j+1)]^{1/2} \chi \begin{Bmatrix} l & \frac{1}{2} & j \\ l & \frac{1}{2} & j' \\ 1 & 0 & 1 \end{Bmatrix} \\ & B^1(j,j',\tilde{l},\tilde{l'};\tilde{\eta_\sigma};\tilde{\lambda_0},\tilde{\mu_0},\tilde{\kappa_0},\tilde{L_0},\tilde{S_0}), \end{aligned} \tag{3.27}$$

$$\begin{aligned} & C^1_s(\tilde{\eta};\tilde{\lambda_0},\tilde{\mu_0},\tilde{\kappa_0},\tilde{L_0},\tilde{S_0}) = \\ & \sum_l \sum_{j,j'} [(3/2)(2l+1)/(2j+1)]^{1/2} \chi \begin{Bmatrix} l & \frac{1}{2} & j \\ l & \frac{1}{2} & j' \\ 0 & 1 & 1 \end{Bmatrix} \\ & B^1(j,j',\tilde{l},\tilde{l'};\tilde{\eta_\sigma};\tilde{\lambda_0},\tilde{\mu_0},\tilde{\kappa_0},\tilde{L_0},\tilde{S_0}), \end{aligned} \tag{3.28}$$

where the abbreviation,

$$\begin{aligned} & B^1(j,j',\tilde{l},\tilde{l'};\tilde{\eta_\sigma};\tilde{\lambda_0},\tilde{\mu_0},\tilde{\kappa_0},\tilde{L_0},\tilde{S_0}) = \\ & (-1)^\eta \sqrt{\frac{2j+1}{2j_0+1}} \chi \begin{Bmatrix} \tilde{l} & \frac{1}{2} & j \\ \tilde{l'} & \frac{1}{2} & j' \\ \tilde{L_0} & \tilde{S_0} & 1 \end{Bmatrix} \langle (\tilde{\eta},0)\tilde{l};(0,\tilde{\eta})\tilde{l'} \| (\tilde{\lambda_0},\tilde{\mu_0})\tilde{\kappa_0}\tilde{L_0}\rangle, \end{aligned} \tag{3.29}$$

has been used.

The tensorial coefficients for the electric quadrupole transition operator are given by

$$C^2_t(\tilde{\eta_\sigma};\tilde{\lambda_0},\tilde{\mu_0},\tilde{\kappa_0},\tilde{L_0},\tilde{S_0}) = e_\sigma C^2_q(\tilde{\eta_\sigma};\tilde{\lambda_0},\tilde{\mu_0},\tilde{\kappa_0},\tilde{L_0},\tilde{S_0}), \tag{3.30}$$

where the expression for the C^2_q coefficient is:

$$\begin{aligned} & C^2_q(\tilde{\eta_\sigma};\tilde{\lambda_0},\tilde{\mu_0},\tilde{\kappa_0},\tilde{L_0},\tilde{S_0}) = \\ & \sum_{l,l'} \sum_{j,j'} [8(2l+1)C_2(\eta_\sigma,0)/(2j+1)]^{1/2} \langle (\eta_\sigma,0)l';(1,1)12 \| (\eta_\sigma,0)l\rangle \\ & \chi \begin{Bmatrix} l & \frac{1}{2} & j \\ l & \frac{1}{2} & j' \\ 2 & 0 & 2 \end{Bmatrix} B^2(j,j',\tilde{l},\tilde{l'};\tilde{\eta_\sigma};\tilde{\lambda_0},\tilde{\mu_0},\tilde{\kappa_0},\tilde{L_0},\tilde{S_0}). \end{aligned} \tag{3.31}$$

Finally, it should be noted that if the tilde is removed from the quantum labels and the symmetry and orthogonality properties of the unitary $9j$ and $SU(3) \supset SO(3)$ coupling coefficients are used, one will recover the tensor coefficients given in Eq. (2.89) for the normal case.

Chapter 4

Shell-Model Calculations for Upper fp-shell Nuclei

While the models presented in Chapters 2 and 3 were very successful for the description of a variety of characterisics of ds-shell nuclei and rare-earth/actinide species, respectively, a similar approach has never been used for the nuclei in the region between these two, namely, the nuclei of the fp shell. For the lower fp-shell (nuclei like ^{44}Ti, ^{48}Cr), it is known that the SU(3) symmetry is broken by the spin-orbit interaction [70]. Despite some earlier results [45, 71] on the pseudo-SU(3) quality for the upper-fp nuclei, the use of pseudo-SU(3)-symmetry-based models has never been justified.

In this chapter, we perform calculations using realistic interactions in a model space including the upper fp-shell plus the intruder $g_{9/2}$ level and further discuss to what extent the results favor the introduction of a symmetry-adapted model that is our ultimate goal. This is done by exploration of several nuclear observables, namely, the low-lying energy spectra, B(E2) transition strengths and the single-particle occupancy. Moreover, the pseudo-SU(3) symmetry of the low-lying eigenstates is examined by calculating the spectral distribution of the second order Casimir invariant of pseudo-$SU(3)$.

As a result of this study, we conclude that although not of the same quality as the one found in heavier rare-earth nuclear systems, reasonably good pseudo-$SU(3)$ symmetry is observed primarily in the vicinity of the N=Z line. Specifically, many of the low-lying eigenstates for these isotopes are described at the level of 50% up to 60% by using only the leading irrep. Adding a reasonable number of adjacent in C_2 value irreps can improve the overlap to 70% and even 80%. Even though this kind of dominance tends to disappear away from the N=Z line and also diminishes with growing mass number A along it, in these heavier isotopes an effect of clusterization is observed which still allows one to build a truncated space, using only 2-3 irreducible (although not necessarily the first 2-3 in the order of decreasing C_2 value) irreps and achieve similar truncation effect. This, along with the fact that only some of the configurations contribute significantly to the correct description of the studied physical quantities, serves as a sufficient proof for the introduction and use of a pseudo-SU(3) based model.

4.1 Upper fp-shell Nuclei and Methods for Their Study

Upper fp-shell nuclei are interesting systems which have received a lot of attention for dozens of reasons over the years. Some of them actively participate in the processes of nucleosynthesis, more specifically, in the rapid proton capture - a fast process responsible for energy production and element synthesis in x-ray binary stellar systems. In addition, N=Z systems from this region are the preferred source of information on the competition between the isovector ($T = 1$) and the isoscalar ($T = 0$) pairing terms. These are transitional nuclei with competitive pairing and quadrupole-quadrupole modes. The region also allows the study of long chains of isotopes (isotones). Finally, these nuclei are known to come in variety of shapes and even to display shape coexistence effects [72, 73].

From computational point of view, these systems are attractive, since the upper-fp shell is the lightest domain where the intruder levels penetrate into the lower-lying shell. Model spaces are still of reasonable size, so full-space calculations are feasible, even though sometimes at the limit of today's computational capabilities. For these reasons, the region seems the most appropriate one for a first attempt to probe an extended SU(3) model with active intruder levels and learn valuable lessons during the process needed for its future development elsewhere.

Currently, shell-model calculations in the full fp shell are doable, but adding the $g_{9/2}$ intruder level to the active configuration space takes one beyond the computational reach provided by even the best of modern day supercomputers. Because of this, researchers have focused their attention on the addition of the intruder level to the upper-fp shell, which is the fp shell less its lowest-lying $f_{7/2}$ orbital. This choice is supported whenever the lowest-lying $f_{7/2}$ level may be considered inactive and part of an inert core. Although, in principle, an effective field theory should be able to provide an interaction in any subspace of the full Hilbert space, there are still only a few interactions for this choice of model space and some of them are just phenomenological [72, 74, 75]. Calculations involving two adjacent shells are even further out of reach, being performed only for the lower-lying combination of the ds and fp shells [76].

Various shell-model computer codes have been developed over the years. Some of them use a basis of good J values, others - of good M_J values. Some of these codes are capable of solving a matrix on the order of 10^8 and even pushed up to 10^9 [77], others have more modest capabilities [78]. In our calculations we used the so-called Glasgow code [78], developed in the early eighties, which uses a basis of good M_J values. This code allowed us to perform calculations in model spaces up to $\approx 10^6$. Although about 3 orders down from the best of today's achievements, this code was adequate for our needs. As with any tool for large scale calculations, the code should have an effective method for solving the eigenvalue problem. One such method is the Lanczos algorithm.

The Lanczos algorithm is an effective scheme for obtaining a small number of eigenvectors corresponding to the lowest or highest eigenvalues [79, 80]. It has been

applied successfully to spatial dimensions on the order of 10^6 and even pushed up to 10^8 [81]. This algorithm is a simple and very efficient method to build a basis of the Hilbert space associated with an eigenvalue problem for an operator H. In its simplest form, one starts with a trial state and applies H over and over to generate new states; the process can be applied as many times as desired. This way one generates an orthonormal basis in which the corresponding matrix of the operator is tri-diagonal. The method is recursive and could be used in numerical, as well as in analytical calculations [82]. For the calculations in nuclei, a numerical matrix realization has been more suitable due to the Fock representation of the states.

Our task is to see to what extent a symmetry-adapted model can be relevant and useful for a description of the upper fp-shell nuclei. Although the energy spectra of interest are not typically highly rotational in nature, various theoretical predictions report on reasonably high values for $B(E2)$ transition strengths which suggest such collectivity. This has been confirmed to some extent by recent experiments [83, 84, 85, 86] .

To benchmark the benefit of the SU(3) scheme in this region (pseudo-SU(3) for the upper-fp shell and normal SU(3) for the $g_{9/2}$ configurations extended to the full gds shell), we first generated results in a standard m-scheme representation for a group of $N \approx Z$ upper-fp shell nuclei with valence nucleons distributed across the $p_{1/2}, p_{3/2}, f_{5/2}, g_{9/2}$ model space with the $f_{7/2}$ level considered to be fully occupied and part of a ^{56}Ni core. The Hamiltonian we used is a G-matrix with a phenomenologically adjusted monopole part [87, 88, 89] that in many cases describes the experimental energies reasonably well. Specifically, this upper-$fp + g_{9/2}$ shell interaction was succesfully used in the past to obtain quite good results for nuclei like ^{62}Ga [85], ^{76}Ge and ^{82}Se [87]. Later, it was applied for exploring the pseudo-SU(4) symmetry in the region from the beginning of the upper fp-shell up to $N = 30$ and for describing related beta decays [90].

4.2 Energy Spectra, Single-Particle Occupation Numbers and B(E2) Transition Strengths

We choose to work with both odd-odd and even-even nuclei. As a whole, the realistic interaction gives very reasonable results for many of the upper fp-shell nuclei. It turns out to be successful beyond the nuclei for which it was designed to be used (^{58}Cu, ^{60}Ni, ^{62}Ga, ^{60}Zn). Specifically, reasonably good results for ^{58,62,64,66}Ni, ^{60}Cu, ^{62,64}Zn have been also obtained. Moreover, the renormalized interaction in the smaller $pf_{5/2}$ space produces similar spectra, which makes it a valuable tool in the evaluation of the symmetry properties of these nuclei.

Unfortunately, there is no universal interaction for this model space such as, for example, the Kuo-Brown-3 interaction [91] for lower fp-shell nuclei, or the Wildenthal interaction [92] for the ds shell. Indeed, the use of the $pf_{5/2}g_{9/2}$ interaction sometimes leads to deviations from the experimental spectra, which for the odd-odd species happens very soon along the Cu and Ga isotope chain. An example

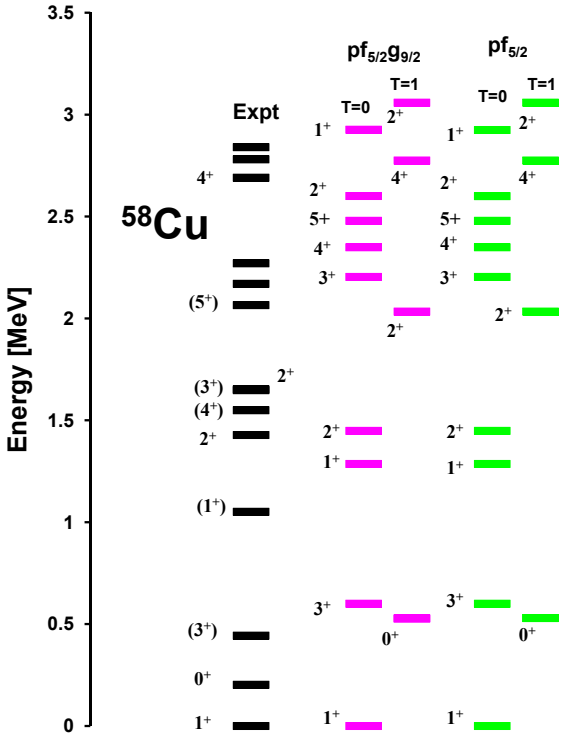

Figure 4.1: Calculated low-energy spectra of ^{58}Cu in the full $pf_{5/2}g_{9/2}$ (magenta) and $pf_{5/2}$ (green) model spaces compared to experimental results (black).

of such deviations is the shifting of the spin value for the ground state. The only isotope chain we are able to describe well consists of the zinc isotopes ^{60}Zn, ^{62}Zn, ^{64}Zn. Nevertheless, as we will see below, this partial success turns out to be quite rewarding.

In this study, we will focus on a description of the N=Z nuclei. The first spectrum is for the odd-odd ^{58}Cu (Fig. 4.1) nucleus. This is an interesting nucleus since it is the only odd-odd N=Z isotope which has a ground state with isospin $T = 0$. In other nuclei it is $T = 1$. There is relatively little recent experimental information on the B(E2) transition strengths. What is available is shown in Table 4.1 where it is compared with the realistic predictions, obtained with the value for the effective charge of $e_{eff} = 0.5$. The results suggest that theory does not appropriately take account of some core polarization effects as it underestimates the values for these transitions.

Next we consider results for the odd-odd nucleus ^{62}Ga. In this case the theoretical spectrum is close in character and agrees with experiment (Fig. 4.2). The only experimental information on B(E2) strengths is for the transition $3^+_1 \rightarrow 1^+_1$ which has a value of B(E2; $3^+_1 \rightarrow 1^+_1$)=197(69) e^2fm^4 [85] which agrees with our theoretical prediction (Table 4.2). This suggests that the core polarization effects referred to above in the ^{58}Cu case seem to no longer be an issue for this nucleus.

Table 4.1: B(E2) transition strengths for ^{58}Cu in units of $[e^2fm^4]$. Data is taken from [83] and [84].

J_i, T_i	J_f, T_f	$B(E_2; J_i \to J_f)$ $[e^2fm^4]$			J_i, T_i	J_f, T_f	$B(E_2; J_i \to J_f)$ $[e^2fm^4]$		
		Exp	$pf_{5/2}$	$pf_{5/2}g_{9/2}$			Exp	$pf_{5/2}$	$pf_{5/2}g_{9/2}$
$3_1, 0$	$1_1, 0$	101(18)	39.628	39.602	$1_2, 0$	$3_1, 0$	–	1.588	1.583
$1_2, 0$	$1_1, 0$	–	48.388	48.904	$2_1, 0$	$3_1, 0$	–	19.123	19.019
$2_1, 0$	$1_1, 0$	–	34.359	33.621	$2_2, 1$	$3_1, 0$	2^{+9}_{-2}	2.161	2.213
$2_2, 1$	$1_1, 1$	< 60	5.636	5.774	$2_1, 0$	$1_2, 0$	–	31.58	30.826
$2_1, 0$	$0_1, 1$	–	0.461	0.562	$2_2, 1$	$1_2, 0$	–	2.179	2.31
$2_2, 1$	$0_1, 1$	122(47)	39.941	38.737	$2_2, 1$	$2_1, 0$	–	1.964	1.938

Table 4.2: B(E2) transition strengths for ^{62}Ga in units of $[e^2fm^4]$. Data is taken from [85].

J_i, T_i	J_f, T_f	$B(E_2; J_i \to J_f)$ $[e^2fm^4]$		J_i, T_i	J_f, T_f	$B(E_2; J_i \to J_f)$ $[e^2fm^4]$	
		$pf_{5/2}$	$pf_{5/2}g_{9/2}$			$pf_{5/2}$	$pf_{5/2}g_{9/2}$
$2_1, 1$	$0_1, 1$	195.39	188.79	$3_1, 0$	$1_1, 0$	32.701	24.745
$2_2, 0$	$0_1, 1$	0.04	0.017	$2_1, 1$	$1_2, 0$	0.458	0.359
$3_1, 0$	$1_1, 0$	141.14	141.18	$2_2, 0$	$1_2, 0$	182.89	175.79
$2_1, 1$	$1_1, 0$	0.091	0.035	$2_1, 1$	$3_1, 0$	0.712	0.749
$2_2, 0$	$1_1, 0$	4.606	8.74	$2_2, 0$	$3_1, 0$	12.856	13.018

The low-energy bands in the even-even nuclei ^{60}Zn and ^{64}Ge are shown in Fig. 4.3 and 4.4. The description is reasonable for the g.s. band in ^{60}Zn and the g.s. and the gamma bands in ^{64}Ge. Also, the existence of a possible beta (K=0) band is predicted in ^{64}Ge. Experimental data on B(E2) transition strengths are even more scarce for these nuclei. There is no experimental information for the transition strengths for ^{60}Zn and for ^{64}Ge some results are given in [86].

Calculations with different cuts of the full model space were done in order to evaluate the relative importance of various configurations for describing essential nuclear characteristics. Results from the examination of the low-energy spectrum (Fig. 4.5) and the B(E2) transition strengths (Table 4.3) for ^{64}Ge suggest that by taking all configurations with up to 2 protons and 2 neutrons for a total of 4 particles in the $g_{9/2}$ level one is able to very closely reproduce the full-model results.

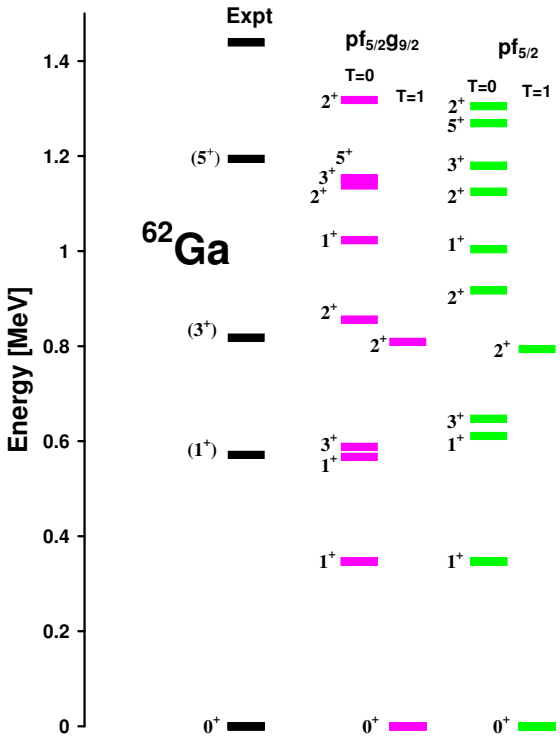

Figure 4.2: Calculated low-energy spectra of ^{62}Ga in the full $pf_{5/2}g_{9/2}$ (magenta) and $pf_{5/2}$ (green) model spaces compared to experimental results (black).

The occupancy of the single-particle levels was also estimated in various model spaces. In Fig. 4.6, a comparison is made between the occupancies for ^{64}Ge as determined in a restricted basis, where at most two particles (protons/neutrons) are allowed in the $g_{9/2}$ level, and the full-space resuls. The upper (yellow) bars show the contribution to occupations from basis states with an occupied intruder level while the lower (blue) portion represents those where the intruder level is empty. The calculated results suggest that the occupancy probability for the intruder level is approximately 0.3 particles for the low-lying states of ^{64}Ge. Calculations with no particles allowed in the intruder level, or with just one identical-particle (or proton-neutron) pair (Fig. 4.6 (a) and (b)), cannot describe either its occupancy or the gradual change in the occupancy of the single-particle levels in the ground-state (g.s.) band that is found in the full-model-space results. However, using a restricted space with at most two identical particles occupying the intruder level (in Fig. 4.6 (e)) is sufficient to describe both features. Similar results were observed for the $K = 2^+$ band of this nucleus, and a comparison between the outcome within the full and a restricted model space is presented in Fig. 4.7. As expected, calculations for ^{68}Se performed in a truncated basis with at most 2 nucleons allowed in the intruder level produce a slighlty higher $g_{9/2}$ occupancy compared to ^{64}Ge. These are given in Fig. 4.8.

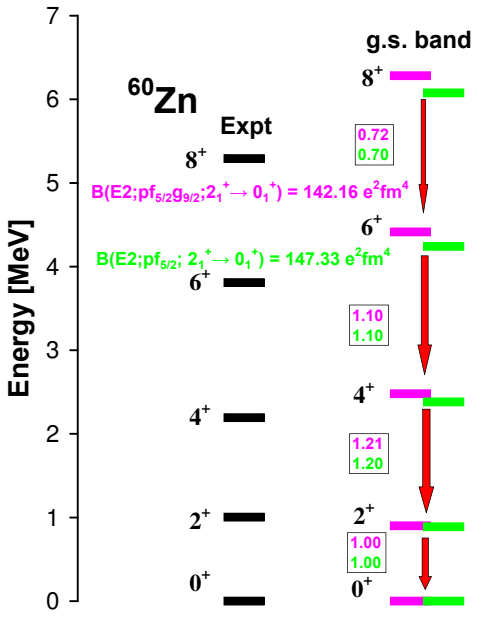

Figure 4.3: Band structure for ^{60}Zn obtained in the full $pf_{5/2}g_{9/2}$ (magenta) and $pf_{5/2}$ (green) model spaces compared to the experimental data. The numbers in the boxes represent the ratio between specific transitions and the B(E2; $2_1^+ \rightarrow 0_{g.s.}^+$). The width of the arrows corresponds to the intensity of the transition.

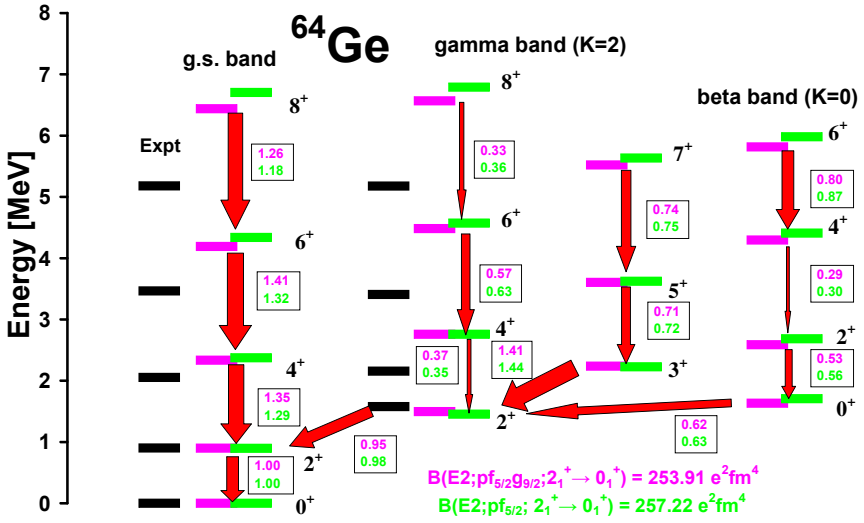

Figure 4.4: Band structure for ^{64}Ge obtained in the full $pf_{5/2}g_{9/2}$ (magenta) and $pf_{5/2}$ (green) model spaces compared to experimental data [93]. The numbers in the boxes represent the ratio between a certain transition and the B(E2; $2_1^+ \rightarrow 0_{g.s.}^+$) The width of the arrows corresponds to the intensity of the transition.

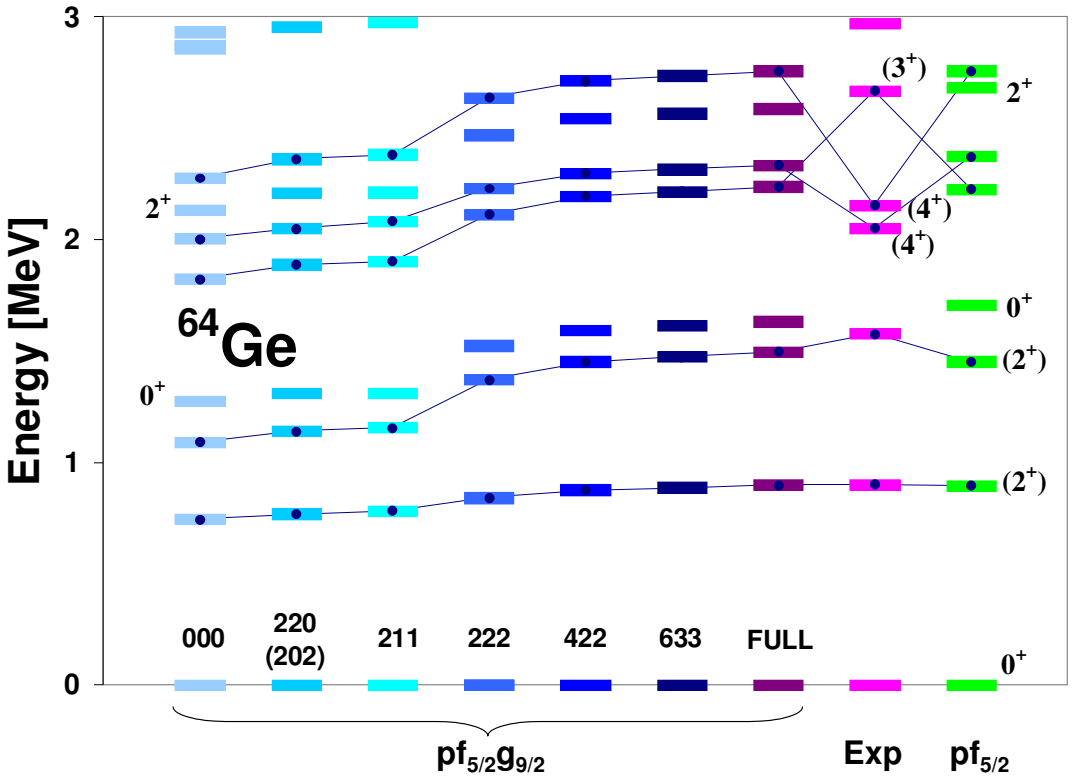

Figure 4.5: Energies of the low-lying states in ^{64}Ge calculated in different truncated spaces. The labels TPN for each restricted-space calculation represent the maximum total number of particles T, and the maximum number of protons P (and neutrons N) allowed in the intruder $g_{9/2}$ level.

Table 4.3: B(E2) transition strengths between the low-lying states in ^{64}Ge in units of $[e^2fm^4]$ calculated in different truncated spaces. The labels TPN for each restricted-space calculation have the same meaning as the ones in Fig. 4.5.

transition	000	211	222	422	full	$pf_{5/2}$
$2_1 \rightarrow 0$	223.18	236.96	252.75	254.09	253.94	257.22
$2_2 \rightarrow 0$	6.51	1.09	1.17	1.27	1.42	1.99
$2_2 \rightarrow 2_1$	334.69	337.37	255.26	248.21	241.41	251.68
$0_2 \rightarrow 2_1$	41.09	53.87	50.22	43.6	38.95	52.92
$0_2 \rightarrow 2_2$	310.06	254.18	171.08	163.69	157.49	161.00
$3_1 \rightarrow 2_1$	9.12	1.18	2.75	3.05	3.40	4.21
$3_1 \rightarrow 2_2$	317.61	334.37	354.63	356.75	357.79	371.15
$4_1 \rightarrow 2_1$	218.72	276.60	338.09	341.47	342.51	332.54
$4_1 \rightarrow 2_2$	93.95	49.96	5.96	3.91	2.73	9.81
$4_1 \rightarrow 3_1$	21.89	37.79	69.88	75.77	79.57	45.47

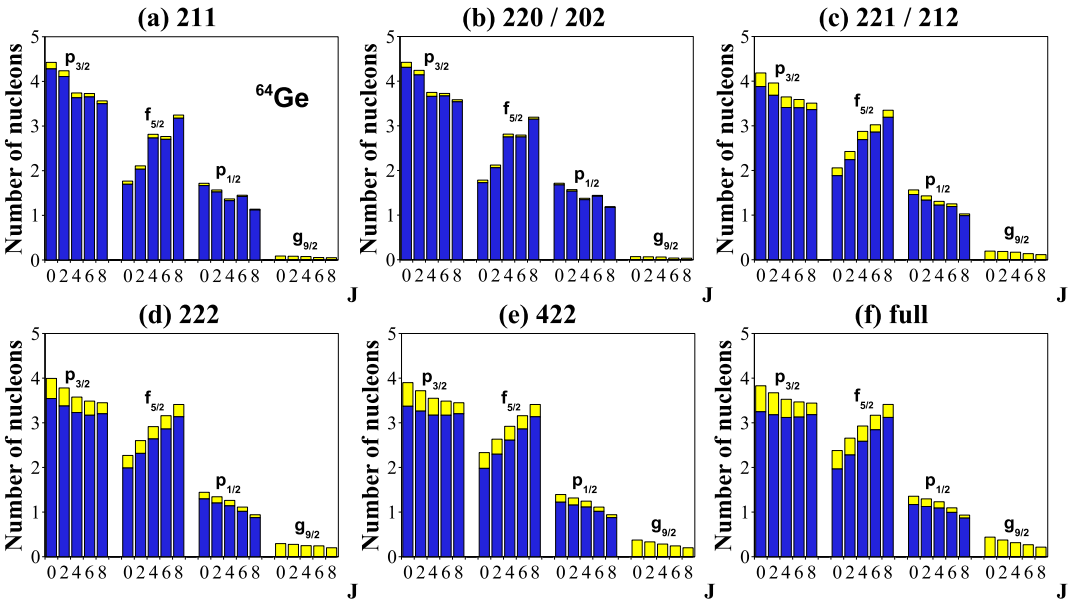

Figure 4.6: Single-particle occupation numbers for eigenstates of the g.s. band of ^{64}Ge calculated in different restricted model spaces (from (a) to (e)) and the full space (f). The labels TPN over each restricted-space calculation have the same meaning as the ones in Fig. 4.5.

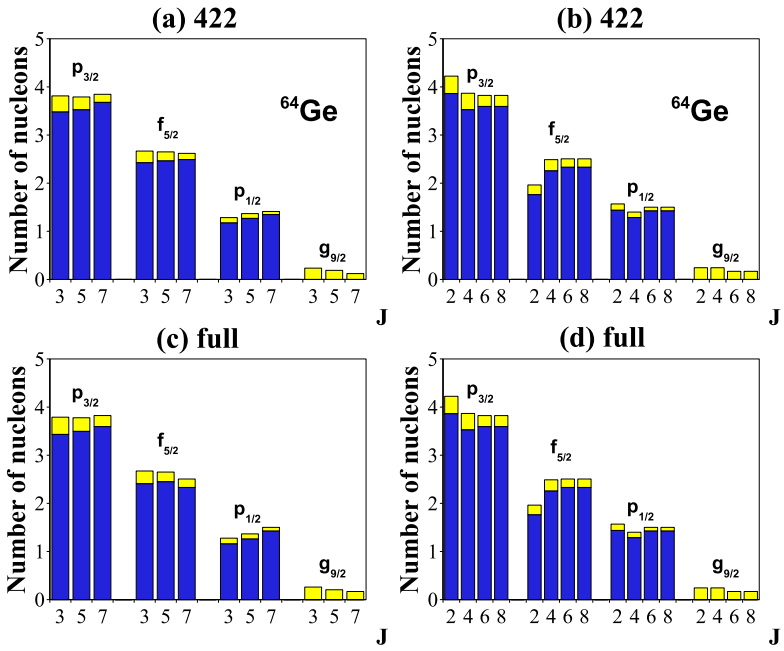

Figure 4.7: Single-particle occupation numbers for eigenstates of the $K = 2$ (gamma) band of ^{64}Ge in the TPN=422 restricted model space ((a) and (b)) and the full space ((c) and (d)). The labels TPN over each restricted-space calculation have the same meaning as the ones in Fig. 4.5.

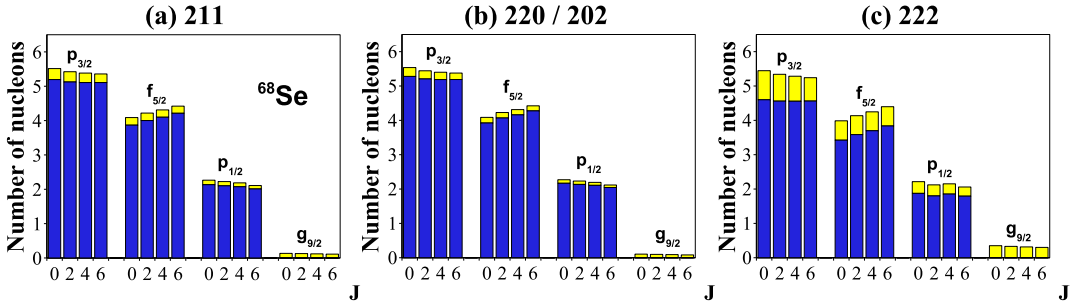

Figure 4.8: Single-particle occupation numbers for eigenstates of the g.s. band of ^{68}Se calculated in different restricted model spaces. The labels TPN over each restricted-space calculation have the same meaning as the ones in Fig. 4.5.

4.3 Evaluation for the Goodness of the Pseudo-SU(3) Symmetry

The goodness of the pseudo-SU(3) symmetry in the upper fp-shell nuclei was tested using a renormalized version of the same realistic interaction in the $pf_{5/2}$ space [90]. The matrix of the second-order Casimir operator of pseudo-SU(3), $C_2 = \frac{1}{4}(3\hat{L}^2 + Q.Q)$, was generated and the method of moments [78] used to diagonalize this matrix by starting the Lanczos procedure with specific eigenvectors of the Hamiltonian for which a pseudo-SU(3) decomposition was desired. Although the procedure provides distributions only over the C_2 values (and not over the actual (λ, μ) irreps), this analysis is quite useful and gives valuable information about the structure of certain eigenstates.

Results presented in Table 4.4 suggest that the symmetry is quite good for all of the ten lowest-lying eigenstates in both odd-odd and even-even nuclei. In particular, for most states this translates into between 60-70% contribution coming from the leading irrep in each of these nuclei. It is quite remarkable that this is the case in both odd-odd and even-even nuclei. Results for some Ni and other isotopes are shown in Table 4.5 and Table 4.6, respectively.

Now we will comment in a little more detail on the pseudo-SU(3) symmetry results for the nuclei ^{64}Ge and ^{68}Se, since these will be the object of special attention in the last chapter. The distribution of the second order Casimir operator C_2 of pseudo-SU(3) yields contributions of about 50-60% from the leading pseudo-SU(3) irrep in the g.s. band of ^{64}Ge (Fig. 4.9(a)) which suggests that the pseudo-SU(3) symmetry is quite good. In the $K = 2^+$ band (Fig. 4.9 (c) and (d)) this contribution appears to be somewhat lower, ranging from approximately 37% for the 8_2^+ state to about 62% in the 3_1^+ state. The analysis also reveals that using only five irreps which have the highest C_2 value one may take account of at least 70% and up to about 95% of the wavefunction for the states in these bands.

In the case of ^{68}Se, the outcome turns out to be quite similar for the states from the g.s. band (Fig. 4.9(b)). Although the irreps with the maximal value of $C_2 = 180$ participate with only between about 40% and 50%, the first eleven irreps with distinct values of λ and μ account for 88-93% of the wavefunction. In addition, the 0_3^+ state at 2.51 MeV is also dominated (64%) by irreps with the biggest C_2 value. However, other states are predicted to be highly-mixed SU(3) configurations. This includes the 0_2^+ state found at 1.05 MeV - a value very similar to the ones reported in [72, 73] for a low-lying state of prolate shape.

The behavior away from the N=Z line was also studied by means of the Zn chain of isotopes. In Fig. 4.10, one can see very similar behavior to that in the transition from ^{64}Ge to ^{68}Se. Namely, instead of dominance of the leading irrep (as is the case for ^{64}Ge and ^{60}Zn), first some fragmentation builds up (^{62}Zn) with part of the contribution redistributed to other still adjacent irreps which further goes into more distant ones (the cases of ^{64}Zn shown in Fig. 4.10 (c)). This behavior cannot be simply explained by saying that certain C_2 values are not allowed for some J values. Indeed, for the $J = 0$ states in ^{68}Se the irreps $(\lambda, \mu) = (9, 3)$ and

Table 4.4: Pseudo-$SU(3)$ symmetry in low-lying states of some $N = Z$ upper fp-shell nuclei. The entries without any subscripts represent the contribution (in percentages) from the irrep(s) with the largest C_2 value. The subscripts in the rest of the data denote the number of irreps with distinct values of λ and μ that are needed to achieve the indicated level of overlap with the realistic eigenstates.

J	^{58}Cu	J	^{60}Zn	J	^{62}Ga	J	^{64}Ge	J	^{68}Se
1_1	81.42	0_1	54.93 $(93.67)_3$	0_1	54.53 $(73.54)_3$ $(92.35)_6$	0_1	51.13 $(63.33)_3$ $(90.41)_{10}$	0_1	40.89 $(72.59)_7$ $(90.38)_{11}$
0_1	72.65	2_1	59.03 $(95.41)_3$	1_1	46.56 $(73.62)_3$	2_1	57.92 $(73.37)_3$	2_1	43.60 $(76.53)_7$
3_1	89.6	4_1	73.99 $(98.83)_3$	1_2	40.18 $(61.27)_3$	2_2	47.01 $(53.75)_3$	0_2	11.03 $(20.47)_7$
1_2	71.99	0_2	16.43 $(78.32)_3$	3_1	66.02 $(86.23)_3$	0_2	12.7 $(25.02)_3$	4_1	45.99 $(79.20)_7$
2_1	92.55	2_2	20.06 $(78.34)_3$	2_1	57.5 $(79.68)_3$	3_1	62.03 $(70.56)_3$	2_2	30.30 $(48.24)_7$
2_2	69.07	1_1	0 $(87.38)_3$	2_2	41.66 $(66.38)_3$	4_1	61.81 $(81.45)_3$	0_3	63.67 $(69.96)_7$
3_2	83.96	2_3	0.21 $(64.89)_3$	1_3	72.63 $(80.03)_3$	2_3	27.42 $(37.48)_3$	3_1	0 $(35.25)_7$
4_1	100	6_1	83.91 $(99.75)_3$	2_3	79.63 $(85.33)_3$	4_2	55.4 $(64.49)_3$	2_3	17.27 $(46.10)_7$
5_1	100	1_2	0 $(81.75)_3$	3_2	31.55 $(59.75)_3$	1_1	0 $(52.25)_3$	4_2	0 $(11.75)_7$
2_3	0.02	3_1	0 (86.2)	5_1	69.54 $(85.38)_3$	2_4	7.16 $(16.07)_3$	1_1	0 $(44.75)_7$

Table 4.5: Pseudo-$SU(3)$ symmetry in low-lying states of some Ni isotopes. Notation is the same as in Table 4.4.

J	^{58}Ni	J	^{60}Ni	J	^{62}Ni	J	^{64}Ni	J	^{66}Ni
0_1	72.65	0_1	80.54	0_1	68.03	0_1	67.72	0_1	73.85
			$(83.67)_3$		$(76)_3$		$(76.76)_3$		
2_1	69.07	2_1	78.48	2_1	64.84	2_1	69.95	2_1	86.80
			$(90.33)_3$		$(82.7)_3$		$(83.82)_3$		
4_1	92.94	2_2	46.23	2_2	64.97	2_2	50.56	2_2	2.04
			$(66.40)_3$		$(90.45)_3$		$(79.6)_3$		
2_2	15.55	2_3	12.32	0_2	69.25	0_2	2.08	3_1	0
			$(74.88)_3$		$(91.93)_3$		$(29.07)_3$		
0_2	0.13	4_1	70.79	1_1	0	3_1	33.49	0_2	25.47
			$(77.22)_3$		$(66.98)_3$		$(60.58)_3$		
1_1	0	3_1	47.05	4_1	28.94	2_3	12.19	4_1	49.48
			$(89.56)_3$		$(95.18)_3$		$(50.4)_3$		
2_3	0.36	1_1	0	0_3	10.39	1_1	0	2_3	9.42
			$(43.04)_3$		$(69.91)_3$		$(77.35)_3$		
3_1	0	0_2	2.85	3_1	0	4_1	74.41	4_2	50.52
			$(49.62)_3$		$(93.15)_3$		$(84.05)_3$		
1_2	0	2_4	2.85	1_2	0	2_4	10.91	1_1	0
			$(49.62)_3$		$(94.99)_3$		$(35.04)_3$		
2_4	4.05	4_2	39.61	2_3	12.28	1_2	0	1_2	0
			$(69.99)_3$		$(71.1)_3$		$(48.11)_3$		

Table 4.6: Pseudo-$SU(3)$ symmetry in low-lying states of some Cu and Zn isotopes. Notation is the same as the one in Table 4.4.

J	^{60}Cu	J	^{62}Zn	J	^{64}Zn
2_1	64.34	0_1	54.54	0_1	33.76
	$(90.06)_3$		$(73.55)_3$		$(46.27)_3$
1_1	69.04	2_1	57.5	2_1	43.88
	$(89.21)_3$		$(79.68)_3$		$(52.88)_3$
1_2	73.33	2_2	44.08	0_2	29.7
	$(89.83)_3$		$(66.35)_3$		$(46.95)_3$
2_2	44.99	4_1	57.32	2_2	3.11
	$(81.72)_3$		$(84.01)_3$		$(33.11)_3$
1_3	34.02	3_1	44.7	4_1	54.95
	$(74.5)_3$		$(70.94)_3$		$(61.49)_3$
3_1	57.84	0_2	1.81	2_3	18.03
	$(85.81)_3$		$(37.58)_3$		$(38.5)_3$
2_3	9.42	0_1	80.68	1_1	0
	$(94.12)_3$		$(46.37)_3$		$(58.69)_3$
4_1	77.74	2_3	4.73	0_3	10.28
	$(96.2)_3$		$(52.79)_3$		$(22.83)_3$
3_2	64.51	4_2	43.16	1_1	0
	$(88.78)_3$		$(70.41)_3$		$(31.61)_3$
1_2	0	2_3	74.07	2_4	9.11
	$(87.72)_3$		$(39.72)_3$		$(43.32)_3$

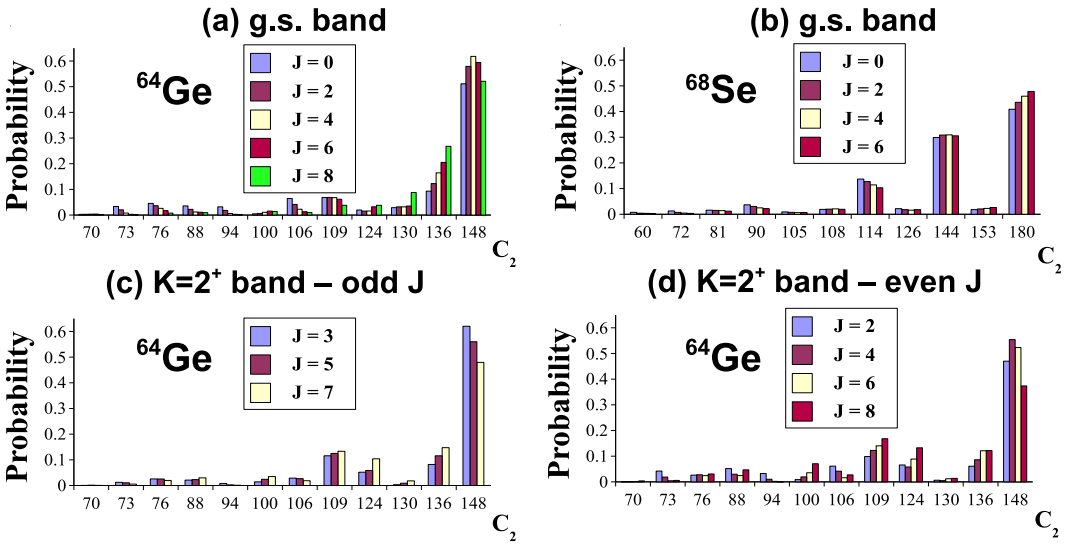

Figure 4.9: Pseudo-SU(3) content of the low-lying states in (a) the g.s. band of ^{64}Ge, (b) the g.s. band of ^{68}Se, and (c) and (d) - the $K = 2^+$ band of ^{64}Ge using the renormalized counterpart of the G-matrix realistic interaction.

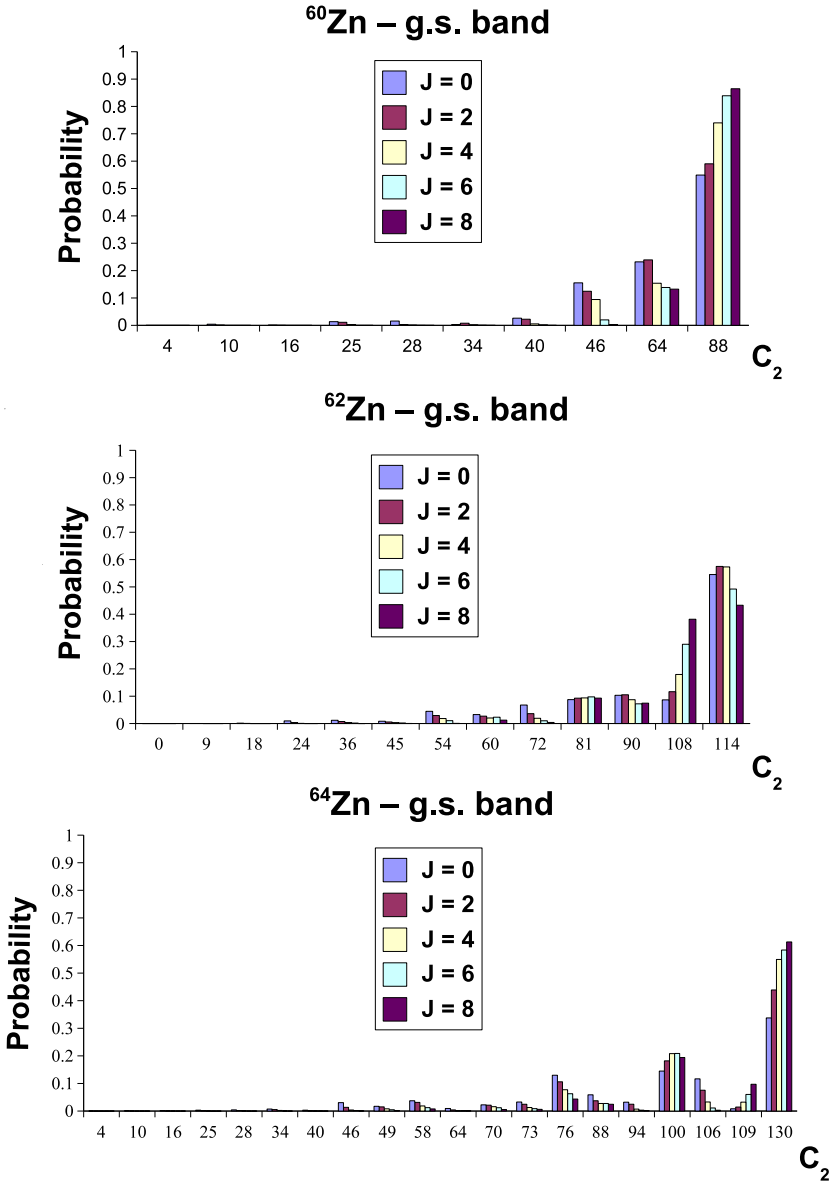

Figure 4.10: Evolution of the pseudo-SU(3) symmetry away from the N=Z line demonstrated for the isotopes of ^{60}Zn, ^{62}Zn and ^{64}Zn.

$(3,9)$ which have $C_2 = 153$ (the second right cluster of bars in Fig. 4.10) and those with $(\lambda,\mu) = (7,4)$ and $(4,7)$ with $C_2 = 126$ (the fourth cluster) are not among the allowed ones for $S = 0$ and the dominance. So, the small contribution may be attributed to the higher importance of the $S = 0$ irreps compared to $S = 1$ ones for low-lying states. However, this is not the case for higher J values and still the contribution is suppressed for the same C_2 values. It seems that the result reflects some properties of the Hamiltonian itself and not just the character of the SU(3) model space.

In summary, the outcome of this study has demonstrated that only part of the configurations are relevant for the structure of the low-lying states in the upper fp-shell nuclei. This along with the results from the pseudo-SU(3) spectral decomposition of the states establishes the validity of a SU(3)-based truncation scheme in $N \approx Z$ upper fp-shell nuclei.

As for the unique-parity spaces, the so-called quasi-SU(3) concept [9, 10, 59, 60, 94] may also be applicable. This symmetry was uncovered in full fp and gds shell-model calculations for even-even [60] and odd-even [94] nuclei. It owes its importance to the dominance of the quadrupole-quadrupole and single-particle terms in a Hamiltonian used to describe well-deformed nuclei. Other terms such as pairing are crucial in determining the observed moments of inertia but most of these effects can be accounted for perturbatively because they introduce small changes in the wavefunctions [95].

The quasi-SU(3) symmetry also leads to an efficient truncation scheme. In shell-model calculations it has been shown that the single-particle levels with $j = l + \frac{1}{2}$ play a dominant role in the low-energy spectra, allowing significant reductions in the size of the Hilbert space [60]. It was also reported [68] that, when a single-particle plus quadrupole-quadrupole Hamiltonian is diagonalized in a SU(3) basis, very few SU(3) irreps are needed to describe the yrast band. The ground state band is built from the $S = 0$ leading irrep, which strongly mixes with the leading $S = 1$ irreps in the proton and neutron subspaces.

The question of how good is the quasi-$SU(3)$ symmetry in the unique-parity spaces is deferred to a follow-on investigation. Since (as we will see below) the role of the unique-parity spaces for the nuclei we deal with is to introduce only some high-order effects, it is relatively safe to accept this to be true throughout the current work.

Chapter 5

Towards an Extended $SU(3)$ Shell Model with Explicitly Included Intruder Levels

Unlike tests for the goodness of the pseudo-$SU(3)$ symmetry, which have been demonstrated in a variety of ways with the only open question being the use of a more modern realistic interaction based, for example, on an effective field theory rather than simplified phenomenological pairing-plus-quadrupole interactions, the problem of taking the abnormal space into active consideration remains a significant challenge for a variety of reasons. First of all, even the most logical choice for an appropriate system for the introduction of such an extended model is not clear. While one might be tempted to first introduce the extension in the area of the rare-earth and actinide nuclei, where pseudo-SU(3) symmetry is good, the inclusion of higher shells which are heavily populated may lead to large mixing effects. In order to avoid these effects, one will probably need to modify the Hamiltonian by adding a term that can "quench" this tendency toward high mixing. One possible choice would be to key in on the total spin of the system which favors the contribution of $S = 0$ basis states to the low-lying states. If this were done, one would end up with a more complicated Hamiltonian which could further introduce additional complications of computational character. Furthermore, higher mixing between configurations with different distribution of particles can also be expected for these nuclei.

On the other hand, the upper fp-shell nuclei seem to be a more amenable candidate since the unique-parity levels in this domain lie one (and even two) shell(s) lower for the protons (neutrons). Still, some drawbacks exist in this case as well, because protons and neutrons lie in the same shell and this implies they strongly interact with each other, so proton-neutron pairing terms have to be introduced in the interaction. Moreover, good systematics on parameters for the quadrupole-quadrupole, pairing and single-particle terms, which exists for light ds-shell or heavy rare-earth nuclei are not available in the case of the upper fp-shell nuclei.

Although the extension of the model from two to four spaces may appear to be just a technical challenge, it is the associated physics that both creates the

biggest challenge and makes this case so interesting. One must keep in mind that approximations are needed because of the complexity of the system. So, most of the answers will not be "black or white" but of the "how" type. How to choose the appropriate basis, what Hamiltonian makes most sense, etc. And accordingly, it must be appreciated that the choices made "qualify" the results.

In this chapter, we introduce the basics of the extended $SU(3)$ shell model for a real (instead of just model) nuclear system as well as the structure of the code used for the calculations performed.

5.1 Basics of the Model

In Chapter 3, we briefly mentioned the intruder and defector levels when we introduce the pseudo-spin concept. It is now time to elaborate on this picture for the nuclei of interest, namely, the upper-fp shell nuclei. A typical shell structure for the upper-fp or medium-mass nuclei is represented in Fig. 5.1. Both protons and neutrons occupy the same oscillator shell. The highest j-level of the fp oscillator shell is pushed down by the strong spin-orbit interaction and lies among the orbitals of the next lower ds shell, and therefore is considered to be a "defector" and part of the inert core. On the other hand, the $g_{9/2}$ "intruder" from the next higher *gds* shell penetrates down into the valence model space. Although it has the opposite parity, it is important that it be included in the model space since this is the only way that experimentally observed states of higher spin and/or opposite parity can be obtained theoretically. Further, it adds to the collective nature of the model space, yielding larger B(E2) values than are otherwise possible.

Following the series of arguments and motivations presented in the previous chapter, we can now introduce the basics of the extended SU(3) shell model. Like its early precursors [3, 12], it is also a microscopic theory in the sense that both SU(3) generators - the angular momentum ($L_\mu, \mu = 0, \pm 1$) and quadrupole ($Q_\mu; \mu = 0, \pm 1, \pm 2$) operators - are given in terms of individual nucleon coordinate and momentum variables. However, as we can see in Fig. 5.1, the model space has a more complicated structure than the one used in earlier models based on the SU(3) symmetry. Specifically, it consists of two parts for each particle type, a normal (N) parity pseudo-shell ($f_{5/2}, p_{3/2}, p_{1/2} \rightarrow \tilde{d}_{5/2}, \tilde{d}_{3/2}, \tilde{s}_{1/2}$) and a unique (or abnormal) (U) parity shell composed of all levels of opposite parity from the *gds* shell above.(Since the normal-unique space distinction will be obvious from context, we will not place tildes over pseudo-space labels as is normally done.)

So far, in almost all investigations of systems with strong spin-orbit interaction where the old pseudo scheme has been applied to the normal parity orbitals, the unique-parity space was assumed to be spanned by configurations of identical particles in only a single-j shell, namely the $\eta + 3/2$ shell [8,53]. The usual argument for neglecting couplings to the energetically higher orbitals ($j < \eta + 3/2$) of the (η+1)-st major shell is based upon the fact that there is an energy difference between these orbitals and the $j = \eta + 3/2$ intruder level which is of the order of the typical major shell separation. Since in a restricted space (as e.g. in a single

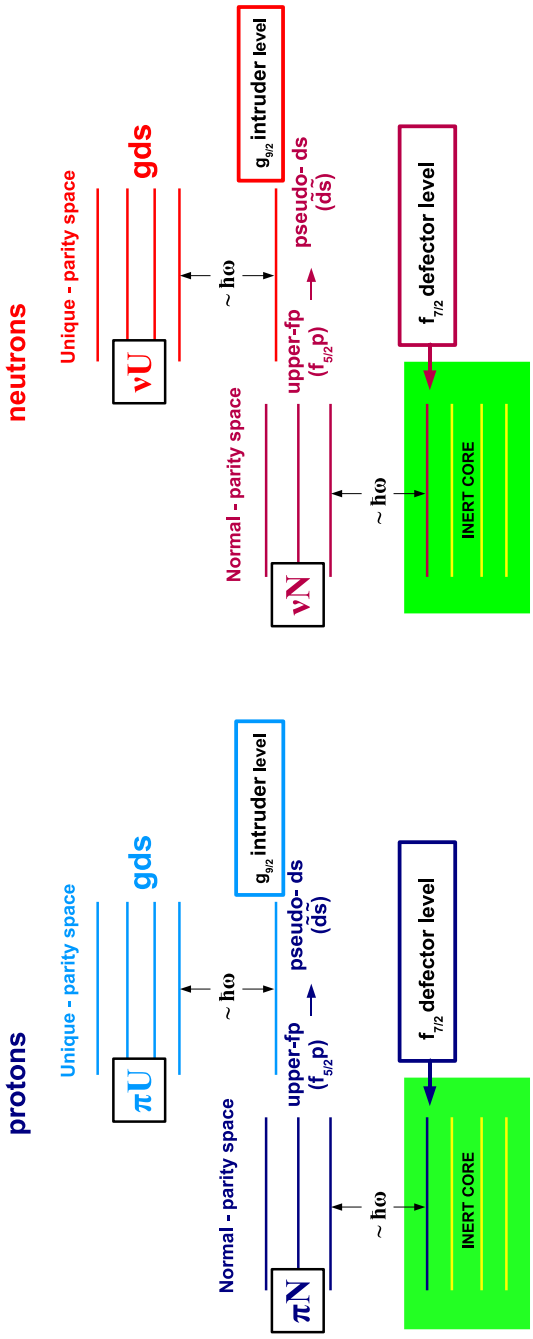

Figure 5.1: Shell structure for the upper fp-shell nuclei.

j-shell) the short-range part of the nucleon-nucleon interaction, which causes pairing correlations, dominates, the energetically most favored state is the seniority zero state, i.e. the one in which all nucleons (except the last one in the case of even-odd nuclei) are paired off to angular momentum zero. In even-even nuclei there is a distinct energy gap ("pairing gap") between this ground state and the first excited state since the excitation involves the decoupling of a pair of nucleons thus yielding a seniority two configuration [96]. The pairing gap is large when compared to the rotational excitation energies, thus considerations of the unique parity space are usually restricted to seniority zero states. In this model, the many-particle basis states for the valence space are given as angular momentum coupled products of pseudo-SU(3) basis states and seniority zero ($J_U = 0$) unique-parity configurations:

$$|\psi_{JM}\rangle = [\Big|\tilde{N}, J_N\Big\rangle \otimes |U, J_U = 0\rangle]^{J=J_N}. \tag{5.1}$$

The seniority-zero restriction is a severe truncation of the unique-parity space that translates into a considerable simplification since angular momentum zero states couple in trivially, affecting only the binding energy while contributing nothing to the overall dynamics of the system. The truncation of the unique-parity levels to low-seniority configurations has been questioned in recent years. Studies in the framework of the "universal" Woods-Saxon and single-shell asymptotic Nilsson models [6] indicate that valence nucleons in the unique-parity intruder orbital contribute significantly to measurable quantities like $B(E2)$ values. Some mean-field theories even claim that the particles in the intruder level play the dominant role in inducing deformation in heavy nuclei [7].

Compared to the models based on the existing (pseudo-)SU(3) symmetry, the novel elements introduced by the extended SU(3) model are:

- it treats particles from the unique-parity space on equal footing with those residing in the normal-parity spaces, i.e. it takes them into active consideration and not through some kind of renormalization procedure;
- it allows for a mixing between configurations with different distribution of particles between the normal- and unique-parity spaces;
- the intruder levels are included along with the rest of the levels from the next shell;
- pn pairing (and pair-scattering) terms are introduced in the SU(3) calculations;
- these terms are included without any imposed restrictions.

5.2 Basis States, Hamiltonian and Matrix Elements

5.2.1 Basis States

Similar to the cases of light and heavy nuclei, for upper-fp shell nuclei, which are of medium mass, the group reduction within the framework of the extended SU(3) shell model has the shape represented in Fig. 5.2. Because of the bigger number of spaces involved, the diagram is more complicated than the one in Fig. 2.2. Nevertheless, it follows a very similar logic.

The many-particle basis states in the extended SU(3) shell model,

$$|\{a_\pi; a_\nu\}\rho(\lambda,\mu)\kappa L, \{S_\pi, S_\nu\}S; JM\rangle \,, \tag{5.2}$$

are built as SU(3) proton (π) and neutron (ν) coupled configurations with well-defined particle number and good total angular momentum. Here, the proton and neutron quantum numbers are indicated by $a_\sigma = \{a_{\sigma N}, a_{\sigma U}\}\rho_\sigma(\lambda_\sigma, \mu_\sigma)$, where the $a_{\sigma\tau} = N_{\sigma\tau}[f_{\sigma\tau}]\alpha_{\sigma\tau}(\lambda_{\sigma\tau}, \mu_{\sigma\tau})$ are the basis-state labels for the four spaces in the model (σ stands for π or ν, and τ stands for N or U). In the last expression, $N_{\sigma\tau}$ denotes the number of particles in the corresponding space, $[f_{\sigma\tau}]$ - the spatial symmetry label and $(\lambda_{\sigma\tau}, \mu_{\sigma\tau})$ - the SU(3) irrep label. Multiplicity indices $\alpha_{\sigma\tau}$ and ρ_σ count different occurrences of $(\lambda_{\sigma\tau}, \mu_{\sigma\tau})$ in $[f_{\sigma\tau}]$ and in the product $\{(\lambda_{\sigma N}, \mu_{\sigma N}) \otimes (\lambda_{\sigma U}, \mu_{\sigma U})\} \rightarrow (\lambda_\sigma, \mu_\sigma)$, respectively. First, the particles from the normal and the unique spaces are coupled for both protons and neutrons. Then, the resulting proton and neutron irreps are coupled to a total final set of irreps. The total angular momentum J results from the coupling of the total orbital angular momentum L with the total spin S. The ρ and κ are, respectively, the multiplicity indices for the different occurrences of (λ, μ) in $\{(\lambda_\pi, \mu_\pi) \otimes (\lambda_\nu, \mu_\nu)\}$ and L in (λ, μ).

5.2.2 Hamiltonian

Since the pn-pairing has proven to be an important ingredient for the description of the $N \approx Z$ nuclei, a more general Hamiltonian than the one used so far is needed. One possible choice is

$$\begin{aligned} H &= \sum_{\sigma,\tau}(H^{\sigma\tau}_{sp} - GS^{\sigma\tau\dagger}S^{\sigma\tau}) - \frac{\chi}{2} : Q.Q : + aJ^2 + bK^2_J + a_{sym}C_2 + c_3C_3 \\ &- G(\sum_{\sigma,\tau\neq\tau'} S^{\sigma\tau\dagger}S^{\sigma\tau'} + \sum_{\tau,\tau'} S^{\pi\nu,\tau\dagger}S^{\pi\nu,\tau'}), \end{aligned} \tag{5.3}$$

which includes spherical Nilsson single-particle energies

$$H^{\sigma\tau}_{sp} = \sum_{i_{\sigma\tau}}(H_0 + C_{\sigma\tau}\mathbf{l}_{i_{\sigma\tau}}.\mathbf{s}_{i_{\sigma\tau}} + D_{\sigma\tau}\mathbf{l}^2_{i_{\sigma\tau}}), \tag{5.4}$$

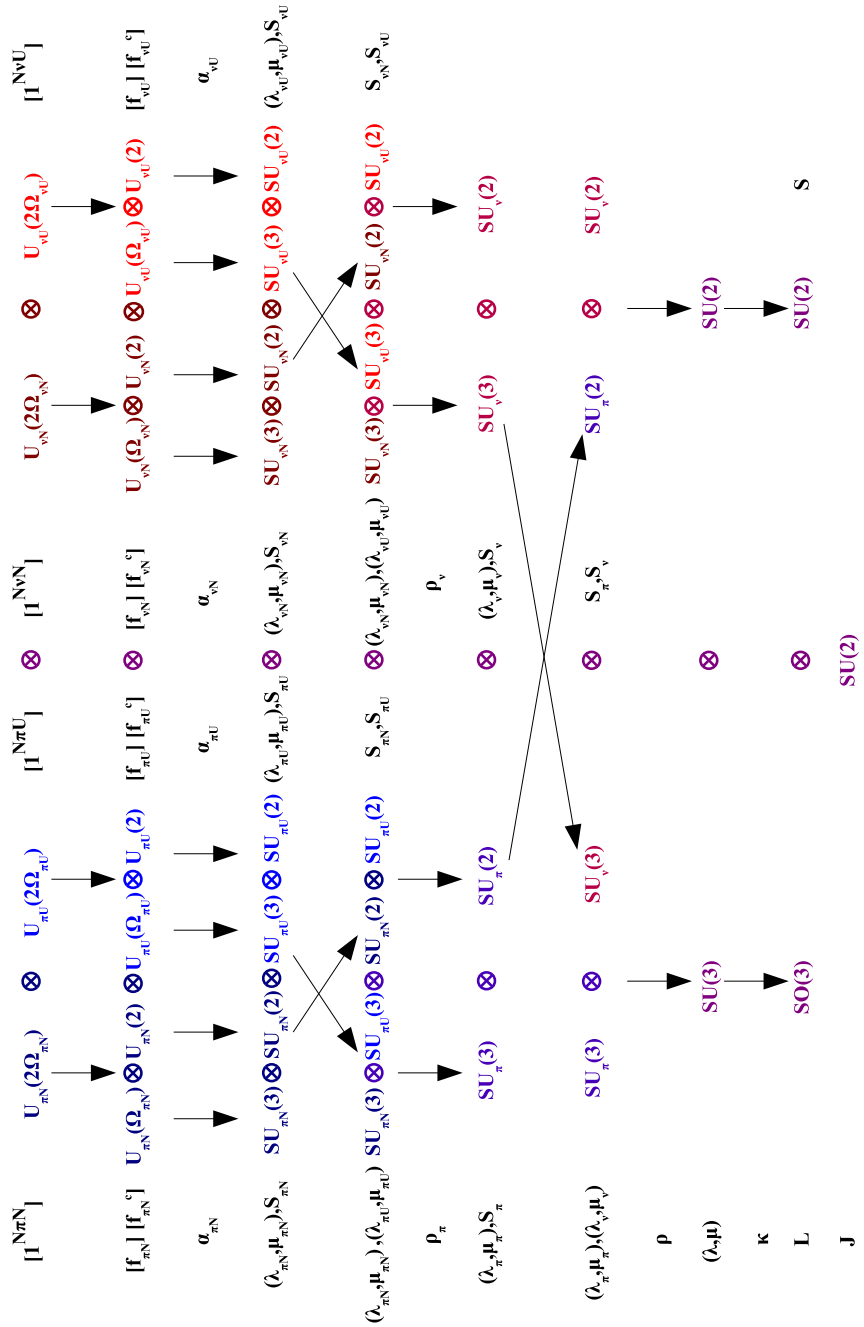

Figure 5.2: Proton-neutron decomposition relevant to the extended SU(3) model applications. The group symbols are represented in color and the associated irrep labels are given on the left for the protons, and on the right for the neutrons.

as well as the quadrupole-quadrupole and pairing interactions (within a shell and between shells) plus two rotor-like terms that are diagonal in the SU(3) basis. In general, the harmonic oscillator term, $H_0 = \hbar\omega(\eta_{i_{\sigma\tau}} + \frac{3}{2})$ where $\hbar\omega \approx \frac{41}{A^{1/3}}$ [22], is essential and its contribution does not cancel out when more than one possible distribution of particles over the shells is involved. The colons in the quadrupole operator notation represent normal-ordered operator since all the one-body effects have already been taken into account by the single-particle terms in the Hamiltonian. In addition, in first approximation, the quadrupole operator in the normal-parity spaces is related to its pseudo counterpart by $Q_{\sigma N} \approx \frac{\tilde{\eta}+1}{\tilde{\eta}}\tilde{Q}_{\sigma N}$ with $\tilde{\eta}$ equal to 2 for both protons and neutrons and $Q = Q_{\pi N} + Q_{\pi U} + Q_{\nu N} + Q_{\nu U} \approx 1.5\ \tilde{Q}_{\pi N} + Q_{\pi U} + 1.5\ \tilde{Q}_{\nu N} + Q_{\nu U}$.

The second line in Eq.(5.3) consists of pairing terms that are included for the first time in SU(3) shell-model calculations. In particular, the first term represents the scattering of an identical-particle pair between the normal- and unique-parity spaces. The second one stands for the proton-neutron pairing (or simply pn-pairing) interaction within the normal- or unique-parity space (terms with $\tau = \tau'$) and for the pn-pair scattering between the normal- and unique-parity spaces (terms with $\tau \neq \tau'$). Finally, the two rotor-like terms J^2 and K_J^2 (the square of the total angular momentum and its projection on the intrinsic body-fixed axis) are used to "fine tune" the energy spectra, adjusting the moment of inertia of the g.s. band and the position of the $K = 2^+$ bandhead, respectively.

The expression for the identical-particle pairing within a shell (and the identical-particle pair-scattering between two shells) in terms of SU(3) irreducible operators is given in [36]:

$$
\begin{aligned}
S^{\sigma\tau\dagger}S^{\sigma\tau'} = \frac{1}{2} \sum_{\substack{(\lambda_1,\mu_1)(\lambda_2,\mu_2)\\ \rho(\lambda,\mu)}} \sum_{ll'} (-)^{l-l'} \sqrt{(2l+1)(2l'+1)} \\
\langle (\eta,0)l;(\eta,0)l \| (\lambda_1,\mu_1)10\rangle \langle (0,\eta')l';(0,\eta')l' \| (\mu_2,\lambda_2)10\rangle \qquad (5.5)\\
\langle (\lambda_1,\mu_1)10;(\mu_2,\lambda_2)10 \| (\lambda,\mu)10\rangle_\rho \\
\left[\left[a^\dagger_{(\eta,0)\frac{1}{2}} \otimes a^\dagger_{(\eta,0)\frac{1}{2}} \right]^{(\lambda_1,\mu_1),S_1=0} \otimes \left[\tilde{a}_{(0,\eta')\frac{1}{2}} \otimes \tilde{a}_{(0,\eta')\frac{1}{2}} \right]^{(\mu_2,\lambda_2),S_2=0} \right]^{\rho(\lambda,\mu),S=0;\ J=0}_{\kappa=1 L=0 \qquad M_J=0},
\end{aligned}
$$

where $\sigma = \pi$ or ν with $\eta = \eta'$ ($\eta \neq \eta'$) and $\tau = \tau'$ ($\tau \neq \tau'$) for the case of pairing (pair-scattering). Here, $\langle\ ;\ \|\ \rangle$ denotes a reduced SU(3) $\supset$ SO(3) Clebsch-Gordan coefficient and $\tilde{a}$ is a proper SU(3) tensor defined by $\tilde{a}_{(0,\eta)ljm} = (-)^{\eta+j+m} a_{(\eta,0)lj-m}$.

A similar relation to the one above holds if we have proton-neutron pair creation and annihilation operators instead. Then inside the brakets there will be an operator product of the type $a^\dagger \otimes b^\dagger$ or $a \otimes b$ where $a^\dagger$ represents creation of a proton and $b^\dagger$ - of a neutron. However, in order to make this relation useful, we also need to find a way to transform to the order of coupling adopted in the extended SU(3) calculations. It can be done by using the fact that the $9 - \lambda\mu$ $(9j)$ coefficients connect composite tensors corresponding to different coupling schemes of four SU(3)

(SU(2)) tensors. In this way, one can derive the corresponding expressions for the pn-pairing (pair-scattering) operators:

$$\Big[\Big[a^\dagger_{(\eta,0)\frac{1}{2}}\otimes b^\dagger_{(\eta,0)\frac{1}{2}}\Big]^{(\lambda_1,\mu_1)S=0}\otimes\Big[\tilde{a}_{(0,\eta')\frac{1}{2}}\otimes\tilde{b}_{(0,\eta')\frac{1}{2}}\Big]^{(\mu_2,\lambda_2)S=0}\Big]^{\rho_0(\lambda,\mu),S=0;\ J=0}_{\kappa=1L=0\quad M_J=0}=$$

$$\sum_{M_LM_S}\Big[\Big[a^\dagger_{(\eta,0)\frac{1}{2}}\otimes b^\dagger_{(\eta,0)\frac{1}{2}}\Big]^{(\lambda_1,\mu_1)S=0}\otimes\Big[\tilde{a}_{(0,\eta')\frac{1}{2}}\otimes\tilde{b}_{(0,\eta')\frac{1}{2}}\Big]^{(\mu_2,\lambda_2)S=0}\Big]^{\rho_0(\lambda,\mu),S=0}_{\kappa=1L=0M_L=0,M_S=0}$$

$$\langle LM_L;SM_S|\,JM_J\rangle$$

$$=\sum_{\substack{(\lambda_\pi,\mu_\pi)(\lambda_\nu,\mu_\nu)\\ \rho_\tau(\lambda,\mu)}}\chi\begin{Bmatrix}(\eta,0)&(\eta,0)&(\lambda_1,\mu_1)&1\\(0,\eta')&(0,\eta')&(\mu_2,\lambda_2)&1\\(\lambda_\pi,\mu_\pi)&(\lambda_\nu,\mu_\nu)&(\lambda,\mu)&\rho_\tau\\1&1&\rho_0&\end{Bmatrix}\sum_{\mathcal{S}}\chi\begin{Bmatrix}\frac{1}{2}&\frac{1}{2}&0\\\frac{1}{2}&\frac{1}{2}&0\\\mathcal{S}&\mathcal{S}&0\end{Bmatrix}$$

$$\Big[\Big[a^\dagger_{(\eta,0)\frac{1}{2}}\otimes\tilde{a}_{(0,\eta')\frac{1}{2}}\Big]^{(\lambda_\pi,\mu_\pi)\mathcal{S}}\otimes\Big[b^\dagger_{(\eta,0)\frac{1}{2}}\otimes\tilde{b}_{(0,\eta')\frac{1}{2}}\Big]^{(\lambda_\nu,\mu_\nu)\mathcal{S}}\Big]^{\rho_0(\lambda,\mu),S=0}_{\kappa=1L=0M_L=0,M_S=0}. \tag{5.6}$$

In the third line $\langle LM_L;SM_S|\,JM_J\rangle=\langle 00;00|\,00\rangle=1$. Further use of the properties of 9-$\lambda\mu$ and $9j$ coefficients leads to the following result:

$$S^{\pi\nu,\tau\dagger}S^{\pi\nu,\tau'}=\frac{1}{4}\sum_{\substack{(\lambda_\pi,\mu_\pi)(\lambda_\nu,\mu_\nu)\\ \rho'(\lambda,\mu)}}\sum_{\mathcal{L}ll'\kappa_\pi\kappa_\nu}(-)^{l-l'}\sqrt{2\mathcal{L}+1}\sum_{\mathcal{S}}\sqrt{2\mathcal{S}+1}$$

$$\langle(\eta,0)l;(0,\eta')l'\|(\lambda_\pi,\mu_\pi)\kappa_\pi\mathcal{L}\rangle\langle(\eta,0)l;(0,\eta')l'\|(\lambda_\nu,\mu_\nu)\kappa_\nu\mathcal{L}\rangle$$

$$\langle(\lambda_\pi,\mu_\pi)\kappa_\pi\mathcal{L};(\lambda_\nu,\mu_\nu)\kappa_\nu\mathcal{L}\|(\lambda,\mu)10\rangle_{\rho'}$$

$$\Big[\Big[a^\dagger_{(\eta,0)\frac{1}{2}}\otimes\tilde{a}_{(0,\eta')\frac{1}{2}}\Big]^{(\lambda_\pi,\mu_\pi)\mathcal{S}}\otimes\Big[b^\dagger_{(\eta,0)\frac{1}{2}}\otimes\tilde{b}_{(0,\eta')\frac{1}{2}}\Big]^{(\lambda_\nu,\mu_\nu)\mathcal{S}}\Big]^{\rho(\lambda,\mu),S=0;\ J=0}_{\kappa=1L=0\quad M_J=0}. \tag{5.7}$$

Likewise, $\eta=\eta'$ ($\eta\neq\eta'$) and $\tau=\tau'$ ($\tau\neq\tau'$) for pn-pairing (pn-pair scattering). The labels (λ_π,μ_π) and (λ_ν,μ_ν) represent the proton and the neutron SU(3)-coupled irreps and the symbols $\mathcal{L}$ and $\mathcal{S}$ stand for the orbital and spin angular momentum which both must be equal in the coupled proton (and neutron) spaces. The final result is extremely valuable because, contrary to many approximate techniques for handling the pairing operator, this one is exact.

The rules for constructing tensor products from the fermion creation and annihilation operators, such as $a^\dagger a$ which moves a particle from the η_2-th major oscillator shell to the η_1-th shell are well known [97]. The possible (λ,μ) values are given by the coupling rule

$$(\eta_1,0)\otimes(0,\eta_2)=\oplus_{k=0}^{min(\eta_1,\eta_2)}(\eta_1-k,\eta_2-k). \tag{5.8}$$

The total intrinsic spin S can take the values 0 or 1 with projection $M_S=0$ or $M_S=0,\pm1$, respectively.

Similarly, the product $a^\dagger a^\dagger$ (aa) which represents creation (or annihilation) of a pair of particles is given by the rules

$$\begin{aligned}(\eta_1,0)\otimes(\eta_2,0) &= \oplus_{k=0}^{min(\eta_1,\eta_2)}(\eta_1+\eta_2-2k,k),\\ (0,\eta_1)\otimes(0,\eta_2) &= \oplus_{k=0}^{min(\eta_1,\eta_2)}(k,\eta_1+\eta_2-2k),\end{aligned} \tag{5.9}$$

where again $S=0$ or $S=1$ with $M_S=0$ or $M_S=0,\pm1$, respectively.

Another term in the Hamiltonian, whose structure becomes more complicated when one transitions to a model with 4 spaces, is the quadrupole-quadrupole interaction. From the general expression of the quadrupole operator in a space spanned by four different parts

$$Q = Q_{\pi N} + Q_{\pi U} + Q_{\nu N} + Q_{\nu U}, \tag{5.10}$$

we can compose the form of the quadrupole-quadrupole interaction relevant to the extended SU(3) model

$$\begin{aligned} Q.Q &= Q_{\pi N}.Q_{\pi N} + Q_{\nu N}.Q_{\nu N} + Q_{\pi N}.Q_{\pi U} + Q_{\nu N}.Q_{\nu U}\\ &+ 2\,Q_{\pi N}.Q_{\pi U} + 2\,Q_{\nu N}.Q_{\nu U}\\ &+ 2\,Q_{\pi N}.Q_{\nu N} + 2\,Q_{\pi N}.Q_{\nu U} + 2\,Q_{\pi U}.Q_{\nu U} + 2\,Q_{\pi U}.Q_{\nu N}. \end{aligned} \tag{5.11}$$

Let $|1\rangle = |N_{\sigma\tau}[f_{\sigma\tau}]\alpha_{\sigma\tau}(\lambda_{\sigma\tau},\mu_{\sigma\tau}),S_{\sigma\tau}\rangle$, $|2\rangle = |\{a_{\sigma N},a_{\sigma U}\}\rho_\sigma(\lambda_\sigma,\mu_\sigma),S_\sigma\rangle$, and $|3\rangle = |\{a_\pi;a_\nu\}\rho(\lambda,\mu)\kappa L,\{S_\pi,S_\nu\}S\rangle$ are the basis states in each of the 4 spaces, in the coupled proton (or neutron) spaces and in the coupled proton-neutron spaces, respectively.

Having in mind that

$$\begin{aligned} \langle 1|||Q_{\pi N}|||1\rangle &\otimes \langle 1|||Q_{\pi U}|||1\rangle \rightarrow \langle 2|||Q_{\pi N}.Q_{\pi U}|||2\rangle,\\ \langle 1|||Q_{\pi N}.Q_{\pi N}|||1\rangle &\otimes \langle 1|||1|||1\rangle \rightarrow \langle 2|||Q_{\pi N}.Q_{\pi N}|||2\rangle,\\ \langle 2|||Q_x.Q_y|||2\rangle &\otimes \langle 2|||1|||2\rangle \rightarrow \langle 3|||Q_x.Q_y|||3\rangle, \end{aligned} \tag{5.12}$$

where the arrow means "the result of the coupling, and the formula used to evaluate is of the form given by Eq. (2.83)", we can easily obtain the matrix elements for the terms from the first and the second row of Eq. (5.11). For the last row, we perform the following second coupling

$$\langle 2|||Q_\pi|||2\rangle \otimes \langle 2|||Q_\nu|||2\rangle \rightarrow \langle 3|||Q_{\pi\nu}|||3\rangle, \tag{5.13}$$

where

$$\langle 2|||Q_\pi|||2\rangle = \langle 2|||Q_{\pi N}+Q_{\pi U}|||2\rangle = \langle 2|||Q_{\pi N}|||2\rangle + \langle 2|||Q_{\pi U}|||2\rangle, \tag{5.14}$$

$$\langle 2|||Q_\nu|||2\rangle = \langle 2|||Q_{\nu N}+Q_{\nu U}|||2\rangle = \langle 2|||Q_{\nu N}|||2\rangle + \langle 2|||Q_{\nu U}|||2\rangle. \tag{5.15}$$

This way, we can evaluate the matrix elements of all the parts in Eq. (5.11).

5.2.3 Calculation of the Matrix Elements

To calculate the matrix elements of an operator when four spaces are involved one can still use Eq. (2.83) but has to keep in mind that now the triple-barred matrix elements have "internal" structure - they are also obtained from the triple-barred matrix elements in two of the four spaces. If, in order to underscore this, instead of ${}^{\pi}T^{\rho_{\pi_0}(\lambda_{\pi_0},\mu_{\pi_0})S_{\pi_0}}$ we use ${}^{\pi}T^{\rho_{\pi_0}(\lambda_{\pi_0},\mu_{\pi_0})S_{\pi_0}}_{\alpha_{\pi N}(\lambda_{\pi N},\mu_{\pi N})\alpha_{\pi U}(\mu_{\pi U},\lambda_{\pi U})S_{\pi N}S_{\pi U}}$ for the elements in (2.83) then

$$
\begin{aligned}
&\langle N'_{\pi}[f'_{\pi}]\alpha'_{\pi}(\lambda'_{\pi},\mu'_{\pi})S_{\pi'}|||{}^{\pi}T^{\rho_{\pi_0}(\lambda_{\pi_0},\mu_{\pi_0})S_{\pi_0}}_{\alpha_{\pi N}(\lambda_{\pi N},\mu_{\pi N})\alpha_{\pi U}(\mu_{\pi U},\lambda_{\pi U})S_{\pi N}S_{\pi U}}|||N_{\pi}[f_{\pi}]\alpha_{\pi}(\lambda_{\pi}\mu_{\pi})S_{\pi}\rangle_{\rho_{\pi}} = \\
&\chi\begin{Bmatrix} S_{\pi N} & S_{\pi N_0} & S'_{\pi N} \\ S_{\pi U} & S_{\pi U_0} & S'_{\pi U} \\ S_{\pi} & S_{\pi_0} & S'_{\pi} \end{Bmatrix} \\
&\sum_{\rho_{\pi N}\rho_{\pi U}} \chi\begin{Bmatrix} (\lambda_{\pi N},\mu_{\pi N}) & (\lambda_{\pi N_0},\mu_{\pi N_0}) & (\lambda_{\pi N},\mu'_{\pi N}) & \rho_{\pi N} \\ (\lambda_{\pi U},\mu_{\pi U}) & (\lambda_{\pi U_0},\mu_{\pi U_0}) & (\lambda'_{\pi U},\mu'_{\pi U}) & \rho_{\pi U} \\ (\lambda_{\pi},\mu_{\pi}) & (\lambda_{\pi_0},\mu_{\pi_0}) & (\lambda'_{\pi},\mu'_{\pi}) & \tilde{\rho_{\pi}} \\ \rho_{\pi} & \rho_{\pi_0} & \rho_{\pi'} & \end{Bmatrix} \\
&\langle N'_{\pi N}[f'_{\pi N}]\alpha'_{\pi N}(\lambda'_{\pi N},\mu'_{\pi N})S'_{\pi N}|||{}^{\pi N}T^{(\lambda_{\pi N},\mu_{\pi N}),S_{\pi N}}|||N_{\pi N}[f_{\pi N}]\alpha_{\pi N}(\lambda_{\pi N},\mu_{\pi N})S_{\pi N}\rangle_{\rho_{\pi N}} \\
&\langle N'_{\pi U}[f'_{\pi U}]\alpha'_{\pi U}(\lambda^{'}_{\pi U},\mu^{'}_{\pi U})S'_{\pi U}|||{}^{\pi U}T^{(\lambda_{\pi U},\mu_{\pi U}),S_{\pi U}}|||N_{\pi U}[f_{\pi U}]\alpha_{\pi U}(\lambda_{\pi U},\mu_{\pi U})S_{\pi U}\rangle_{\rho_{\pi U}},
\end{aligned}
\tag{5.16}
$$

and the same can be done for the triple-barred matrix elements for the neutrons. During the two-step process of calculations, namely, the first and the second coupling, most pieces in the Hamiltonian couple twice to the unit matrix. The three exceptions are the pn-pairing, the pair-scattering and the quadrupole-quadrupole interaction (excluding the Q.Q part within each of the four spaces). To calculate them, expression (2.83) in its most general form has to be used. Similarly, the expressions for electromagnetic transitions (Eq. (2.86)) given in Chapter 2 need to be generalized where the sums must go over all four (instead of just two) spaces.

While our choice throughout the current investigation is first to couple separately the irreps for each type of particles and then to couple the proton and the neutron irreps, in priniciple, one could use a different coupling scheme, for example one in which the particles from the normal- and unique-parity sector are first coupled and then the normal space is coupled to the unique one. The easiest way to transform between these two approaches is by using the relations between the basis states and the operators in these two couplings. These are given by the 9-(λ,μ) $(9j)$ coefficients for the SU(3) (and SU(2) part, respectively) of the coupled state (or tensor). Knowing this relation is useful because it resolves any complications that may come up when devising new procedures for different coupling schemes.

5.3 Method of Calculation

In the rest of this chapter, we would like to familiarize the reader with the algorithms in use and the codes available (some of them developed specifically for the problems

addressed in this dissertation) to perform the calculations in the framework of the extended SU(3) shell model.

An elaborate testing and further development of a code [42] designed to perform calculations in model spaces which consist of one, two and even four parts has been performed. Along with building the appropriate matrix elements and solving the eigenvalue problem, it calculates B(E2) and B(M1) transition strengths as well as other observables. Earlier versions of this code were used in one (or at most two) space(s) [98].

A schematic representation of the basic ingredients of the code and its connections to some peripheral packages and subroutines is given in Fig. 5.3. Since giving details would serve little purpose, the input and output files are not included; we only give the general structure of the program, with each arrow on the figure representing output information from one of the main codes that serves as an input for the next one.

The code shares two auxiliary subroutines: the SU(3) coupling (Wigner and Racah) coefficient package [32, 33] and the weighted searched tree (WST) package [99, 100]. The former is used mainly for building tensor operators and generating reduced matrix elements and the latter is a numerical database which allows for a convenient storage and retrieval of data that is used multiple times and that on a relative scale is costly to calculate.

The formatted output files are used to show intermediate results of a calculation. They further serve as formatted input files for the next main program. Also, unformatted files produced by the SU3RME package are used for storing information in WST arrays that can then be used in subsequent steps of the program.

Many results published for real nuclei were performed using another SU(3) shell-model code - the one written by [101]. It had similar capabilities as the one we use but its main drawback is that it was not a simple task to extend it for use for more than 2 spaces. Nevertheless, that code is also useful and includes some ideas that were incorporated in the current investigation.

In short, we made several improvements and extensions to existing codes and added a number of important new elements to this overall program. These consist of:

- devising a program **ircoup.f** which generates all the possible SU(3) coupled irreps and selects those which are allowed according to a specific truncation scheme of choice. The output of this code is needed in the construction of the coupled basis states, so its output file serves as an input for the main code **hamrme2.f**.

- including the pn-pairing interaction which is essential for the $N \approx Z$ nuclear systems;

- introducing terms in the Hamitonian that mix configurations with different distribution of particles among the four spaces:

  (a) pp(nn) pair-scattering between the normal and unique spaces;

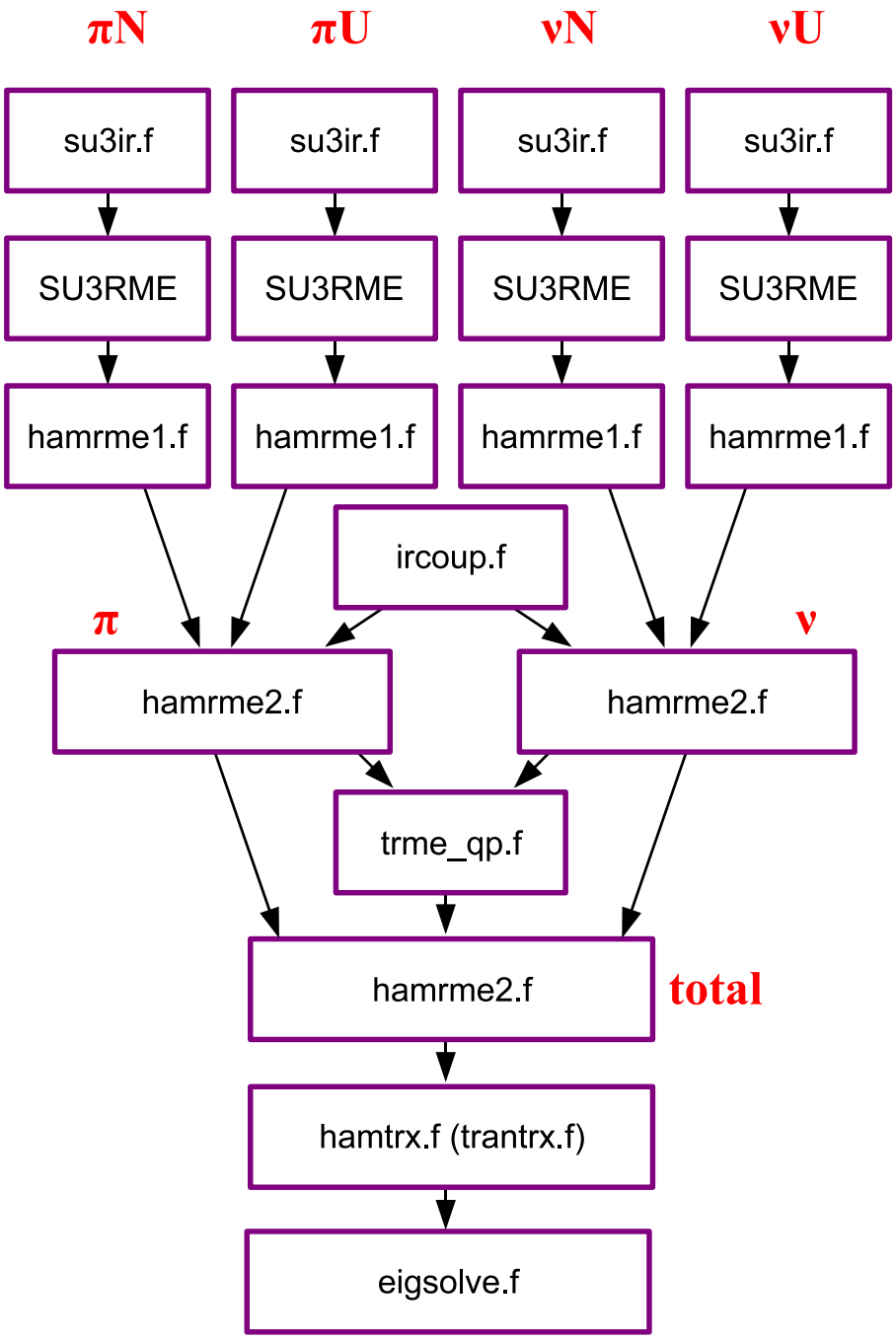

Figure 5.3: Algorithm used for the calculations within the framework of the extended $SU(3)$ shell model. There are seven main programs (**su3ir.f**, **hamrme1.f**, **hamrme2.f**, **hamtrx.f**, **trantrx.f**, **eigsolve.f** and **trme_qp.f** plus the SU3RME package which can run separately or be put together (shown by the arrows).

(b) pn pair scattering between the normal and unique spaces.

- adding the angular momentum, spin and quadrupole operators in a form, useful for calculating the $B(M1)$ and $B(E2)$ transition strengths;
- adding the rotor-like terms J^2, C_2, C_3, K_J^2 and S^2;
- With the view of further extension of the pseudo-SU(3) model for rare-earth and actinide nuclei, some array dimensions in the subroutines from the $SU3$ package have been increased. This is related to the fact that when higher shells and more than two spaces are involved in the calculation, the multiplicities can go beyond the previously established limits.

The calculation starts with the **su3ir.f** program [102] which generates all possible irreps in each of the four sub-spaces (for N=Z nuclei the list will be the same for protons and neutrons in both the normal- and the unique-parity spaces). Then, lists of irreps in the proton, neutron, and the proton-neutron coupled spaces are selected by the **ircoup.f** program based upon an automated truncation criterion and then stored in an output file for a further possible later use.

The next step is to find the matrix elements of the $SU(3)$ elementary tensor operators of the type ($a^\dagger, a^\dagger a^\dagger, a, aa, a^\dagger a a^\dagger a^\dagger a, a^\dagger aa$ and $a^\dagger a^\dagger aa$) which are of vital importance in the evaluation for the matrix elements of any one- (or two-) body operator. This is done with the use of the SU3RME package [57]. Next, **hamrme1.f** program calculates the triple-barred matrix elements for each operator in the Hamiltonian or used for obtaining electromagnetic transitions.

From that point forward, one performs the coupling of two spaces with **hamrme2.f**, first the normal and unique spaces for each type of particles are coupled and then the proton and the neutron spaces are coupled. Before the last coupling made, we also had to construct the matrix elements of Q_π and Q_ν according to Eqs. (5.14) and (5.15), performed with the code **trme_qp.f** . After the run, we have the basis states, operators and the triple-barred matrix elements in the final coupled space. In **hamtrx.f** (**trantrx.f**) code the double-barred elements for the Hamiltonian (transition operators) are obtained from the triple-barred ones for the operators. The rotor terms are also calculated here.

Finally, the code **eigsolve.f** solves the eigenvalue problem for the Hamiltonian matrix with the option of using two different methods: Jacobi method, applicable for smaller matrices (up to about 1000 basis states) and Lanczos method - for larger matrices (usually, above 1000 basis states). Information about the normal- and unique-parity space occupancy as well as the wave-function content can also be obtained. The program is also designed to perform a fit of the theoretical predictions with available experimental results. The methods which are used to do that are either simple estimate of the χ^2 statistics in a grid of points chosen in an interval for a certain number of fit parameters or more elaborate (but in many cases to a great extent time saving) methods, like the one of Levenberg-Marquardt which has been implemented in the MINPACK package [103]. In the calculations presented here, we used the first option, since it was found to fit our needs.

Chapter 6

Results for ^{64}Ge and ^{68}Se in the Extended SU(3) Shell Model

Up to this point we have justified the use of a new effective symmetry-adapted truncation scheme (Chapter 4), introduced the basics of the extended SU(3) shell model, and briefly described the algorithms and the computer codes that have been developed (Chapter 5). What remains to be done is some calculations using this new approach followed by an analysis of our outcome by comparing it with results obtained with some realistic interactions.

In this chapter, following a motivation for the choice of the isotopes studied, we present results for the energy spectra, B(E2) transition strengths and the wave function content as well as observation on the dominance of different configurations and the role that several terms play in the Hamiltonian. In addition, the size of the model spaces used in the two approaches are compared pointing to the advantages provided by the symmetry-adapted and severely-truncated basis. It is concluded that the investigation, even though being performed with some key approximations, proves that the extended-SU(3) scheme is useful for the description of many of the upper-fp-nuclear characteristics. More elaborate choices of Hamiltonian and/or model space(s) can lead to improvements in some of the problematic observables. Finally, a discussion about the future of the model and its application for nuclei from adjacent or more distant domains is included.

6.1 Role of the Upper fp-shell Nuclei ^{64}Ge and ^{68}Se

The choice of ^{64}Ge and ^{68}Se as isotopes for our detailed study of the extended SU(3) model is motivated mainly by their interesting properties. The proton-rich unstable nucleus ^{64}Ge is known to be a typical example for a nucleus showing soft structure with respect to quadrupole and octupole deformations, according to both experimental evidence and theoretical calculations [104]. In ^{68}Se shape coexistence effects have been predicted [72, 73] and await experimental confirmation. The nature of the first excited 0^+ state is currently a hot topic for many N$\sim$Z nuclei. Some

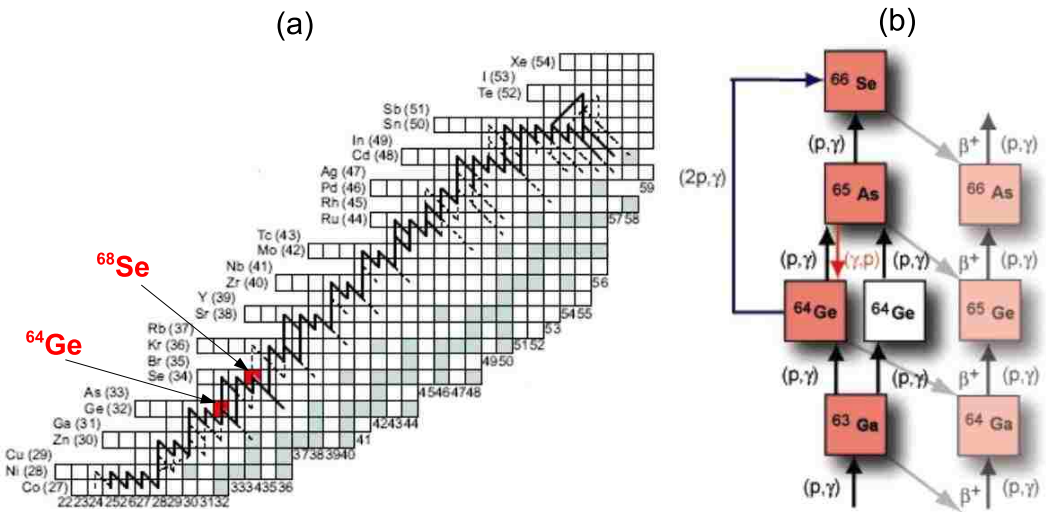

Figure 6.1: (a) A typical rp-process reaction flow taken from [106] and (b) a more detailed representation of the reactions running in the vicinity of ^{64}Ge. (The bridging of the waiting-point nucleus via an isomeric state is also possible and is depicted by the white square.)

investigations predict the one in ^{68}Se to be a low-lying isomeric state [105]. Both of these nuclei are heavy enough so that the effect of the pair-scattering terms on the single-particle occupancies is expected to be of a reasonable size. At the same time, these upper-fp systems belong to a region where full shell-model calculations are still feasible even though at the limit of the current computational abilities, when the intruder $g_{9/2}$ level is included in the model space.

^{64}Ge and ^{68}Se are both active participants in nucleosynthesis. Specifically, they are key nuclei in the rapid proton capture process (rp-process) (Fig.6.1 (a)) which runs close to the proton drip line and is characterized by proton capture reaction rates that are orders of magnitude faster than β-decay rates [107]. The reaction path follows a series of fast (p,γ)-reactions until further proton capture is inhibited, either by proton decay or photodisintegration (Fig. 6.1 (b)). Then the process stalls waiting for the relatively slow β-decay or may proceed through the rapid capture of two protons to bypass the so-called "waiting-point" nucleus. ^{64}Ge and ^{68}Se are such nuclei. The process continues towards heavier nuclei until it ends in the Sn-Sb-Te region [106]. The total lifetimes of the waiting points along the reaction path (including all destructive processes like β-decay and net proton capture) entirely determine the speed of nucleosynthesis towards heavier nuclei and the produced isotopic abundances, since at any given time essentially all the material is stored in the waiting points. Knowledge of the nuclear structure along the rp-process path is needed for its further understanding, as means for network simulations, exploring the nuclear structure at the extreme and testing model-based predictions.

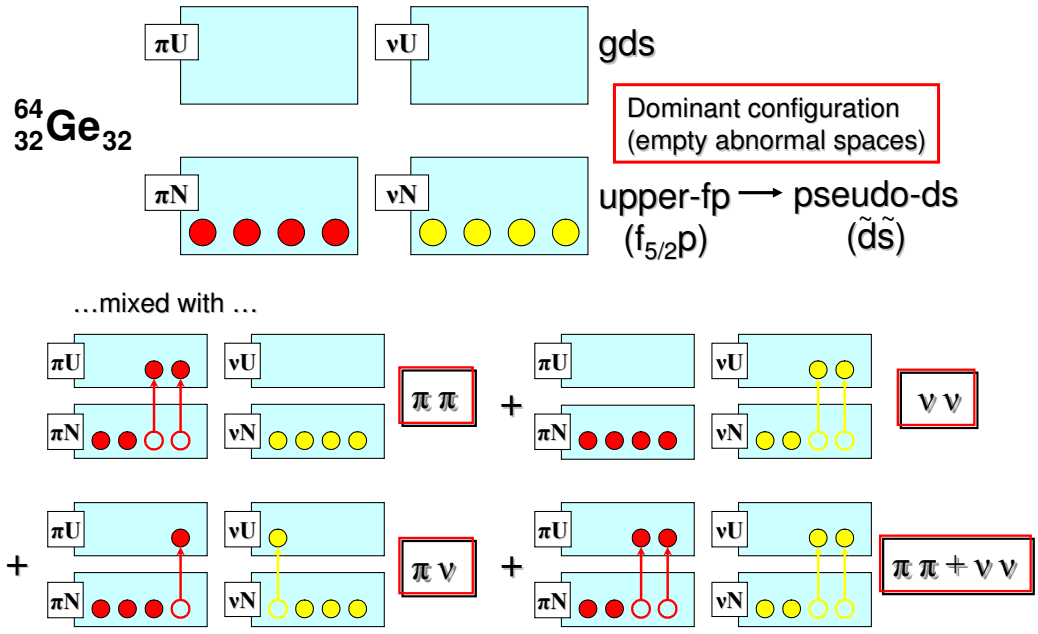

Figure 6.2: The five different types of configurations for ^{64}Ge included in the extended-SU(3)-shell-model calculations.

6.2 Choice of Basis States and Hamiltonian.

Calculations within the framework of the extended SU(3) model were performed using irreps from 5 types of configurations - for example, $[N_{\pi N}, N_{\pi U}; N_{\nu N}, N_{\nu U}]$ = $[4,0;4,0]$, $[4,0;2,2]$, $[2,2;4,0]$, $[3,1;3,1]$ and $[2,2;2,2]$ for the ^{64}Ge case. (See Fig. 6.2 and Table 6.1 where the list of configurations for ^{68}Se is also given.) For each of these groups, irreps in the proton and neutron spaces with (pseudo-) spin $S_{\sigma\tau}$ = 0, 1/2, 1 and 3/2 in both the normal- and the unique-parity spaces were generated. Then, from all the possible couplings between these we chose those with the largest value of the second order Casimir operator of SU(3) and spin S = 0, 1 and 2. Here, we present results obtained with five (seven) coupled proton-neutron irreps with distinct values of λ and μ for each distribution of particles between the normal and unique spaces for ^{64}Ge (^{68}Se). (This number was even pushed up to eleven for the [6,0;6,0] configuration in ^{68}Se). The complete set, listed in Table 6.1, consists of 492 (580) coupled irreps in the case of ^{64}Ge (^{68}Se). This number is bigger by a factor of about 20 than the one typically handled up to now within the framework of the SU(3) model. Some of the coupled irreps can be constructed in more than one way. For example, the irrep $(\lambda,\mu)S = (10,0)0$ can be obtained by coupling the $(\lambda_\pi,\mu_\pi)S_\pi \otimes (\lambda_\nu,\mu_\nu)S_\nu = (4,2)0 \otimes (4,2)0$ or $(5,0)1 \otimes (5,0)1$ proton and neutron irreps.

The choice of Hamiltonian for ^{64}Ge and ^{68}Se is dictated by two seemingly contradictory principles, namely, **simplicity** and **completeness**. In particular, we

Table 6.1: The irreps in the coupled proton-neutron model space for ^{64}Ge and ^{68}Se that were used in the extended SU(3) shell-model calculations. The subscripts for each spin value denote the multiplicity, that is, the number of different ways the corresponding irrep can be constructed.

$[N_{\pi N}, N_{\pi U}; N_{\nu N}, N_{\nu U}]$	total $(\lambda,\mu)S_{\text{multiplicity}}$				
		^{64}Ge			
$[4,0;4,0]$	$(8,4)0_1$	$(9,2)0_1,1_2$	$(10,0)0_2,1_1,2_1$	$(6,5)0_1,1_2$	$(7,3)0_6,1_8,2_2$
$[4,0;2,2]$ $([2,2;4,0])$	$(16,2)0_2$	$(17,0)1_2$	$(14,3)0_6,1_6$	$(15,1)0_{12},1_{15},2_4$	$(12,4)0_{18},1_{18},2_4$
$[3,1;3,1]$	$(16,2)0_2,1_3,2_1$	$(17,0)0_2,1_3,2_1$	$(14,3)0_8,1_{15},2_5$	$(15,1)0_{16},1_{27},2_{10}$	$(12,4)0_{28},1_{43},2_{15}$
$[2,2;2,2]$	$(24,0)0_1$	$(22,1)0_3,1_4$	$(20,2)0_{16},1_{18},2_4$	$(21,0)0_9,1_{18},2_4$	$(18,3)0_{42},1_{64},2_{16}$
		^{68}Se			
$[6,0;6,0]$	$(12,0)0_1$ $(1,10)0_1,1_2$ $(2,8)0_8,1_{12},2_4$	$(0,12)0_1$ $(6,6)0_4,1_3,2_1$	$(9,3)0_2,1_2$ $(7,4)0_6,1_{11},2_3$	$(3,9)0_2,1_2$ $(4,7)0_6,1_{11},2_3$	$(10,1)0_1,1_2$ $(8,2)0_8,1_{12},2_4$
$[6,0;4,2]$ $([4,2;6,0])$	$(18,2)0_2$ $(17,1)0_{12},1_{16},2_4$	$(19,0),1_2$ $(13,6)0_{10},1_{16},2_4$	$(15,5)0_2,1_2$	$(16,3)0_8,1_{12},2_2$	$(12,8)0_2$
$[5,1;5,1]$	$(18,2)0_2,1_3,2_1$ $(17,1)0_{18},1_{30},2_{14}$	$(19,0)0_2,1_3,2_1$ $(13,6)0_{20},1_{33},2_{15}$	$(15,5)0_4,1_6,2_2$	$(16,3)0_{16},1_{27},2_{13}$	$(12,8)0_2,1_3,2_1$
$[4,2;4,2]$	$(24,4)0_1$ $(24,1)0_{19},1_{31},2_{13}$	$(25,2)0_1,1_2$ $(20,6)0_{16},1_{18},2_6$	$(26,0)0_2,1_1,2_1$	$(22,5)0_3,1_4$	$(23,3)0_{14},1_{20},2_6$

tried to adopt the most general interaction while keeping only the terms which are needed to reproduce the *available* data. Up to now, (pseudo-)SU(3) calculations have employed interactions with the usual (and most complete) choice for realistic nuclear systems (as given in Chapter 3 - Eq. (3.22)) which in Chapter 5 was generalized to Eq. (5.3), that is

$$\begin{aligned} H &= \sum_{\sigma,\tau}(H_{sp}^{\sigma\tau} - GS^{\sigma\tau\dagger}S^{\sigma\tau}) - \frac{\chi}{2} : Q.Q : + aJ^2 + bK_J^2 + a_{sym}C_2 + c_3C_3 \\ &- G(\sum_{\sigma,\tau\neq\tau'} S^{\sigma\tau\dagger}S^{\sigma\tau'} + \sum_{\tau,\tau'} S^{\pi\nu,\tau\dagger}S^{\pi\nu,\tau'}). \end{aligned} \tag{6.1}$$

In the case of ^{64}Ge and ^{68}Se we decided to include only two of the rotor terms, so the last expression reduces to

$$\begin{aligned} H &= \sum_{\sigma,\tau}(H_{sp}^{\sigma\tau} - GS^{\sigma\tau\dagger}S^{\sigma\tau}) - \frac{\chi}{2} : Q.Q : + aJ^2 + bK_J^2 \\ &- G(\sum_{\sigma,\tau\neq\tau'} S^{\sigma\tau\dagger}S^{\sigma\tau'} + \sum_{\tau,\tau'} S^{\pi\nu,\tau\dagger}S^{\pi\nu,\tau'}). \end{aligned} \tag{6.2}$$

The arguments for these simplifications are the following. First, there is no experimental information about any excited 0^+ states for these nuclei, so the presence in the Hamiltonian of a term proportional to the third-order Casimir invariant C_3, whose primary role is to adjust their excitation energy, becomes irrelevant. Also, no 1^+ states have been measured so far, which allows us to skip the term proportional to the second-order Casimir operator C_2 since there is no "anchor configuration" to fix the a_{sym} strength. The only other consequence of ignoring it could be that the higher-J states may appear at some higher energies.

As a result of these simplifications, we are left with only two of the four rotor-like terms. Therefore, the simpler procedure of adjusting the appropriate values of parameters a and b can be used, namely, by choosing a grid of points within a carefully selected interval of reasonable values for both parameters and search for the global minimum of the χ^2 statistics where $\chi^2 = \sum_{i=1}^{N} W(i)\frac{(E_{th}(i)-E_{exp}(i))^2}{N-m}$ with $E_{exp}(i)$ standing for the experimental energies and $E_{th}(i)$ for their theoretical predictions for the i-th state, respectively, N is the total number of states used in the fitting procedure, $m = 2$ is the number of parameters, and the W(i) weight factors. Since many of the spin assignments in the experimental energy spectra are uncertain, only the experimental excitation energies for the g.s. bands and the 2_2^+ bandhead are used.

The single-particle terms together with the proton, neutron and proton-neutron pairing interactions mix the SU(3) basis states, which allows for a realistic description of the energy spectra of the nuclei. The values of the parameters used in Hamiltonian (6.2) can be found in Table 6.2. The single-particle energies in the Hamiltonian for the normal spaces are fixed with the numbers provided by the

Table 6.2: Parameters (in MeV) used in the extended SU(3) model Hamiltonian.

Nucleus	G	χ	a	b
^{64}Ge	0.280	0.0176	−0.002	0.020
^{68}Se	0.263	0.0152	−0.002	0.000

upper-fp shell single-particle energies and for the strengths in the unique-parity spaces the numbers from systematics are used [22]. The values for the parameters G and χ in the Hamiltonian which are taken from [75] are found to be in agreement with the ones [22, 108] used in previous calculations for some ds-shell and rare-earth nuclei. For simplicity, we take both identical-particle and proton-neutron pairing strengths to be equal.

6.3 Results

6.3.1 Energies and Role of the Pairing Terms

For both ^{64}Ge and ^{68}Se, proton-neutron configurations with no particles in the unique space are found, as expected, to lie lowest and determine, by-and-large, the structure of the low-lying eigenstates. Only a small portion of all proton-neutron coupled irreps - 27 (112) in the case of ^{64}Ge (^{68}Se) - belong to these types of configurations, which we will refer to as the dominant ones. Since the only possible irrep in the unique-parity spaces for this case is $(\lambda_{\pi U}, \mu_{\pi U}) = (0, 0)$ (and $(\lambda_{\nu U}, \mu_{\nu U}) = (0, 0)$), these configurations are the exact pseudo analog of the ones encountered in the ds-shell nuclei ^{24}Mg and ^{28}Si which have been studied earlier [9]. Using only the principal part of the Hamiltonian (6.2), namely, the part with both rotor term strengths equal to zero, we are able to provide a good description of the low-lying states. Specifically, all the energies from the g.s. bands (with the exception of the 2_1^+ state in ^{68}Se) differ by no more than 15% from the experimental values [93]. In order to conform with this result and prevent any further changes in the structure of the wave function, the range of values for the parameters a and b were severely restricted so that these terms only introduce small ("fine tuning") changes to the overall fit.

Proton-neutron configurations with two and four particles in the unique-parity space prevail at higher energies. The former starts to dominate from about 3.5 MeV (5 MeV) in the case of ^{64}Ge (^{68}Se), usually for states of higher spin values, and the latter at even higher energies. The amount of mixing found between configurations with different distribution of particles is due to the pair-scattering interactions between the normal- and unique-parity spaces. While the expected behavior of the unique-parity-space occupancy is observed - it goes up with the rise of both G and/or χ strengths - with the choice of parameters from Table 6.2 the absolute values appear to be underestimated by at least a factor of 3 in ^{64}Ge (see the result shown in Fig. 4.6) and by even more for the case of ^{68}Se. This may indicate that

the model space has to be further expanded to acommodate more mixing from the pair-scattering interaction terms, that the pn-interaction indeed should enter with different, possibly bigger strength than the identical-particle pairing, or the possible need to include other terms in the Hamiltonian like the quadrupole and isoscalar pairing interactions.

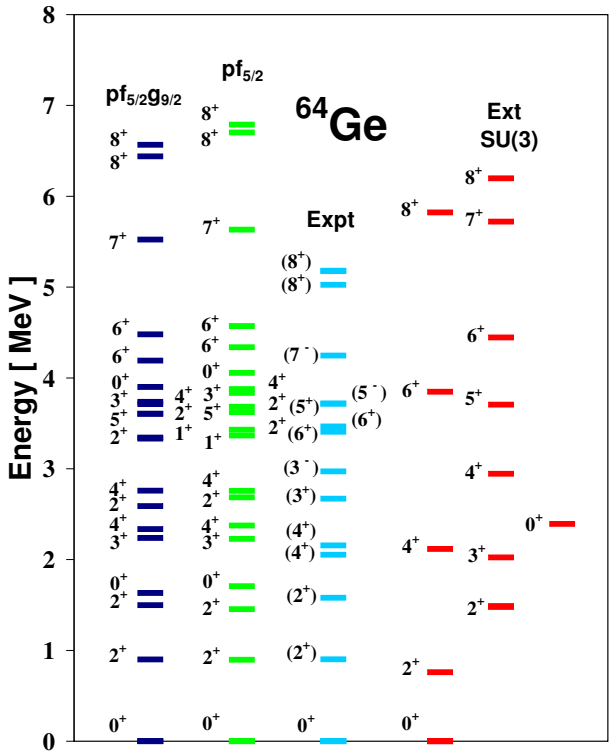

Figure 6.3: Low-energy spectra of ^{64}Ge obtained with (from left to right) the realistic interaction in the full $pf_{5/2}g_{9/2}$ and $pf_{5/2}$ model spaces compared with experiment [93] and the extended-SU(3)-model results.

Results for the excitation spectra of ^{64}Ge are presented in Fig. 6.3. The realistic G-matrix interaction gives a reasonable result for the low-lying states consistent with the one obtained in [72, 75]. Moreover, a description of a similar quality is provided by the extended SU(3) model. The existence of two prolate bands, as predicted by the calculations with the realistic interactions, is also observed, that is, a g.s. $K = 0^+$ and an excited $K = 2^+$ band, both dominated by the $(8, 4)$ irrep. The first excited 0^+ (0_2^+) state, not reported yet experimentally, is found at 2.39 MeV which is higher than the prediction made by the realistic interactions.

Consistent with the outcome for ^{64}Ge, in the case of ^{68}Se we found a reasonable description for the energies of the states from the g.s. band (Fig.6.4). Even the use of a restricted space with at most 2 nucleons allowed in the intruder $g_{9/2}$ level produces result which reflects some basic characterisics of the full-space spectrum reported in [72]. For example, the first excited 0^+ state (0_2^+) is also positioned

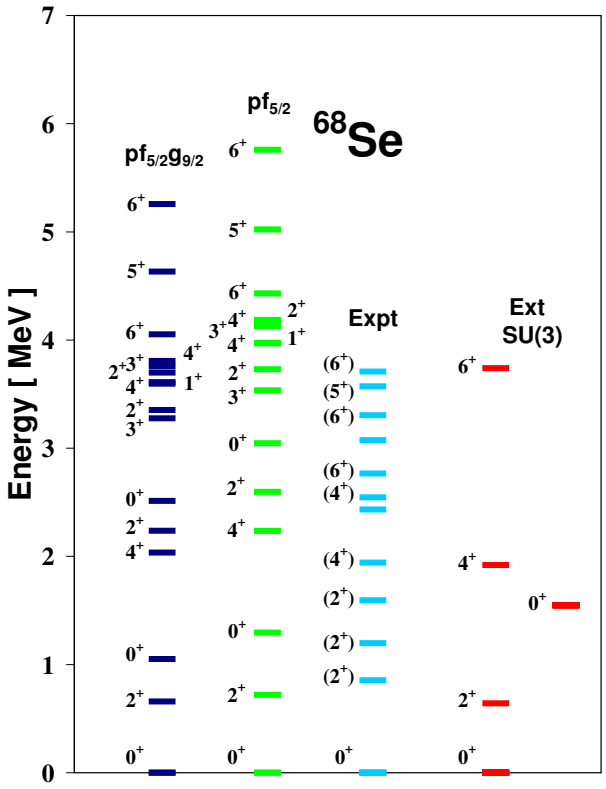

Figure 6.4: Low-energy spectra of ^{68}Se obtained with (from left to right) the realistic interaction in the restricted $pf_{5/2}g_{9/2}$ (at most 2 particles allowed in the intruder $g_{9/2}$ level) and full $pf_{5/2}$ model spaces compared with experiment [93] and the extended-SU(3)-model results.

below the 2_2^+ state. A new feature observed in our results is that the 0_3^+ state at 2.51 MeV was found to be dominated by the shapes with $C_2 = 180$ (see Section II). Within the framework of the extended SU(3) shell model, ^{68}Se is predicted to be a mid-shell nucleus, a fact which may explain the existence of shape coexistence effects. Unlike the case of ^{28}Si [9], now the g.s. band is dominated by the irrep $(12, 0)$ which corresponds to a prolate shape. This result mainly follows due to the presence of the orbit-orbit terms in the Hamiltonian and is in agreement with some earlier discussions [109, 110]. Specifically, it favors the scenario in which the lower eigenstates in the g.s. band are prolate and throughout the band the shape changes to oblate [109]. Because of the nature of the leading representation, the model can not easily account for a $K = 2^+$ band with the same shape characteristic, neither can it give a simple explanation for a low-lying $K = 0^+$ band, facts which are in support of the realistic prediction made in Section II for a highly-mixed nature of the 0_1^+ as well as many other low-lying states in this nucleus. With only the J^2 term used in the Hamiltonian for adjusting the energies, the 0_2^+ state is predicted by the model at 1.55 MeV.

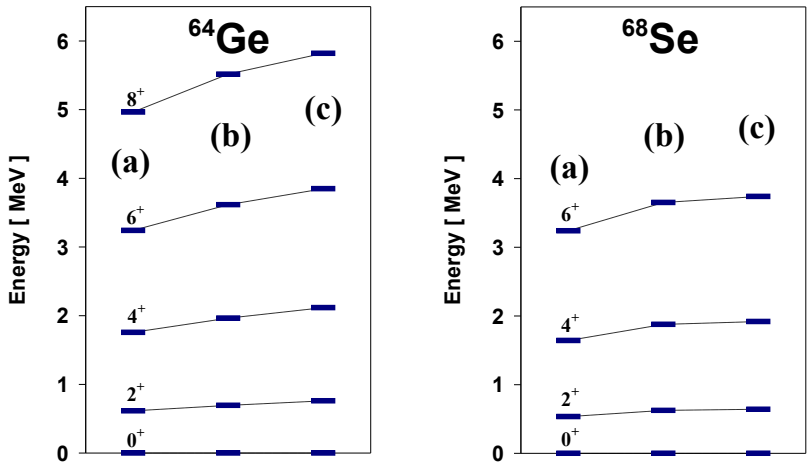

Figure 6.5: Role of the pn-pairing and the pair-scattering terms for the states in the g.s. band of ^{64}Ge and ^{68}Se: (a) both pair-scattering and pn-pairing contributions excluded, (b) only pair-scattering contribution excluded and (c) total interaction.

The effect of adding the proton-neutron pairing and the pair-scattering terms in the Hamiltonian is illustrated in Fig. 6.5. For our choice of model space (Table 6.1), the results for the g.s. bands demonstrate comparable size effects from both interactions, especially for ^{64}Ge, with the only clear exception being the 4_1^+ and 6_1^+ states in ^{68}Se. When a smaller number of irreps is included in the calculation, the pn-pairing interaction has a much bigger impact, an effect mainly visible for higher-spin states, while the role of the pair-scattering terms is strongly diminished.

6.3.2 B(E2) Transition Strengths and Wave Function Content

Electromagnetic transition strengths are normally calculated with the E2 transition operator of the form [8, 37, 56]:

$$\begin{aligned} T(E2) &\approx \sqrt{5/16\pi}A^{1/3}(e_\pi \frac{\tilde{\eta_\pi}+1}{\eta_\pi}\tilde{Q}_{\pi N} + e_\pi Q_{\pi U} \\ &+ e_\nu \frac{\tilde{\eta_\nu}+1}{\eta_\nu}\tilde{Q}_{\nu N} + e_\nu Q_{\nu U}). \end{aligned} \tag{6.3}$$

Instead, in this work we simply used the single dominant component in the pseudo-SU(3) expansion of the quadrupole operators in the normal-parity space. The effective charges e_π and e_ν were taken as $e_\pi = 1.5$ and $e_\nu = 0.5$ for the two versions of the realistic interaction and the extended-SU(3) calculations. The overall agreement between the results for both nuclei (Table 6.3 for ^{64}Ge and Table 6.4 for the g.s. band in ^{68}Se) is good, although some recent experimental findings for the $2^+_{g.s.} \rightarrow 0^+_{g.s.}$ transition strength in ^{64}Ge [86] seem to be underestimated by approximately a factor of 1.4. The correct behavior of the interband transitions is also nicely reproduced.

Table 6.3: B(E2) transition strengths for ^{64}Ge in units of e^2fm^4 calculated using the G-matrix interaction in full $pf_{5/2}$ and $pf_{5/2}g_{9/2}$ model spaces, and the extended SU(3) model. Entries in parentheses show the result when only the normal spaces are used in the calculations.

$(J+2)^+ \rightarrow J^+$	$pf_{5/2}$	$pf_{5/2}g_{9/2}$	Ext. SU(3)
$2^+_{g.s.} \rightarrow 0^+_{g.s.}$	257.22	253.91	292.80 (280.10)
$4^+_{g.s.} \rightarrow 2^+_{g.s.}$	332.54	342.51	346.26 (334.10)
$6^+_{g.s.} \rightarrow 4^+_{g.s.}$	340.51	356.92	380.39 (370.56)
$8^+_{g.s.} \rightarrow 6^+_{g.s.}$	303.31	320.14	273.84 (268.08)
$4^+_{\gamma} \rightarrow 2^+_{\gamma}$	89.26	93.13	67.25 (65.73)
$6^+_{\gamma} \rightarrow 4^+_{\gamma}$	164.23	144.19	207.18 (204.78)
$8^+_{\gamma} \rightarrow 6^+_{\gamma}$	92.12	84.38	74.79 (79.39)
$(J+1)^+ \rightarrow J^+$			
$3^+_{\gamma} \rightarrow 2^+_{\gamma}$	371.15	357.79	505.27 (493.39)
$5^+_{\gamma} \rightarrow 4^+_{\gamma}$	238.48	240.40	137.48 (135.48)
$7^+_{\gamma} \rightarrow 6^+_{\gamma}$	159.44	161.24	10.26 (10.17)
$J^+_{\alpha} \rightarrow J^+_{\beta}$			
$2^+_{\gamma} \rightarrow 0^+_{g.s.}$	1.98	1.42	5.71 (5.74)
$2^+_{\gamma} \rightarrow 2^+_{g.s.}$	251.68	241.41	183.16 (178.96)
$3^+_{\gamma} \rightarrow 2^+_{g.s.}$	4.21	3.40	9.90 (9.93)
$4^+_{\gamma} \rightarrow 4^+_{g.s.}$	72.10	74.69	47.11 (46.89)
$4^+_{\gamma} \rightarrow 2^+_{g.s.}$	18.86	19.31	6.70 (6.75)

More significant deviations are observed for the transitions between members of the $K = 2^+$ band and the $(J+1)^+ \rightarrow J^+$ transitions in ^{64}Ge. These could be attributed to the fact that some of the states from this band (e.g. 4^+_2 and 6^+_2) are found to be highly mixed with $S = 1$ irreps and differ more significantly from the rest thus displaying a less regular structure pattern throughout the band, for example, to what has been observed in the same bands of some rare-earth nuclei. It seems that the orbit-orbit interaction is the part of the Hamiltonian responsible for this feature. Results when only the normal-parity spaces are included in the calculation (shown in parentheses) reveal a contribution of the unique-parity sector of only up to 2-3%. An increase in this number is expected for higher-lying states or heavier nuclei where the dominant configurations are the ones with an occupied unique-parity space.

Finally, let us look at the content of the eigenfunctions for the states in the different bands. In the g.s. ($K = 0^+$) band of ^{64}Ge, one can clearly see the dominance of the leading and most deformed SU(3) irrep $(8, 4)$ (Fig.6.6 (a)) which gradually declines throughout the band from about 80% for $J = 0^+_{g.s.}$ to less than 40% for $J = 8^+_1$. Since the spin-orbit interaction is not as strong as in the case of the ds-shell nuclei, the mixing of irreps is smaller compared to the corresponding normal-SU(3) results

for ^{24}Mg and ^{28}Si [9]. On the other hand, as mentioned above, the $K = 2^+$ band follows a less regular pattern with some of the states being of highly mixed nature. The 0_2^+ state is found to be dominated (85%) by the $(\lambda, \mu), S = (9, 2), 1$ irrep. In the case of ^{68}Se, the leading irrep $(12, 0)$ contributes from 75 to 85% (Fig.6.6 (b)). A slight change in the type of Hamiltonian used may help establish the transition from states of prolate shape dominated by the irrep (12,0) in the g.s. band to ones where the (0,12) irrep prevails. To achieve this effect, we need to add a term proportional to the third-order Casimir invariant C_3 of SU(3). It was demonstrated earlier [9] that this term is capable of adjusting the prolate-oblate band crossing by driving irreps with $\mu >> \lambda$ lower in energy than those with $\lambda >> \mu$. The same term can also be used to fix the position of the first excited 0^+ state not assigned yet experimentally but predicted by our G-matrix calculations to lie at 1.05 MeV.

6.3.3 Reduction in the Model Space

Although the extended-SU(3) calculations are performed in a model space that involves the whole *gds* shell, the basis is still much smaller in size even compared with the one used for realistic calculations in the $pf_{5/2}g_{9/2}$ space. This drastic reduction translates into the use of only hundreds or at most a few thousand basis states (Table 6.5). For example, the size of the basis used in the extended-SU(3) calculations for ^{64}Ge represents only between 0.02% to 0.3% of that for unrestricted calculations in the $pf_{5/2}g_{9/2}$ model space. This means that a space spanned by a set of extended-SU(3) basis states may be computationally manageable beyond the limit accessible for the modern full-space shell-model calculations as is the case for the combination of the upper-*fp* and the *gds* shells. While some refinements in the model certainly could be done (like trying different and more sophisticated types of Hamiltonians, using different strengths for identical-particle and pn-pairing interactions, etc.) and the role of the model-space truncation may be further explored, the results presented in this dissertation suffice to demonstrate that the SU(3) scheme in its extended formulation can be a valuable tool for studying nuclei of the upper-*fp*-shell region.

Table 6.4: B(E2) transition strengths for the states in the g.s. band of ^{68}Se in units of e^2fm^4 calculated using the G-matrix interaction in full $pf_{5/2}$ model space and the extended SU(3) model. Entries in parentheses show the result when only the normal spaces are used in the calculations.

$(J+2)^+ \rightarrow J^+$	$pf_{5/2}$	Ext. SU(3)
$2^+_{g.s.} \rightarrow 0^+_{g.s.}$	322.71	354.17 (346.37)
$4^+_{g.s.} \rightarrow 2^+_{g.s.}$	448.07	486.65 (477.18)
$6^+_{g.s.} \rightarrow 4^+_{g.s.}$	441.58	473.89 (467.09)

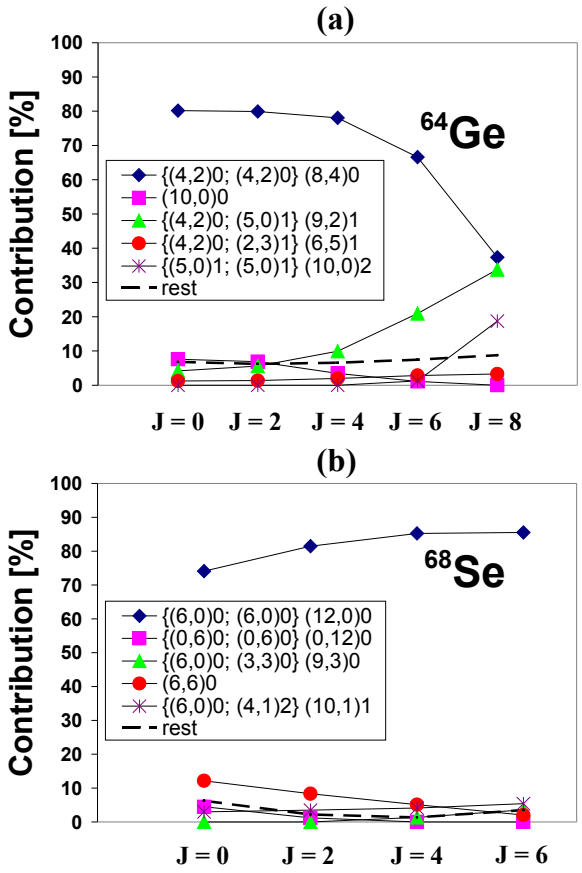

Figure 6.6: Wave-function decomposition of the calculated extended SU(3) eigenstates in the g.s. band of (a) ^{64}Ge and (b) ^{68}Se. The leading irreps from the dominant type configurations are listed explicitly while the effect of those with less than 3% contribution for any state as well as from configurations with two and four particles in the unique space is represented with a dashed line.

6.4 The Extended SU(3) Model - Future and Open Questions

The benefits of the extended SU(3) model will show up even more prominently in the more general and complicated case, namely, when the dominant configuration is no longer the one with an empty unique-parity space and/or in situations when two or more competing configurations are closer to one another in energy and as a consequence experience strong mixing.

The first case is realized in some heavier upper-*fp* shell nuclei. For example, the krypton isotopes, with distribution of particles between the normal- and unique-parity spaces represented in Fig. 6.7 (b), have as dominant configurations those with four particles in the unique-parity space. (For comparison, the distribution of particles for ^{64}Ge and ^{68}Se in the dominant configuration is shown in Fig. 6.7

Table 6.5: Model-space dimensions for the G-matrix calculations in the full (restricted) $pf_{5/2}g_{9/2}$ space for ^{64}Ge (^{68}Se) as well as for the complete $pf_{5/2}$ spaces and for the extended SU(3) shell model with the irreps listed in Table 6.1. (The entry marked with a $*$ is smaller by about a factor of two due to our taking advantage of time-reversal symmetry, which we did not invoke in the other cases as machine storage for them was not an issue.)

	J				
	0	2	4	6	8
		^{64}Ge			
$pf_{5/2}g_{9/2}$	1,831,531	1,728,929	1,454,930	1,090,581	724,318
$pf_{5/2}$	28,503	24,246	14,760	6,183	1,638
Ext. $SU(3)$	322	1,421	2,098	2,225	2,208
		^{68}Se			
$pf_{5/2}g_{9/2}$	1,929,014*	3,611,680	2,973,404	2,138,391	
$pf_{5/2}$	93,710	81,122	52,175	37,086	
Ext. $SU(3)$	397	1,765	2,640	3,115	

(a)). One challenge for such heavier upper-*fp* members is related to an expected evolution of the values for key parameters like χ and G [108], whose origin can be explained by the theory of effective interactions. This change does not seem to affect signifficantly the results for ^{64}Ge and ^{68}Se since it appears as a higher-order effect caused by the low mixing of the dominant type of configurations with the rest.

While the focus in this dissertation has been primarily directed towards the study of the upper-fp shell nuclei, a similar extension of the pseudo-SU(3) shell model is also possible and under development for other species. These include the rare-earth and actinide nuclei for which even more particles occupy the unique-parity spaces of the dominant configurations (Fig. 6.7(c)). The advantage for such systems is that they will be described with a somewhat simplified Hamiltonian, namely, the pn pairing and pair-scattering terms will disappear since the protons and the neutrons occupy different shells.

On the other hand, some stronger spin-orbit mixing effects are expected since the unique-parity spaces for the dominant configurations are occupied with particles residing in higher shells. As a result, the basis states of spin $S = 1$ will tend to enter more prominently in the low-lying states of the rare-earths and actinides. In order to oppose this effect, one can introduce the S^2 term in the Hamiltonian where S is the total spin. In short, there is expected to be strongly competition between basis states of spin $S = 1$ to those of higher C_2 values. As a result, the interplay between the spin and quadrupole modes is expected to prove interesting and should be studied.

Once established, the extension of the pseudo-SU(3) model for this region could improve the predictive capabilities of the theory. First, the richer model

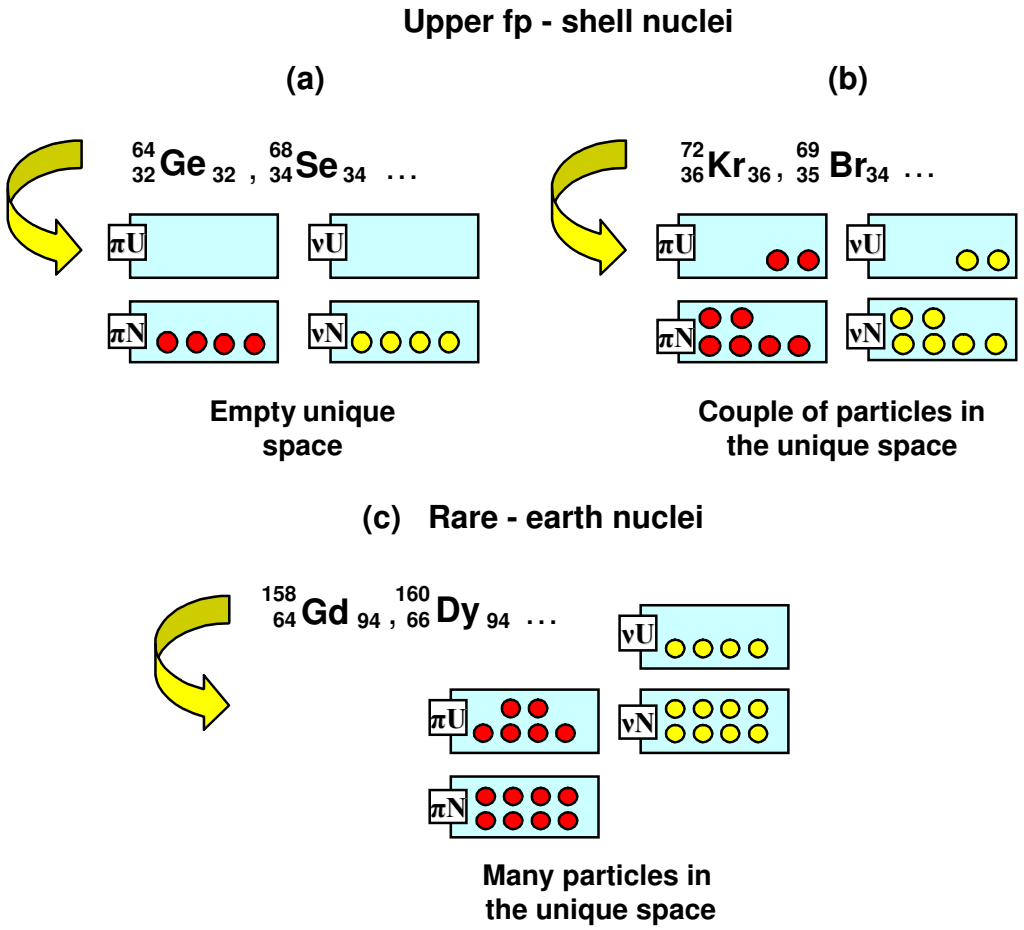

Figure 6.7: Dominant type of configurations for different nuclei.

space provided by the new model will revise the outcome for the fragmentation and clusterization in the B(M1) transition strengths. Secondly, the effective charge used in the B(E2) transition strengths will be strongly diminished. And finally, the role of the intruder levels is expected to be explored in a much less restrictive, but still manageable environment with model spaces that are of workable sizes.

Recent high resolution (p,t) experiments have established the existence of a large number of low-lying excited 0^+ levels in the deformed ^{158}Gd [111], ^{168}Er [112] and some actinide nuclei [113]. In addition, enhanced B(E2) transition strengths have been reported to members of the g.s. bands [114]. This abundance of 0^+ states is difficult to be explained within collective models like the geometric collective model or the interacting boson model [115]. The reason is that within such models, the number of collective degrees of freedom is limited. Other attempts to achieve theoretical descriptions have also been made [73, 116]. While all these models (in their simple or more elaborated version) manage to produce enough low-lying 0^+ states, they still lack the correct description of the enhanced B(E2) strengths.

The extended SU(3) shell model seems to be a superb candidate to resolve both problems since the explicit inclusion of the particles from the unique-parity space ensures a robust number of collective degrees of freedom and the Hamiltonian provides various means of obtaining the correct wave function structure.

Chapter 7

Conclusions

The main goal of this dissertation was to extend the usual pseudo-SU(3) shell model for upper-fp shell nuclei by integrating the intruder level(s) explicitly into the model space. This was accomplished in two ways: firstly by integrating only the $g_{9/2}$ level into the dynamics; and secondly by taking into account the entire *gds*-shell, organized via its SU(3) structure. We dubbed the latter the extended SU(3) shell model.

In order to develop a measured approach, we first calculated various nuclear characteristics using a realistic interaction. Specifically, the energy spectra, B(E2) transition strengths and the single-particle occupancy were calculated and the outcome of these calculations in different truncated model spaces were used to determine the most important configurations, sufficient for their reasonable description. Examination of the goodness of the pseudo-SU(3) symmetry revealed that many of the eigenstates in N=Z upper fp shell can be described at the 50 to 60 percent level by using only the leading pseudo-SU(3) representation. Including a reasonable number of irreps, which span a computationally manageable basis, this contribution raises from 80 to about 90 percent. In addition, it was found that the states from the g.s. band in some $N \neq Z$ isotopes tend to cluster the contributions in basis states even when they are for irreps of considerably smaller values of the second order Casimir operator. In the final analysis, seems that only a few representations (usually 2 or 3) constitute a very good approximation.

Various existing computational tools were extensively tested and some others developed. A newly implemented code allows the construction of an appropriate and based on some truncation principle extended-SU(3) basis in the coupled space originated from 4 separate subspaces. The Hamiltonian which was previously used in the SU(3) based models was extended by adding the proton-neutron pairing terms, an essential part of the residual interaction for N=Z nuclear systems. Also, the option for an interaction which mixes configurations with two different distributions of particles among the normal- and unique-parity spaces is added. Specifically, the terms which describe the scattering of pairs of particles between the normal- and unique-parity spaces were included in the Hamiltonian. Finally, procedure for parameter optimization was developed which in further and more elaborated studies will prove useful in determining the reasonable values of the interaction parameters.

While the work presented here only deals with the simplest case in which one configuration (the one with no particles in the unique-parity space) dominates all others, it is still possible to appreciate the strength of this new approach. Specifically, the model offers a richer model space compared to the previous SU(3) schemes by taking particles from the unique-parity space explicitly into account. As a result, the current approach presents an opportunity for a better description of the collectivity properties of the systems considered by reducing the effective charge needed in the description of their B(E2) transition strengths. These results will be even more pronounced for heavier systems where the intruder space is expected to have higher occupancy. This approach also offers an opportunity to explore the role of the intruder levels in the dynamics of the system as in the current study they are treated on the same footing as the normal parity orbitals. It is important to underscore that these advantages are accomplished within a highly truncated and symmetry-adapted basis, which possibly allows one to reach into otherwise computationally challenging (if not inaccessible) domains.

The findings for the nuclei ^{64}Ge and ^{68}Se reproduce results obtained with a realistic interation. Specifically, many of the states in the energy spectra and the B(E2) transition strengths are nicely reproduced. While the results are satisfactory for the states from the g.s. bands, there still seem to be some need for a more precise description of the nuclear characteristics related to the properties of the eigenfunctions. These could be addressed in the future by including some corrections with the use of more elaborate interactions. Nevertheless, the results certainly suggest that the extended SU(3) model can be a valuable tool in studying properties of nuclei of special interest from this region, such as those lying close to the proton drip line or/and actively participating in the processes of nucleosynthesis. They also point to an excellent opportunity to reveal the role the intruder levels play in the dynamics of the system in an exciting and completely new way, namely, considering their connection to their like-parity partners within the framework of a severely-truncated symmetry-adapted model space.

An extension of the SU(3) shell model for the rare-earth and actinide nuclei is also underway. It will be able to provide some valuable new information and a better understanding of the fragmentation and clusterization phenomena in the B(M1) transition strengths. Also, it will signifficantly reduce the values of the effective charges used in estimates of the B(E2) transition strengths. In addition, an expected new emerging structure of the states in the excited $K = 0^+$ bands could give an explanation for the enhanced B(E2) transition strengths to members of the g.s. band. Finally, the new model provides a powerful means of explanation for the abundance of low-lying $K = 0^+$ states found experimentally.

Bibliography

[1] M. G. Mayer, Phys. Rev. **75**, 1969 (1949); **78**, 16 (1950); O. Haxel, J. H. D. Jensen and H. E. Suess, Phys. Rev. **75**, 1766 (1949); Z. Physik 128, 295 (1950).

[2] S. E. Koonin, D. J. Dean, and K. Langanke, Phys. Rep. **577**, 1 (1996).

[3] J. P. Elliott, Proc. Roy. Soc. A **245**, 128 (1958).

[4] J. P. Draayer, T. Beuschel and J. G. Hirsch, J. Phys. G **25**, 605 (1999).

[5] J. Escher, J. P. Draayer, A. Faessler, Nucl. Phys. **A586**, 73 (1995).

[6] K. H. Bhatt, C. W. Nestor, Jr. and S. Raman, Phys. Rev. C **46**, 164 (1992).

[7] S. Åberg, H. Flocard, and W. Nazarewicz, Annu. Rev. Nucl. Part. Sci. **40**, 469 (1990).

[8] K. H. Bhatt, S. Kahane, and S. Raman, Phys. Rev. C **61**, 034317 (2000).

[9] C. Vargas, J. G. Hirsch, and J. P. Draayer, Nucl. Phys. **A690**, 409 (2001).

[10] C. E. Vargas, J. G. Hirsch, and J. P. Draayer, Nucl. Phys. **A697**, 655 (2002).

[11] C. Vargas, J. G. Hirsch, T. Beuschel, and J. P. Draayer, Phys. Rev. C **61**, 031301 (2000).

[12] R. D. Ratna Raju, J. P. Draayer and K. T. Hecht, Nucl. Phys. **A202**, 433 (1973).

[13] H. Schatz et al., Phys. Rep. **294**, 167 (1998).

[14] A. Arima and F. Iachello, Ann. Phys. **99**, 253 (1976); ibid. **111**, 201 (1978).

[15] J. P. Elliott, Proc. Roy. Soc. A **245**, 562 (1958); J. P. Elliott and M. Harvey, Proc. Roy. Soc. A **272**, 557 (1963); J. P. Elliott and C. E. Wilsdon, Proc. Roy. Soc. A **302**, 509 (1968).

[16] A. Messiah, *Quantum Mechanics*, North Holland: Wiley and Sons (1958).

[17] J. P. Elliott, *Proceedings of the international school of physics "Enrico Fermi"*, Academic Press, New York (1966).

[18] R. F. Casten, J. P. Draayer, K. Heyde, P. Lipas, T. Otsuka, and D. Warner, *Algebraic Approaches to Nuclear Structure: Interacting Boson and Fermion Models*, Harcourt, Brace, and Jovanovich, New York, 436 (1993).

[19] J. P. Draayer and D. Troltenier, *Geometric interpretation for SU(3) outer multiplicity label*, (LSU 1994).

[20] J. F. Cornwell in: *Techniques in Physics 7: Group theory in Physics, Vol. 2*, Academic Press, Orlando (1985).

[21] Y. Leschber, Hadronic Journal Supplement **3**, 1 (1987).

[22] P. Ring and P. Schuck, *The Nuclear Many-Body Problem*, Springer-Verlag, 1980.

[23] H. A. Naqvi and J. P. Draayer, Nucl. Phys. **A516**, 351 (1990).

[24] H. A. Naqvi and J. P. Draayer, Nucl. Phys. **A536**, 297 (1992).

[25] W. Heisenberg, Z Phys. 33, 879 (1925); M. Born, P. Jordan, Z. Phys. 34, 858 (1925).

[26] E. Schrödinger, Ann. Phys. 79, 361 (1926); ibid. 79, 489 (1926), Ann. Phys. 79, 734 (1926); Ann. Phys. 80, 437 (1926).

[27] H. B. G. Casimir: Rotation of a Rigid Body in Quantum Mechanics, Thesis (The Hague, J. B. Wolters, 1931).

[28] O. Castaños, J. P. Draayer, and Y. Leschber, Z. Phys. **A329**, 71 (1988).

[29] Y. Leschber and J. P. Draayer, Phys. Lett. **B190**, 1 (1987).

[30] J. Carvalho: Ph. D. Thesis, University of Toronto (1984).

[31] B. R. Judd, W. Miller Jr, J. Patera, and P. Winternitz, J. Math. Phys. **15**, 1787 (1974).

[32] Y. Akiyama and J. P. Draayer, Comp. Phys. Commun. **5**, 405 (1973).

[33] J. P. Draayer and Y. Akiyama, J. Math. Phys. **14**, 1904 (1973).

[34] S. T. Belyaev, Dan. Mat. Fys. Medd. **31**, 11 (1959).

[35] D. R. Bes and R. A. Sorensen, Advances in Nuclear Physics **2**, 129 (1969).

[36] C. Bahri, J. Escher, and J. P. Draayer, Nucl. Phys. **A592**, 171 (1995); **A 594**, 485 (1995).

[37] O. Castaños, J. P. Draayer, and Y. Leschber, Ann. Phys. **180**, 290 (1987).

[38] D. Troltenier, C. Bahri, J. P. Draayer, Nucl. Phys. **A586**, 53 (1995).

[39] H. A. Jahn and J. Hope, Phys. Rev. **93**, 318 (1954).

[40] D. A. Varshalovich, A. N. Moskalev, and V. K. Khersonskii, *Quantum Theory of Angular Momentum*, World Scientific, Singapore (1988).

[41] D. J. Millener, J. Math. Phys. 19, 1513 (1978).

[42] C. Bahri et al., in preparation.

[43] P. J. Brussard and P. M. Glaudemans, *Shell-Model Applications in Nuclear Spectroscopy*, North-Holland, Amsterdam, 1997.

[44] J. P. Draayer and G. Rosensteel, Nucl. Phys. **A439**, 61 (1985).

[45] A. Arima, M. Harvey and K. Shimizu, Phys. Lett. B **30**, 517 (1969).

[46] K. T. Hecht and A. Adler, Nucl. Phys. **A137**, 129 (1969).

[47] C. Bahri, J. P. Draayer, and S. A. Moszkowski, Phys. Rev. Lett. **68**, 2133 (1992).

[48] J. P. Draayer, *Pseudospin in Perspective*, in Group Theory in Physics, Cocoyoc, Morelos, Mexico, June 3-7, 1991, ed. by A. Frank, T. H. Seligman, and K. B. Wolf (American Institute of Physics, Cocoyoc, Morelos, Mexico, 1991).

[49] O. Castaños, M. Moshinsky, and C. Quesne, Phys. Lett. **B277**, 238 (1992).

[50] A. L. Blokhin, C. Bahri, and J. P. Draayer, Phys. Rev. Lett. **74**, 4149 (1995); A. L. Blokhin, T. Beuschel, J. P. Draayer, and C. Bahri, Nucl. Phys. **A612**, 163 (1997).

[51] A. Bohr and B. R. Mottelson, Nuclear Structure, Vol. I & II (Benjamin, Reading, Mass., 1975).

[52] Y. Nambu and G. Jona-Lasinio, Phys. Rev. **124**, 246 (1961); ibid. **122**, 345 (1961); H. Reinhardt, Phys. Lett. **B 188**, 263 (1987).

[53] B. D. Serot and J. D. Walecka, Advances in Nuclear Physics **16**, (1986).

[54] J. Zimanyi and S. A. Moszkowski, Phys. Rev. C **42**, 1416 (1990).

[55] J. P. Draayer, K. J. Weeks, and K. T. Hecht, Nucl. Phys. **A381**, 1 (1982).

[56] J. P. Draayer and K. J. Weeks, Ann. Phys. **156**, 41 (1984).

[57] C. Bahri, J. P. Draayer, Compt. Phys. Comm. **83**, 59 (1994).

[58] D. Troltenier, C. Bahri, J. P. Draayer, Nucl. Phys. **A589**, 75 (1995).

[59] C. Vargas, J. G. Hirsch, P. O. Hess, and J. P. Draayer, Phys. Rev. C **58**, 1488 (1998).

[60] A. P. Zuker, J. Retamosa, A. Poves, and E. Caurier, Phys. Rev. C **52**, R1741 (1995).

[61] T. Beuschel, J. P. Draayer, D. Rompf, J. G. Hirsch, Phys. Rev. C **57**, 1233 (1998).

[62] T. Beuschel, J. G. Hirsch, and J. P. Draayer, Phys. Rev. C. **61**, 054307 (2000).

[63] D. Troltenier, J. P. Draayer, and J. G. Hirsch, Nucl. Phys. **A601**, 89 (1996).

[64] D. Rompf, T. Beuschel, J. P. Draayer, and W. Scheid, Phys. Rev. C **57**, 1703 (1998).

[65] G. Popa, J. G. Hirsch, and J. P. Draayer, Phys. Rev. C **62**, 064313 (2000).

[66] J. P. Draayer, G. Popa, and J. G. Hirsch, Acta Phys. Pol. B **32**, 2697 (2001).

[67] C. E. Vargas and H. G. Hirsch, Phys. Rev. C **70**, 064320 (2004).

[68] C. E. Vargas, J. G. Hirsch, J. P. Draayer, Nucl. Phys. **A673**, 219 (2000).

[69] C. E. Vargas, J. G. Hirsch, J. P. Draayer, Phys. Rev. C **66**, 064309 (2002).

[70] V. G. Gueorguiev, J. P. Draayer, and C. J. Johnson, Phys. Rev. C **63**, 014318 (2000).

[71] D. Strottman, Nucl. Phys. **A188**, 488 (1972).

[72] K. Kaneko, M. Hasegawa, and T. Mizusaki, Phys. Rev. C **70**, 051301(R) (2004).

[73] Y. Sun, A. Aprahamian, J. Zhang, and C. T. Lee, Phys. Rev. C **68**, R061301 (2003).

[74] S. M. Vincent et al., Phys. Rev. C **60**, 064308 (1999).

[75] K. Kaneko, M. Hasegawa, and T. Mizusaki, Phys. Rev. C **66**, 051306(R) (2002).

[76] E. Caurier, F. Nowacki, and A. Poves, Phys. Rev. Lett. **95**, 042502 (2005).

[77] E. Caurier and F. Nowacki, Acta Phys. Pol. B **30**, 705 (1999).

[78] R. R. Whitehead, A. Watt, B. J. Cole and I. Morrison, Adv. Nucl. Phys. **9**, 123 (1977).

[79] H. G. Golub and C. F. Van Loan, "Matrix Computations" The Johns Hopkins University Press, Baltimor (1989). J. K. Cullum and R. A. Wiloughby, "Lanczos algorithms for large symmetric eigenvalue computations", Birkhauser, Boston (1995).

[80] C. Lanczos, J. Res. Nat. Bur. Stan. B **45**, 255 (1950).

[81] C. A. Ur et al., Phys. Rev. C **58**, 3163 (1998).

[82] M. Kaluza, Comp. Phys. Comm. **79**, 425 (1994).

[83] A. Costin, N. Pietralla, T. Koike, C. Vaman, T. Ahn, and G. Rainovski, Phys. Rev. C **72**, 054305 (2005).

[84] A. Lisetskiy et al., Phys. Rev. C **68**, 034316 (2003).

[85] S. M. Vincent et al., Phys. Lett. **B437**, 264 (1998).

[86] K. Starosta et al., Phys. Rev. Lett. **99**, 042503 (2007).

[87] E. Caurier, F. Nowacki, A. Poves, J. Retamosa, Phys. Rev. Lett. **77** (1996) 1954.

[88] F. Nowacki, Ph. D. thesis, ULP Strasbourg, 1995 (unpublished).

[89] A. Abzouzi, E. Caurier, and A. P. Zuker, Phys. Rev. C **66**, 1134 (1991).

[90] P. Van Isacker, O. Juillet and F.Nowacki, Phys. Rev. Lett. **82**, 2060 (1999).

[91] T. Kuo and G. E. Brown, Nucl. Phys. **A114**, 241 (1968); A. Poves and A. P. Zuker, Phys. Rep. **70**, 235 (1981).

[92] B. H. Wildenthal, Prog. Part. Nucl. Phys. **11**, 5 (1984).

[93] National Nuclear Data Center, http://www.nndc.bnl.gov.

[94] G. Martinez-Pinedo, A. P. Zuker, A. Poves, and E. Caurier, Phys. Rev. C **55**, 187 (1997).

[95] E. Caurier, J. L. Egido, G. Martinez-Pinedo, A. Poves, J. Retamosa, L. M. Robledo, and A. P. Zuker, Phys. Rev. Lett. **75**, 2466 (1995).

[96] K. L. G. Heyde, *The Nuclear Shell Model* (Springer-Verlag, Berlin, Heidelberg, New York, 1990).

[97] M. F. O'Reilly, J. Math. Phys. **23**, 2022 (1982).

[98] C. Bahri, Ph. D. Dissertation - "Pairing and quadrupole interactions in the pseudo-$SU(3)$ shell model", unpublished.

[99] S. C. Park, J. P. Draayer, and S. Zheng, *Time-Space Optimal Numerical Database for Large-Scale Scientific Applications*, in Interanational Computer Symposium 1990, December 17-19, edited by Hsinchu, Taiwan, ROC, 1990.

[100] S. C. Park, C. Bahri, J. P. Draayer, and S.-Q. Zheng, Comp. Phys. Comm., **82**, 247 (1994).

[101] D. Troltenier, SU(3) shell model code, unpublished.

[102] J. P. Draayer, Y. Leschber, S. C. Park and R. Lopez, Comp. Phys. Comm. **56**, 279 (1989).

[103] http://www.netlib.org/minpack/

[104] P. J. Ennis et al., Nucl. Phys. **A535**, 392 (1991).

[105] Y. Sun, M. Wiescher, A. Aprahamian, J. Fisker, Nucl. Phys. **A758**, 765c (2005).

[106] H. Schatz et al., Phys. Rev. Lett. **86**, 3471 (2001).

[107] R. K. Wallace and S. E. Woosley, Astrophys. J. Suppl. **45**, 389 (1981).

[108] M. Dufour, A. P. Zuker, Phys. Rev. C **54**, 1641 (1996).

[109] K. C. Tripathy and R. Sahu, Int. Journ. Mod. Phys. E **11**, 531 (2002).

[110] S. M. Fischer, D. P. Balamuth, P. A. Hausladen, C. J. Lister, M. P. Carpenter, D. Seweryniak, and J. Schwartz, Phys. Rev. Lett. **84**, 4064 (2000).

[111] S. R. Lesher et al., Phys. Rev C **66**, 051305(R) (2002).

[112] D. Bucurescu et al., Annual Report of the Meier-Leibbnitz Laboratory (University and Technical University of Munich).

[113] H.-F. Wirth et al., Phys. Rev. C **69**, 044310 (2004).

[114] S. R. Lesher et al., in *Nuclear Physics in the 21-st century*, ed. by E. Norman et al., AIP Conf. Proc. 610, 798 (AIP, Melville, NY, 2002).

[115] N. V. Zamfir, Jing-ye Zhang, and R. F. Casten, Phys. Rev. C **66**, 057303 (2002).

[116] N. Lo Iudice, A. V. Sushkov, and N. Yu. Shirikova, Phys. Rev. C **70**, 064316 (2004).

[117] D. Troltenier, J. P. Draayer, P. O. Hess and O. Castaños, Nucl. Phys. **A576**, 351 (1994).

Appendix A

$SU(3)$ Wigner Coefficients

Using the notation defined in [32], the Wigner SU(3) coupling coefficients

$$\langle (\lambda_1, \mu_1)\alpha_1; (\lambda_2, \mu_2)\alpha_2 | \, (\lambda_3, \mu_3)\alpha_3 \rangle_\rho \tag{A.1}$$

are defined as the elements of a unitary transformation between coupled and uncoupled orthonormal irreps of SU(3) in the α scheme. In the case of the $SU(3) \supset SO(3)$ reduction with $\alpha = \kappa l m$ used throughout this dissertation (versus the other possibility, the $SU(3) \supset SU(2) \otimes U(1)$ reduction with $\alpha = \epsilon \Lambda M_\Lambda$), we have that

$$\begin{aligned} &|\rho(\lambda_3, \mu_3)\kappa_3 l_3 m_3\rangle = \\ &\sum_{\kappa_1 l_1 m_1 \kappa_2 l_2 m_2} \langle (\lambda_1, \mu_1)\kappa_1 l_1 m_1; (\lambda_2, \mu_2)\kappa_2 l_2 m_2 | \, (\lambda_3, \mu_3)\kappa_3 l_3 m_3 \rangle_\rho \\ &|(\lambda_1, \mu_1)\kappa_1 l_1 m_1\rangle \, |(\lambda_2, \mu_2)\kappa_2 l_2 m_2\rangle \, , \end{aligned} \tag{A.2}$$

and the inverse transformation is given by

$$\begin{aligned} &|(\lambda_1, \mu_1)\kappa_1 l_1 m_1\rangle \, |(\lambda_2, \mu_2)\kappa_2 l_2 m_2\rangle = \\ &\sum_{\rho(\lambda_3, \mu_3)\kappa_3 l_3 m_3} \langle (\lambda_1, \mu_1)\kappa_1 l_1 m_1; (\lambda_2, \mu_2)\kappa_2 l_2 m_2 | \, (\lambda_3, \mu_3)\kappa_3 l_3 m_3 \rangle_\rho \\ &|\rho(\lambda_3, \mu_3)\kappa_3 l_3 m_3\rangle \, . \end{aligned} \tag{A.3}$$

The orthonormality relations for the Wigner SU(3) coupling coefficients are

$$\begin{aligned} &\sum_{\kappa_1, l_1, m_1, \kappa_2, l_2, m_2} \langle (\lambda_1, \mu_1)\kappa_1 l_1 m_1; (\lambda_2, \mu_2)\kappa_2 l_2 m_2 | \, (\lambda_3, \mu_3)\kappa_3 l_3 m_3 \rangle_\rho \\ &\langle (\lambda_1, \mu_1)\kappa_1 l_1 m_1; (\lambda_2, \mu_2)\kappa_2 l_2 m_2 | \, (\lambda_3', \mu_3')\kappa_3 l_3 m_3 \rangle_{\rho'} = \\ &\delta_{\lambda_3 \lambda_3'} \delta_{\mu_3 \mu_3'} \delta_{\rho \rho'}, \end{aligned} \tag{A.4}$$

and

$$\sum_{\rho(\lambda_3,\mu_3)\kappa_3,l_3,m_3} \langle(\lambda_1,\mu_1)\kappa_1 l_1 m_1;(\lambda_2,\mu_2)\kappa_2 l_2 m_2|\,(\lambda_3,\mu_3)\kappa_3 l_3 m_3\rangle_\rho$$
$$\langle(\lambda_1,\mu_1)\kappa_1' l_1' m_1';(\lambda_2,\mu_2)\kappa_2' l_2' m_2'|\,(\lambda_3,\mu_3)\kappa_3 l_3 m_3\rangle_\rho =$$
$$\delta_{\kappa_1\kappa_1'}\delta_{l_1 l_1'}\delta_{m_1 m_1'}\delta_{\kappa_2\kappa_2'}\delta_{l_2 l_2'}\delta_{m_2 m_2'}. \tag{A.5}$$

It is possible to factor out the dependence of the $SU(3) \supset SO(3)$ Wigner coupling coefficients on the m subgroup labels by defining so-called double-barred or "reduced" SU(3) Wigner coupling coefficients:

$$\langle(\lambda_1,\mu_1)\kappa_1 l_1 m_1;(\lambda_2,\mu_2)\kappa_2 l_2 m_2|\,(\lambda_3,\mu_3)\kappa_3 l_3 m_3\rangle_\rho =$$
$$\underbrace{\langle(\lambda_1,\mu_1)\kappa_1 l_1;(\lambda_2,\mu_2)\kappa_2 l_2\|(\lambda_3,\mu_3)\kappa_3 l_3\rangle_\rho}_{\text{reduced Wigner coefficient}}\underbrace{\langle l_1 m_1; l_2 m_2|\, l_3 m_3\rangle}_{\text{geometric part}}. \tag{A.6}$$

From the unitarity of the full SU(3) Wigner and the ordinary SU(2) Clebsch-Gordan coefficients it follows that the double-barred coefficients are also unitary. With the phase convention from [32] they become real, and therefore orthogonal.

Next, we list several symmetry relations for $SU(3)$ coupling coefficients [32]; equivalent relations for reduced $SU(3)$ coupling coefficients can easily be derived by making use of the proper symmetry relations for Clebsch-Gordan coefficients [40]. For example, one finds that $1 \leftrightarrow 3$ interchange of the quantum labels is given by:

$$\langle(\lambda_1,\mu_1)\kappa_1 l_1 m_1;(\lambda_2,\mu_2)\kappa_2 l_2 m_2|\,(\lambda_3,\mu_3)\kappa_3 l_3 m_3\rangle_\rho =$$
$$(-1)^{\phi+\chi_2}\sqrt{\frac{\dim(\lambda_3,\mu_3)}{\dim(\lambda_1,\mu_1)}}$$
$$\langle(\lambda_3,\mu_3)\kappa_3 l_3 m_3;(\mu_2,\lambda_2)\kappa_2 l_2 - m_2|\,(\lambda_1,\mu_1)\kappa_1 l_1 m_1\rangle_\rho, \tag{A.7}$$

where the dimension of a SU(3) irrep is given by $\dim(\lambda,\mu) = \frac{1}{2}(\lambda{+}1)(\mu{+}1)(\lambda{+}\mu{+}1)$, $\phi = (\lambda_1+\mu_1)+(\lambda_2+\mu 2)-(\lambda_3+\mu_3)$ and $\chi_i = (\lambda_i-\mu_i)+l_i-m_i$.

The $1 \leftrightarrow 2$ interchange is more complicated:

$$\langle(\lambda_1,\mu_1)\kappa_1 l_1 m_1;(\lambda_2,\mu_2)\kappa_2 l_2 m_2|\,(\lambda_3,\mu_3)\kappa_3 l_3 m_3\rangle =$$
$$\sum_{\rho'}\Phi_{\rho\rho'}[(\lambda_1,\mu_1),(\lambda_2,\mu_2);(\lambda_3,\mu_3)]$$
$$\langle(\lambda_2,\mu_2)\kappa_2 l_2 m_2;(\lambda_1,\mu_1)\kappa_1 l_1 m_1|\,(\lambda_3,\mu_3)\kappa_3 l_3 m_3\rangle_{\rho'}, \tag{A.8}$$

since it requires a phase matrix Φ. If the $SU(3)$ coupling $(\lambda_1,\mu_1)\otimes(\lambda_2,\mu_2) \to (\lambda_3,\mu_3)$ is unique, i.e. when $\rho_{\max}=1$, the matrix reduces to a simple phase factor: $\Phi_{11}[(\lambda_1,\mu_1),(\lambda_2,\mu_2);(\lambda_3,\mu_3)] = (-1)^\phi$.

Appendix B

Algebraic Relations for $SU(3)$ Wigner Coefficients: Wigner-Eckart Theorem

A set of quantities $\{T\}$ form an irreducible tensor $T^{(\lambda,\mu)}$ with respect to $SU(3)$ if the elements of $\{T\}$ transform under $SU(3)$ in the same way as the corresponding basis states, i.e. if the elements of $\{T\}$ transform under $SU(3)$ as

$$\left[C^{11}_{\alpha}, T^{(\lambda,\mu)}_{\beta}\right] = \sum_{\gamma} \langle (\lambda,\mu)\gamma | C^{11}_{\alpha} | (\lambda,\mu)\beta \rangle T^{(\lambda,\mu)}_{\gamma}, \tag{B.1}$$

where C^{11}_{α} are the generators with (λ,μ) and, α, β and γ respectively, the irrep and intra-irrep labels of $SU(3)$. With the $SU(3)$ coupling coefficients introduced in Appendix A, irreducible tensors can be coupled according to the rules for coupling $SU(3)$ tensors to give a new tensor:

$$\left[T^{(\lambda_1,\mu_1)} \otimes T^{(\lambda_2,\mu_2)}\right]^{\rho(\lambda_3,\mu_3)}_{\kappa_3 l_3 m_3} =$$

$$\sum_{\kappa_1 l_1 m_1 \kappa_2 l_2 m_2} \langle (\lambda_1,\mu_1)\kappa_1 l_1 m_1; (\lambda_2,\mu_2)\kappa_2 l_2 m_2 | \, (\lambda_3,\mu_3)\kappa_3 l_3 m_3 \rangle \tag{B.2}$$

$$T^{(\lambda_1,\mu_1)}_{\kappa_1 l_1 m_1} T^{(\lambda_2,\mu_2)}_{\kappa_2 l_2 m_2}. \tag{B.3}$$

The Wigner-Eckart theorem, known from angular momentum theory, allows one to express the matrix element of a tensor operator in terms of the product of a reduced matrix element that is only a function of the angular momenta and a Clebsch-Gordan coefficient that contains the projection quantum numbers [16]:

$$\langle l_3 m_3 | T^{l_2}_{m_2} | l_1 m_1 \rangle = \frac{(-1)^{l_2}}{\sqrt{2l_3+1}} \langle l_1 m_1 l_2 m_2 | l_3 m_3 \rangle \, \langle l_3 \| T^{l_2} \| l_1 \rangle. \tag{B.4}$$

This factorization into a geometric part and a reduced matrix element allows one to calculate and store relatively few reduced matrix elements before running a computer

code to evaluate the full set of matrix elements which can then be easily generated by just multiplying these reduced matrix elements with a Clebsch-Gordan coefficient.

This procedure can be generalized for the $SU(3)$ case where the matrix element of a $SU(3)$ irreducible tensor operator can be written as the product of a $SU(3)$ Clebsch-Gordan coefficient and a so-called double-barred reduced matrix element [33]. For the $SU(3) \supset SU(2)$ subgroup chain this generalized $SU(3)$ Wigner-Eckart theorem has the form

$$\begin{aligned}
&\langle(\lambda_3,\mu_3)\kappa_3 l_3 m_3|T^{(\lambda_2,\mu_2)\kappa_2 l_2 m_2}|(\lambda_1,\mu_1)\kappa_1 l_1 m_1\rangle = \\
&\langle l_1 m_1; l_2 m_2|\, l_3 m_3\rangle\langle(\lambda_3,\mu_3)\kappa_3 l_3\|T^{(\lambda_2,\mu_2)\kappa_2 l_2}\|(\lambda_1,\mu_1)\kappa_1 l_1\rangle, \qquad \text{(B.5)}
\end{aligned}$$

with $\langle(\lambda_3,\mu_3)\kappa_3 l_3\|T^{(\lambda_2,\mu_2)\kappa_2 l_2}\|(\lambda_1,\mu_1)\kappa_1 l_1\rangle$ being a (double-barred) SU(2)-reduced matrix element. Analogously, it is possible to extend this scheme in defining a $SU(3)$-reduced (= triple-barred) matrix element. The important difference is the summation over the multiplicity index ρ

$$\begin{aligned}
&\langle(\lambda_3,\mu_3)\kappa_3 l_3 m_3|T^{(\lambda_2,\mu_2)\kappa_2 l_2 m_2}|(\lambda_1,\mu_1)\kappa_1 l_1 m_1\rangle \\
= &\sum_\rho \langle(\lambda_1,\mu_1)\kappa_1 l_1 m_1; (\lambda_2,\mu_2)\kappa_2 l_2 m_2|\, (\lambda_3,\mu_3)\kappa_3 l_3 m_3\rangle_\rho \\
&\langle(\lambda_3,\mu_3)|||T^{(\lambda_2,\mu_2)}|||(\lambda_1,\mu_1)\rangle_\rho \\
= &\sum_\rho \langle l_1 m_1; l_2 m_2|\, l_3 m_3\rangle\langle(\lambda_1,\mu_1)\kappa_1 l_1; (\lambda_2,\mu_2)\kappa_2 l_2\|(\lambda_3,\mu_3)\kappa_3 l_3\rangle_\rho \\
&\langle(\lambda_3,\mu_3)|||T^{(\lambda_2,\mu_2)}|||(\lambda_1,\mu_1)\rangle_\rho. \qquad \text{(B.6)}
\end{aligned}$$

Often, one has to consider a quantum-mechanical system which consists of two subsystems, 1 and 2 (for example, protons and neutrons). Reduced matrix elements for the irreducible tensor product of two operators, $T^{(\lambda_t,\mu_t)}(1)$ and $U^{(\lambda_u,\mu_u)}(2)$, which depend only on the variables of the first and second subsystem, respectively, may be evaluated with the help of the following reduction rule:

$$\begin{aligned}
&\langle[(\lambda_1,\mu_1)\otimes(\lambda_2,\mu_2)]^{\rho(\lambda,\mu)} \\
&||| \,[T^{(\lambda_t,\mu_t)}(1)\otimes U^{(\lambda_u,\mu_u)}(2)]^{\rho_0(\lambda_0,\mu_0)} \,||| \\
&[(\lambda_1',\mu_1')\otimes(\lambda_2',\mu_2')]^{\rho'(\lambda',\mu')}\rangle_{\tilde\rho} = \\
&\sum_{\rho_1\rho_2}\chi\begin{Bmatrix}
(\lambda_1',\mu_1') & (\lambda_t,\mu_t) & (\lambda_1,\mu_1) & \rho_1 \\
(\lambda_2',\mu_2') & (\lambda_u,\mu_u) & (\lambda_2,\mu_2) & \rho_2 \\
(\lambda',\mu') & (\lambda_0,\mu_0) & (\lambda',\mu') & \tilde\rho \\
\rho' & \rho_0 & \rho &
\end{Bmatrix} \\
&\langle(\lambda_1,\mu_1)|||T^{(\lambda_t,\mu_t)}(1)|||(\lambda_1',\mu_1')\rangle_{\rho_1}\langle(\lambda_2,\mu_2)|||U^{(\lambda_u,\mu_u)}(2)|||(\lambda_2',\mu_2')\rangle_{\rho_2}. \qquad \text{(B.7)}
\end{aligned}$$

Appendix C

On the Evaluation of Operators with $SU(3)$ Character

The evaluation of many-body operators with $SU(3)$ tensor character can be simplified with the use of the $SU(3)$ Wigner-Eckart theorem. It is known that a one-body tensor operator $\mathcal{F}^{(\lambda_0,\mu_0),S_0}_{\kappa_0 L_0 M_{L_0},M_{S_0}}$ of rank (λ_0,μ_0) and spin S_0 can be expressed in second quantization formalism as [37]:

$$\mathcal{F}^{(\lambda_0,\mu_0),S_0}_{\kappa_0 L_0 M_{L_0},M_{S_0}} = \sum_{\{-\}} \langle (\eta,0) l' m'; \frac{1}{2} m'_s \| f^{(\lambda_0,\mu_0),S_0}_{\kappa_0 L_0 M_{L_0},M_{S_0}} \| (\eta,0) l m; \frac{1}{2} m_s \rangle$$
$$a^{\dagger}_{(\eta,0) l' m'; \frac{1}{2} m'_s} a_{(\eta,0) l m; \frac{1}{2} m_s}, \tag{C.1}$$

where $\{-\}$ stands for $\{ll'mm'm_sm'_s\}$. In general, the $SU(3)$ irreps of the initial and final single-particle state could be different, corresponding to an "excitation" operator that shifts a particle from shell η to shell η'. In this work, however, the so-called symplectic extension of the $SU(3)$ model which describes such shell mixing effects [117] are not used and only operators that act within a single shell are considered.

By applying the Wigner-Eckart theorem and the symmetry properties of the $SU(3)$ and $SU(2)$ coupling coefficients, the above expression for a second quantized operator can be rewritten in terms of a triple-barred reduced matrix element:

$$\mathcal{F}^{(\lambda_0,\mu_0),S_0}_{\kappa_0 L_0 M_{L_0},M_{S_0}} = \langle (\eta,0); \frac{1}{2} ||| f^{(\lambda_0,\mu_0),S_0} ||| (\eta,0); \frac{1}{2} \rangle$$
$$\left[\frac{2\mathrm{dim}(\eta,0)}{(2S_0+1)\mathrm{dim}(\lambda_0,\mu_0)} \right]^{\frac{1}{2}} \{ \sum_{ll'} \sum_{mm'm_sm'_s} (-1)^{\eta+l-m+\frac{1}{2}-m_s}$$
$$\left\langle \frac{1}{2} m'_s, \frac{1}{2} - m_s | S_0 M_{S_0} \right\rangle \langle l'm', l-m | L_0 M_{L_0} \rangle$$
$$\langle (\eta,0) l'; (0,\eta) l \| (\lambda_0,\mu_0) \kappa_0 L_0 \rangle a^{\dagger}_{(\eta,0) l' m'; \frac{1}{2} m'_s} a_{(\eta,0) l m; \frac{1}{2} m_s} \}. \tag{C.2}$$

The expression for an operator in second quantized form can be simplified if we use the fact that the creation operator for a spin $\frac{1}{2}$ particle in shell η is a proper $SU(3)$

tensor of rank $(\eta, 0)$,

$$a^{\dagger(\eta,0),\frac{1}{2}}_{lm_l,m_s}|0\rangle = \left|(\eta,0)lm_l,\frac{1}{2}m_s\right\rangle, \tag{C.3}$$

and determine that the corresponding annihilation tensor $\tilde{a}^{(0,\eta),\frac{1}{2}}$ is related to the annihilation operator by

$$a^{(0,\eta),\frac{1}{2}}_{lm_l,m_s} = (-)^{\eta+l+m_l+\frac{1}{2}+m_s}\tilde{a}^{(\eta,0),\frac{1}{2}}_{l-m_l;-m_s}. \tag{C.4}$$

By coupling the single-particle creation and annihilation operators to a tensor of rank (λ_0, μ_0) and spin S_0, we have

$$\begin{aligned}
&[a^{\dagger(\eta,0);\frac{1}{2}}\otimes\tilde{a}^{(0,\eta);\frac{1}{2}}]^{(\lambda_0,\mu_0),S_0}_{\kappa_0 l_0 M_{L_0},M_{S_0}} = \\
&\sum_{ll'}\langle(\eta,0)l';(0,\eta)l\|(\lambda_0,\mu_0)\kappa_0 L_0\rangle \\
&\sum_{mm'm_sm'_s}\left\langle\frac{1}{2}m'_s,\frac{1}{2}m_s|S_0M_{S_0}\right\rangle\langle l'm',lm|L_0M_{L_0}\rangle \\
&a^{\dagger}_{(\eta,0)l'm';\frac{1}{2}m'_s}a_{(0,\eta)lm;\frac{1}{2}m_s}.
\end{aligned} \tag{C.5}$$

As a result, Eq. (C.1) can be simplified to

$$\begin{aligned}
&\mathcal{F}^{(\lambda_0,\mu_0),S_0;J}_{\kappa_0 L_0\quad M} = \left[\frac{2\dim(\eta,0)}{(2S_0+1)\dim(\lambda_0,\mu_0)}\right]^{\frac{1}{2}} \\
&\langle(\eta,0);\frac{1}{2}|||f^{(\lambda_0,\mu_0);S_0}|||(\eta,0);\frac{1}{2}\rangle \\
&[a^{\dagger(\eta,0);\frac{1}{2}}\otimes\tilde{a}^{(0,\eta);\frac{1}{2}}]^{(\lambda_0,\mu_0),S_0;J}_{\kappa_0 L_0\quad M},
\end{aligned} \tag{C.6}$$

where the tensors have been coupled to conserved angular momentum J, namely,

$$\mathcal{F}^{(\lambda_0,\mu_0),S_0;J}_{\kappa_0 L_0\quad M} = \sum_{M_{L_0}M_{S_0}}\langle L_0M_{L_0},S_0M_{S_0}|JM\rangle\,\mathcal{F}^{(\lambda_0,\mu_0),S_0}_{\kappa_0 L_0 M_{L_0},M_{S_0}}, \tag{C.7}$$

and

$$\begin{aligned}
&[a^{\dagger(\eta,0);\frac{1}{2}}\otimes\tilde{a}^{(0,\eta);\frac{1}{2}}]^{(\lambda_0,\mu_0),S_0;J}_{\kappa_0 L_0\quad M} = \\
&\sum_{m_{L_0}m_{S_0}}\langle l_0m_{L_0},S_0m_{S_0}|JM\rangle\,[a^{\dagger(\eta,0);\frac{1}{2}}\otimes\tilde{a}^{(0,\eta);\frac{1}{2}}]^{(\lambda_0,\mu_0),S_0}_{\kappa_0 L_0 m_{L_0},m_{S_0}}.
\end{aligned} \tag{C.8}$$

A two-body tensor operator $\mathcal{G}^{(\lambda_0,\mu_0),S_0}$ in second quantized form can be written as

$$\begin{aligned}
&\mathcal{G}^{(\lambda_0,\mu_0),S_0} = -\frac{1}{2}\sum_{\{-\}}\langle(\lambda_1,\mu_1);s_1|||g^{(\lambda_0,\mu_0);S_0}|||(\lambda_2,\mu_2);s_2\rangle_{\rho_0} \\
&\sqrt{\frac{\dim(\lambda_1,\mu_1)(2s_1+1)}{\dim(\lambda_0,\mu_0)(2S_0+1)}}(-1)^{\varphi}\sum_{\rho'_0}\phi_{\rho\rho'_0}((\lambda_0,\mu_0)(\lambda_2,\mu_2);(\lambda_1,\mu_1)) \\
&\left[\left[a^{\dagger(\eta,0);\frac{1}{2}}\otimes a^{\dagger(\eta,0);\frac{1}{2}}\right]^{(\lambda_1,\mu_1);S_1}\otimes\left[\tilde{a}^{(0,\eta);\frac{1}{2}}\otimes\tilde{a}^{(0,\eta);\frac{1}{2}}\right]^{(\lambda_2,\mu_2);S_2}\right]^{(\lambda_0,\mu_0)\rho'_0,S_0}.
\end{aligned} \tag{C.9}$$

Appendix D

Pseudo-$SU(3)$ Expansion of One-Body Tensor Operators

If a one-body $SU(3)$ tensor operator has to be evaluated in a pseudo-$SU(3)$ basis, it is necessary to rewrite it using pseudo quantum numbers. For this relabeling, it is convenient to express the operator in a J coupled scheme since this quantum number is invariant under the transformation from the real to the pseudo space:

$$\begin{aligned}
\mathcal{F}^{J_0}_{M_0} &= \sum_{ll'} \sum_{jj' m_j m'_j} \langle (\eta,0)l; \frac{1}{2}, j m_j | g^{J_0} | (\eta,0)l'; \frac{1}{2}, j' m_{j'} \rangle \\
&\quad a^{\dagger(\eta,0)l;\frac{1}{2},j}_{m_j} a^{(0,\eta)l';\frac{1}{2},j'}_{m_{j'}} \\
&= \sum_{ll'} \sum_{jj'} \langle (\eta,0)l; \frac{1}{2}, j \| g^{J_0} \| (\eta,0)l'; \frac{1}{2}, j' \rangle \\
&\quad \{(-1)^{\eta} \sqrt{\frac{2j+1}{2J_0+1}} \left[a^{\dagger(\eta,0)l;\frac{1}{2},j} a^{(0,\eta)l';\frac{1}{2},j'} \right]^{J_0}_{M_0} \}. \qquad \text{(D.1)}
\end{aligned}$$

Discarding the terms with $j+\eta+\frac{1}{2}$, the tensor product of creation and annihilation operator can be relabeled using pseudo $SU(3)$ quantum numbers,

$$(-1)^{\eta} \left[a^{\dagger(\eta,0)l;\frac{1}{2},j} \otimes \tilde{a}^{(0,\eta)l';\frac{1}{2},j'} \right]^{j_0}_{m_{j_0}} = (-1)^{\tilde{\eta}} \left[a^{\dagger(\tilde{\eta},0)\tilde{l};\frac{1}{2},j} \otimes \tilde{a}^{(0,\tilde{\eta})\tilde{l}';\frac{1}{2},j'} \right]^{J_0}_{M_0}, \qquad \text{(D.2)}$$

and recoupled into unit tensors

$$\begin{aligned}
&\left[a^{\dagger(\tilde{\eta},0)\tilde{l};\frac{1}{2},j} \otimes \tilde{a}^{(0,\tilde{\eta})\tilde{l}';\frac{1}{2},j'} \right]^{J_0}_{M_0} = \\
&\sum_{\tilde{L}_0 \tilde{S}_0} \chi \begin{Bmatrix} \tilde{l} & \frac{1}{2} & j \\ \tilde{l}' & \frac{1}{2} & j' \\ \tilde{L}_0 & \tilde{S}_0 & j_0 \end{Bmatrix} \left[a^{\dagger(\tilde{\eta},0)l;\frac{1}{2},j} \otimes \tilde{a}^{(0,\tilde{\eta})l';\frac{1}{2},j'} \right]^{\tilde{L}_0,\tilde{S}_0;j_0}_{m_{j_0}} \qquad \text{(D.3)}
\end{aligned}$$

$$= \sum_{(\tilde{\lambda_0},\tilde{\mu_0})\tilde{\kappa_0}} \sum_{\tilde{L_0}\tilde{S_0}} \chi \begin{Bmatrix} \tilde{l} & \frac{1}{2} & j \\ \tilde{l'} & \frac{1}{2} & j' \\ \tilde{L_0} & \tilde{S_0} & J_0 \end{Bmatrix} \langle (\tilde{\eta},0)\tilde{l};(0,\tilde{\eta})\tilde{l'} \| (\tilde{\lambda_0},\tilde{\mu_0})\tilde{\kappa_0}\tilde{L_0} \rangle$$
$$\left[a^{\dagger(\tilde{\eta},0);\frac{1}{2}} \otimes \tilde{a}^{(0,\tilde{\eta});\frac{1}{2}} \right]^{(\tilde{\lambda_0},\tilde{\mu_0}),\tilde{S_0};J_0}_{\tilde{\kappa_0}\tilde{L_0} \qquad M_0}. \tag{D.4}$$

Substituting this result into Eq. (D.1), the matrix element for one-body operator becomes

$$\mathcal{F}^{J_0}_{M_0} = \sum_{(\tilde{\lambda_0},\tilde{\mu_0})\kappa_0} \sum_{\tilde{L_0}\tilde{S_0}} C^{J_0}(\tilde{\eta},\tilde{\lambda_0},\tilde{\mu_0},\tilde{\kappa_0},\tilde{L_0},\tilde{S_0}) \left[a^{\dagger(\tilde{\eta},0)l;\frac{1}{2}} \otimes \tilde{a}^{(0,\tilde{\eta})l';\frac{1}{2}} \right]^{(\tilde{\lambda_0},\tilde{\mu_0}),\tilde{S_0};J_0}_{\tilde{\kappa_0}\tilde{L_0} \qquad M_0}, \tag{D.5}$$

where a coefficient C^{J_0} has been introduced,

$$C^{J_0}(\tilde{\eta};\tilde{\lambda_0},\tilde{\mu_0},\tilde{\kappa_0},\tilde{L_0},\tilde{S_0}) = \sum_{ll'} \sum_{jj'} \langle (\eta,0)l;\frac{1}{2},j \| g^{J_0} \| (\eta,0)l';\frac{1}{2},j' \rangle$$
$$(-1)^{\tilde{\eta}} \sqrt{\frac{2j+1}{2J_0+1}} \chi \begin{Bmatrix} \tilde{l} & \frac{1}{2} & j \\ \tilde{l'} & \frac{1}{2} & j' \\ \tilde{L_0} & \tilde{S_0} & J_0 \end{Bmatrix} \langle (\tilde{\eta},0)\tilde{l};(0,\tilde{\eta})\tilde{l'} \| (\tilde{\lambda_0},\tilde{\mu_0})\tilde{\kappa_0}\tilde{L_0} \rangle$$
$$= \sum_{ll'} \sum_{jj'} \langle (\eta,0)l;\frac{1}{2},j \| g^{J_0} \| (\eta,0)l';\frac{1}{2},j' \rangle$$
$$B^J(j,j',\tilde{l},\tilde{l'};\tilde{\eta};\tilde{\lambda_0},\tilde{\mu_0},\tilde{\kappa_0},\tilde{L_0},\tilde{S_0}). \tag{D.6}$$

The expression $B^{J_0}(j,j',\tilde{l},\tilde{l'};\tilde{\eta};\tilde{\lambda_0},\tilde{\mu_0},\tilde{\kappa_0},\tilde{L_0},\tilde{S_0})$ depends only on the tensorial rank, J_0, of the one-body operator.

Vita

Kalin Pavlov Drumev was born in June, 1974, in Shumen, Bulgaria. He attended the School of Natural Sciences in Shumen and graduated in 1992. Next, he studied physics at the University of Shumen and received his Master of Science Degree in 1997 after defending a thesis entitled "Alpha particle momentum distributions and (alpha,2alpha) reaction cross sections" under the supervision of Professor A. N. Antonov. He began his studies in the Department of Physics and Astronomy at Louisiana State University in 2000. His doctoral degree is expected to be awarded in May 2008.